

DFT INSIGHTS INTO Nb-BASED 211 MAX PHASE CARBIDES: Nb₂AC (A = Ga, Ge, Tl, Zn)



By

Prima Das

M.Sc in Physics

Student ID: 19MSPHY001F

A thesis submitted in partial fulfilment of the requirements for the degree of
MASTER of SCIENCE in Physics

Department of Physics

CHITTAGONG UNIVERSITY OF ENGINEERING AND TECHNOLOGY

September, 2023

Candidate's Declaration

I hereby declare that the work contained in this Thesis has not been previously submitted to meet the requirements for an award at this or any other higher education institution. To the best of my knowledge and belief, the Thesis contains no material previously published or written by another person except where due reference is cited. Furthermore, the Thesis complies with the PLAGIARISM and ACADEMIC INTEGRITY regulations of CUET.

Prima Das
19MSPHY001F
Department of Physics
Chittagong University of Engineering & Technology (CUET)

Copyright © Prima Das, 2023.

This work may not be copied without permission of the author or Chittagong University of Engineering & Technology.

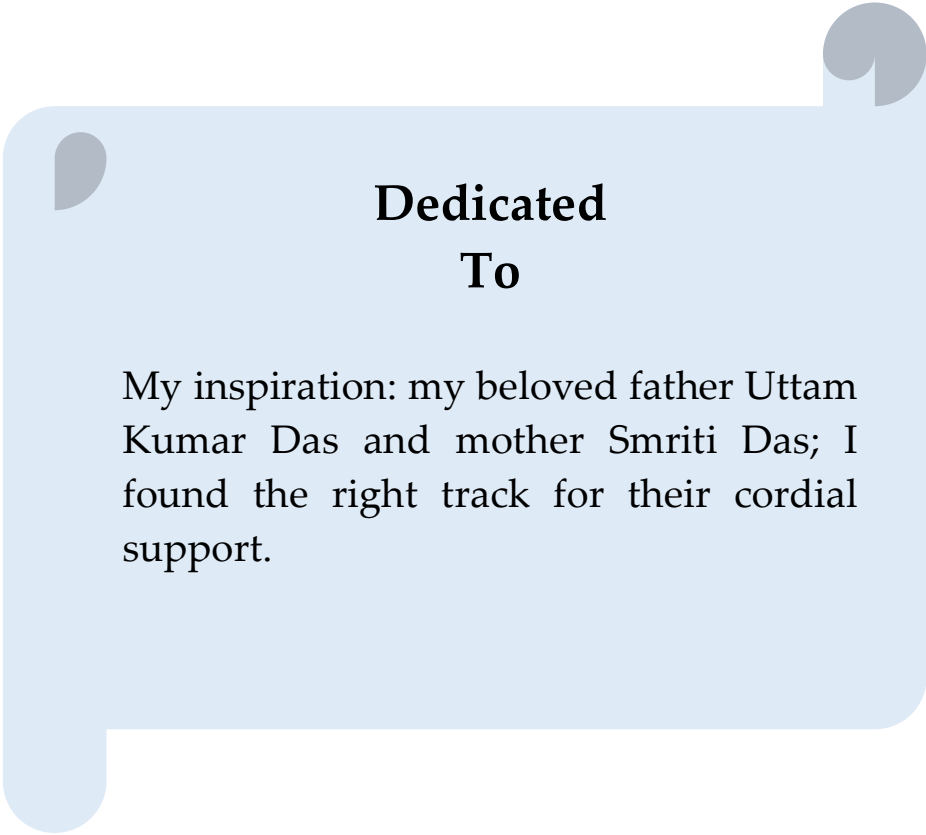
Copyright Declaration

I hereby declare that I am the sole author of the thesis titled "**DFT INSIGHTS INTO Nb-BASED 211 MAX PHASE CARBIDES: Nb₂AC (A = Ga, Ge, Tl, Zn)**". Along with this, submitted a softcopy is true copy of my final hardcopy thesis including any required final revisions, as accepted by the board of examination.

I hereby release my copyright to Chittagong University of Engineering and Technology (CUET) for uploading the electronic version of the same to the 'Digital Repository (Institutional Repository)' of CUET after one year from the day of submission. Apart from this, the existing or to be approved Open Education Resources (OER) policies and procedures of Chittagong University of Engineering and Technology (CUET) shall be applicable to this research work.

I also acknowledge my sincere delivering of copyright to Chittagong University of engineering and Technology (CUET) to reproduce this thesis by reprography or by other means, in total or by part at the necessity of individuals for the purpose of scholarly research.

Signature of the Author



Dedicated To

My inspiration: my beloved father Uttam Kumar Das and mother Smriti Das; I found the right track for their cordial support.

Publication & Conference attended

Publication

Prima Das, N. Jahan, M. A. Ali, "DFT insights into Nb-based 211 MAX phase carbides: Nb₂AC (A = Ga, Ge, Tl, Zn, P, In, Cd)", RSC Advances, volume 13, issue February 2023, page number 5538; published by Royal Society of Chemistry.

Conference attended

Prima Das, N. Jahan, M. A. Ali, "DFT insights into Nb-based 211 MAX Phase Carbides: Nb₂AC (A = Ga, Ge, Tl, Zn)"- has been presented Poster presentation, "International Conference on Physics -2022"- held on 19 to 21 May, organized by Bangladesh Physical Society, Atomic Energy Centre, Dhaka, Bangladesh.

Approval/Declaration by the Supervisor(s)

This is to certify that Prima Das has carried out this research work under my/our supervision and that she has fulfilled the relevant Academic Ordinance of the Chittagong University of Engineering and Technology so that she is qualified to submit the following Thesis in the application for the degree of MASTER of SCIENCE in PHYSICS. Furthermore, the Thesis complies with the PLAGIARISM and ACADEMIC INTEGRITY regulations of CUET.

Dr. Md. Ashraf Ali
Professor
Department of Physics
Chittagong University of Engineering & Technology

Acknowledgement

First of all, I want to thank Almighty God for the successful completion of my M.Sc. journey.

A great thanks from the core of my heart to my supervisor Professor Dr. Md. Ashraf Ali, Department of Physics, Chittagong University of Engineering and Technology (CUET), for his scholastic supervision, valuable guidance and helpful discussion throughout the progress of this work. I learn research work as well as new thinking on the field of materials science under his valuable supervision. I am highly grateful to him for giving me a chance of pursuing this study under his supervision.

I am deeply grateful to Prof. Dr. Swapan Kumar Roy, Head, Department of Physics, Chittagong University of Engineering and Technology (CUET), for his inspiration during the research work.

I am indebted to Prof. Dr. Md. Mohi Uddin and Prof. Dr. Mohammad Belal Hossen, Department of Physics, Chittagong University of Engineering and Technology (CUET) for their helpful and valuable guidance.

I would like to express my gratitude to my teacher Prof. Dr. Nusrat Jahan, Dr. Md. Mukter Hossain, Associate Professor and Md. Abdul Jalil, Assistant Professor, Department of Physics, Chittagong University of Engineering and Technology (CUET) for their encouragement and suggestion throughout the thesis work.

I also express highly thanks to Prof. Dr. H. M. A. R. Maruf, Prof. Dr. Animesh Kumer Chakraborty, Mosammat Arjumanara Bagum, Shaiful Kabir, Md. Zahid Hasan and Sinthia Binte Kholil for their constant support and encouragement.

I am grateful to the Directorate of Planning and Development, CUET and Ministry of Science & Technology (MOST) for providing me scholarship and the authority of CUET, Chattogram, Bangladesh for giving the necessary permission, financial and technical support during this work.

September, 2023

The Author
(Prima Das)

Abstract

In this thesis, to study the 211 MAX phase carbides, the first-principles calculations were performed: Nb₂AC (A = Ga, Ge, Tl, Zn) and the obtained properties of these phases are compared with those of Nb₂AC (A = P, In, Cd, Al). With those from the prior studies, the structural characteristics are in appropriate agreement. Vickers hardness, stiffness constants and elastic modulus have been calculated to explore mechanical behavior. Besides, the structural stability of the studied compounds was checked using the phonon dispersion curves. Based on the elastic constants, the selected MAX phases are mechanically stable. Among the studied compounds, the value of Poisson's ratio and Pugh ratio indicate that Nb₂GaC ($\nu = 0.23$ and $G/B = 0.67$) behaves as brittle solids whereas other studied compounds behave ductile nature. According to the values of Vickers hardness for studied materials can be ordered as follows: Nb₂GaC > Nb₂ZnC > Nb₂TlC > Nb₂GeC. On the contrary, Nb₂PC (10.02 GPa and 9.31 GPa for GGA PBE and GGA PBEsol, respectively) has higher Vickers hardness than selected MAX phases. The anisotropy of the elastic characteristics was exposed through the 2D and 3D plotting of elastic moduli and calculating anisotropy indices. Utilizing the bond overlap and Mulliken atomic population, the mixture of ionic and covalent bonding has been explained among these carbides. To confirm the metallic behavior, the band structure and density of states (DOS) have been calculated. The discussion of the strength and bonding nature of different states also used Partial DOS. To explore the possible relevance in various fields, the optical characteristics of these selected phases have also been computed and analysed. Nb₂AC (A = Ga, Ge, Tl, Zn, P, In, Cd, Al) MAX phases can be considered as prospective absorbing materials in this energy range because of the large absorption coefficients in the high energy range (7-10 eV). In order to bring out the potential relevance in high-temperature technology, the Debye temperature (Θ_D), minimum thermal conductivity (K_{min}), Grünisen parameter (γ) and melting temperature (T_m) were studied. The findings of the present research suggest that the mentioned carbides are suitable for usage as thermal barrier coating (TBC) and solar radiation-protecting coating materials.

বিমূর্ত:

এই থিসিসে, আমরা ২১১ ম্যাক্স ফেজ Nb_2AC ($A = Ga, Ge, Tl, Zn$) কার্বাইডগুলি অধ্যয়ন করার জন্য ফার্স্ট প্রিন্সিপাল গণনা সম্পাদন করেছি এবং এই ফেজগুলির প্রাপ্ত বৈশিষ্ট্যগুলি Nb_2AC ($A = Ga, Ge, Tl, Zn$) এর সাথে তুলনা করা হয়েছে। গঠনগত বৈশিষ্ট্যগুলি পূর্ববর্তী অধ্যয়নের সাথে উপযুক্ত সামঞ্জস্য রয়েছে। দৃঢ়তার গুণক, স্থিতিস্থাপক গুণাংক এবং ভিকারস হার্ডনেস গণনা করে মেকানিক্যাল বৈশিষ্ট্য অধ্যয়ন করা হয়েছে। নির্বাচিত যৌগগুলির গঠনগত স্থিতিশীলতা যাচাই করতে ফোনন ডিম্পারশন রেখা ব্যবহার করা হয়েছে। স্থিতিস্থাপক গুণাংকের উপর ভিত্তিতে, নির্বাচিত ম্যাক্স ফেজগুলি মেকানিক্যালভাবে স্থিতিশীল। অধ্যয়ন করা যৌগগুলির মধ্যে, পয়সনের অনুপাত এবং Pugh অনুপাতের মান নির্দেশ করে যে Nb_2GaC ($\nu = 0.23$ এবং $G/B = 0.67$) ভঙ্গুর কঠিন পদার্থ হিসাবে আচরণ করে যেখানে অন্যান্য অধ্যয়নকৃত যৌগগুলি নমনীয় প্রকৃতির আচরণ করে। ভিকারস হার্ডনেসের মান অনুযায়ী অধ্যয়ন করা যৌগগুলিকে এই ক্রমে অনুসরণ করা যেতে পারে: $Nb_2GaC > Nb_2ZnC > Nb_2TlC > Nb_2GeC$ । পক্ষান্তরে, Nb_2PC (GGA PBE এবং GGA PBEsol এর জন্য যথাক্রমে 10.02 GPa এবং 9.31 GPa) নির্বাচিত ম্যাক্স ফেজগুলির তুলনায় ভিকারস হার্ডনেস বেশি। স্থিতিস্থাপক বৈশিষ্ট্যের ক্ষেত্রে স্থিতিস্থাপক গুণাংকের ২ডি ও ৩ডি গ্রাফ এবং গণনা করা অ্যানাইসোট্রপিক সূচকগুলি যৌগগুলির অ্যানাইসোট্রপিক আচরণ প্রকাশ করে। আমরা এই কার্বাইডগুলির মধ্যে আয়নিক এবং সমযোজী বন্ধনের মিশ্রণ ব্যাখ্যা করতে মুলিকেন এটমিক এবং বন্ড ওভারল্যাপ পপুলেশন ব্যবহার করেছি। ব্যান্ড স্ট্রাকচার এবং ডেনসিটি অব স্টেটস (DOS) অধ্যয়ন করে ধাতব আচরণ নিশ্চিত করা হয়েছে। পার্শিয়াল ডেনসিটি অব স্টেটস (PDOS) বিভিন্ন স্টেটের মধ্যে বন্ধনের প্রকৃতি এবং শক্তি নিয়ে আলোচনা করতে ব্যবহৃত হয়েছে। এই পর্যায়গুলির অপটিক্যাল বৈশিষ্ট্যগুলিও অধ্যয়ন করা হয়েছে এবং বিভিন্ন ক্ষেত্রে সম্ভাব্য প্রাসঙ্গিকতা প্রকাশ করার জন্য বিশ্লেষণ করা হয়েছে। উচ্চ শক্তি পরিসরে (7-10 eV) বৃহৎ শোষণ সহগগুলির কারণে Nb_2AC ($A = Ga, Ge, Tl, Zn$) ম্যাক্স ফেজগুলিকে সম্ভাব্য শোষণকারী উপাদান হিসাবে বিবেচনা করা যেতে পারে। ডিভাই তাপমাত্রা (θ_D), গ্রনিসেন প্যারামিটার (γ), গলনাংকের তাপমাত্রা (T_m) এবং ন্যূনতম তাপ পরিবাহিতা (K_{min}) উচ্চ-তাপমাত্রা প্রযুক্তিতে তাদের সম্ভাব্য প্রাসঙ্গিকতা যাচাই করার জন্য অধ্যয়ন করা হয়েছে। এই গবেষণার ফলাফলগুলি নির্দেশ করে যে শিরোনামযুক্ত কার্বাইডগুলি সূর্যের তাপ থেকে রক্ষার জন্য প্রলেপ এবং তাপীয় বাধার প্রলেপ (TBC) হিসাবে ব্যবহারের জন্য উপযুক্ত।

Table of Contents

Abstract.....	ix
Table of Contents	xi
List of Figures	xiii
List of Tables	xiv
Abbreviations	xvi

CHAPTER 1 INTRODUCTION 1-8

1.1	Background	1
1.2	The Structure of Crystals for the MAX Phase	2
1.3	Structural Aspects	4
1.4	Aims and Objectives of the Present Study	5
1.5	Outline of the Present Study	6
	References	7

CHAPTER 2 LITERATURE REVIEW OF MAX PHASE 9-16

2.1	General	9
2.2	Historical Background	9
2.3	History of C-containing MAX Phases	10
2.4	Conclusion and Impacts	13
	References	14

CHAPTER 3 MATERIALS AND METHODOLOGY 17-35

3.1	CASTEP Code	17
3.2	Many-body Problems in Quantum Mechanics	18
3.3	Density Functional Theory	20
3.4	Pseudopotential	22
3.5	Generalized Gradient Approximation (GGA)	24

3.6	k-Point Sampling	25
3.7	Theory of the Calculated Properties	25
	References	33
CHAPTER 4 RESULTS AND DISCUSSIONS		36-72
4.1	Structural Properties and Phase Stability	36
4.2	Mechanical Properties	40
4.3	Electronic Properties, Mulliken Atomic and Bond Population Analysis	47
4.4	Elastic Anisotropy	52
4.5	Optical Properties	60
4.6	Thermal Properties	64
	References	68
CHAPTER 5 KEY FINDINGS AND CONCLUSIONS		73-75
5.1	General	73
5.2	Key Findings	73
	Limitations of the Study	74
	Practical Implication	74
	Recommendation for Further Study	75

List of Figures

Fig. No.	Figure Caption	Page
Fig. 1.1	MAX phase based periodic table.	1
Fig. 1.2	(i) Crystal structure of $M_{n+1}AC_n$ phase.	3
	(ii) The unit cell of Nb_2GaC .	3
Fig. 3.3.2	Self-Consistent Kohn-Sham equation solution flow chart	21
Fig. 3.4	All electrons (blue lines), pseudo-potentials (red lines), and the analogous wave functions are revealed schematically. The pseudopotentials and electron alignment are r_c .	22
Fig. 4.1.1	The unit cell of Nb_2AC ($A = Ga, Ge, Ti, Zn$).	36
Fig. 4.1.2	Phonon dispersion curves along with phonon DOS of (a) Nb_2GaC , (b) Nb_2GeC , (c) Nb_2TiC , (d) Nb_2ZnC calculated using GGA PBEsol.	48
Fig. 4.2.1	Comparison of (a) stiffness constants and (b) elastic moduli of Nb_2AC ($A = Ga, Ge, Ti, Zn, P, In, Cd, Al$) MAX phases calculated using GGA PBEsol.	43
Fig. 4.3.1	(i) Band Structure of (a) Nb_2GaC , (b) Nb_2GeC , (c) Nb_2TiC , (d) Nb_2ZnC calculated using GGA PBEsol.	48
Fig. 4.3.1	(ii) Total and partial DOS of (a) Nb_2GaC , (b) Nb_2GeC , (c) Nb_2TiC , (d) Nb_2ZnC , calculated using GGA PBEsol.	49
Fig. 4.4.	(i) The 2D and 3D plots of (a) Y , (b) K , (c) G and (d) v of Nb_2GaC for GGA PBEsol.	55
	(ii) The 2D and 3D plots of (a) Y , (b) K , (c) G and (d) v of Nb_2GeC for GGA PBEsol.	56
	(iii) The 2D and 3D plots of (a) Y , (b) K , (c) G and (d) v of Nb_2TiC for GGA PBEsol.	57
	(i) The 2D and 3D plots of (a) Y , (b) K , (c) G and (d) v of Nb_2ZnC for GGA PBEsol.	58
Fig. 4.5	(a) real part (ϵ_1) and (b) imaginary part (ϵ_2) of dielectric function (ϵ), (c) refractive index (n), (d) extinction coefficient (k), (e) absorption coefficient (α), (f) photoconductivity (σ), (g) reflectivity (R) and (h) loss function (LF) of Nb_2AC ($A = Ga, Ge, Ti, Zn, P, In, Cd, Al$) MAX phases as a function of photon energy calculated using GGA PBEsol.	63

List of Tables

Table No.	Table Caption	Page
Table 4.1.1	Calculated lattice constants (a and c), c/a ratio, internal parameter (Z_m), density (ρ), volume (\AA), distortion parameters of octahedra (O_d), and trigonal prism (P_d) of Nb_2AC ($A = \text{Ga, Ge, Tl, Zn}$), along with those of Nb_2AC ($A = \text{P, In, Cd, Al}$) MAX phases.	37
Table 4.2.1	Calculated stiffness constant (C_{ij}), bulk modulus (B), shear modulus (G), Young's modulus (Y), machinability index (B/C_{44}), Cauchy pressure (CP), Poisson's ratio (ν) and Pugh ratio (G/B) of Nb_2AC ($A = \text{Ga, Ge, Tl, Zn}$), along with those of Nb_2AC ($A = \text{P, In, Cd, Al}$) MAX phases.	41
Table 4.2.3	Calculated Mulliken bond number n^μ , bond length d^μ , bond overlap population P^μ , metallic population $P^{\mu'}$, bond volume v_b^μ , bond hardness H_v^μ of μ -type bond and Vickers hardness H_v of Nb_2AC ($A = \text{Ga, Ge, Tl, Zn}$), along with those of Nb_2AC ($A = \text{P, In, Cd, Al}$) MAX phases.	46
Table 4.3.2	(a) Mulliken atomic and bond overlap population (BOP) calculated using GGA PBEsol of Nb_2AC ($A = \text{Ga, Ge, Tl, Zn}$), along with those of Nb_2AC ($A = \text{P, In, Cd, Al}$) MAX phases.	51
	(b) Mulliken atomic and bond overlap population (BOP) calculated using GGA PBE of Nb_2AC ($A = \text{Ga, Ge, Tl, Zn}$), along with those of Nb_2AC ($A = \text{P, In, Cd, Al}$) MAX phases.	52
Table 4.4	(a) Anisotropy factors $A_1, A_2, A_3, k_c/ka, B_a, B_c$ percentage anisotropy factors A_G and A_B and universal anisotropic index A^u , calculated values using GGA PBEsol of Nb_2AC ($A = \text{Ga, Ge, Tl, Zn}$), along with those of Nb_2AC ($A = \text{P, In, Cd, Al}$) MAX phases.	59
	(b) Anisotropy factors $A_1, A_2, A_3, k_c/ka, B_a, B_c$ percentage anisotropy factors A_G and A_B and universal anisotropic index A^u , calculated values using GGA PBE of Nb_2AC ($A = \text{Ga, Ge, Tl, Zn}$), along with those of Nb_2AC ($A = \text{P, In, Cd, Al}$) MAX phases.	59

Table 4.6	(a) Calculated density (ρ), longitudinal, transverse, and average sound velocities (v_l , v_t , and v_m , respectively), Debye temperature (Θ_D), minimum thermal conductivity (K_{min}), and Grüneisen parameter (γ), calculated values using GGA PBEsol of Nb ₂ AC (A= Ga, Ge, Tl, Zn), along with those of Nb ₂ AC (A = P, In, Cd, Al) MAX phases.	65
	(b) Calculated density (ρ), longitudinal, transverse, and average sound velocities (v_l , v_t and v_m respectively), Debye temperature (Θ_D), minimum thermal conductivity (K_{min}), and Grüneisen parameter (γ), calculated values using GGA PBE of Nb ₂ AC (A= Ga, Ge, Tl, Zn), along with those of Nb ₂ AC (A = P, In, Cd, Al) MAX phases.	65

Abbreviations

BZ	Brillouin Zone
CASTEP	Cambridge Serial Total Energy Package
DF	Density Functional
DFT	Density Functional Theory
DOS	Density of States
eV	Electron Volts
GGA	Generalized Gradient Approximation
GPa	Giga Pascals
GS	Ground State
IR	Infrared
KS	Kohn and Sham
LDA	Local Density Approximation
NCP	Norm-conserving Pseudopotential
PBE	Perdew, Burke and Ernzerhof
PBEsol	Perdew, Burke and Ernzerhof for solids
PDOS	Partial Density of States
PP	Pseudopotential
TBC	Thermal Barrier Coating
USP	Ultra-soft Pseudopotential
UV	Ultraviolet
XC	Exchange-correlation

CHAPTER-1

INTRODUCTION

The fundamental concepts are discussed in this chapter and the aim of the whole work is summarized here. An overview of how the several chapters are organized is also shown here.

1.1 Background

Many ternary compounds such as carbides, nitrides, and borides have been included in the MAX phase materials family, which can be expressed as $M_{n+1}AX_n$, where M belongs to the early transition metals group, A is the elements that exist within the groups 13-16, and X can only be C, N, and B, and n is the positive integer with a value of 1-3 [1-4].

I A																		VII A																											
H																		He																											
II A																																													
Li	Be																																												
Na	Mg																																												
K	Ca	Sc	Ti	V	Cr	Mn	Fe	Co	Ni	Cu	Zn	Ga	Ge	As	Se	Br	Kr																												
Rb	Sr	Y	Zr	Nb	Mo	Tc	Ru	Rh	Pd	Ag	Cd	In	Sn	Sb	Te	I	Xe																												
Cs	Ba	La	Hf	Ta	W	Re	Os	Ir	Pt	Au	Hg	Tl	Pb	Bi	Po	At	Rn																												
Fr	Ra	Ac	Rf	Db	Sg	Bh	Hs	Mt	Ds	Rg	Uub	Uut	Uuq	Uup	Uuh	Uus	Uuo																												
<div><div>M = Early transition metal</div><div>A = Group A element</div><div>X = C or N or B</div></div>																																													
<table><tr><td>Ce</td><td>Pr</td><td>Nd</td><td>Pm</td><td>Sm</td><td>Eu</td><td>Gd</td><td>Tb</td><td>Dy</td><td>Ho</td><td>Er</td><td>Tm</td><td>Yb</td><td>Lu</td></tr><tr><td>Th</td><td>Pa</td><td>U</td><td>Np</td><td>Pu</td><td>Am</td><td>Cm</td><td>Bk</td><td>Cf</td><td>Es</td><td>Fm</td><td>Md</td><td>No</td><td>Lr</td></tr></table>																		Ce	Pr	Nd	Pm	Sm	Eu	Gd	Tb	Dy	Ho	Er	Tm	Yb	Lu	Th	Pa	U	Np	Pu	Am	Cm	Bk	Cf	Es	Fm	Md	No	Lr
Ce	Pr	Nd	Pm	Sm	Eu	Gd	Tb	Dy	Ho	Er	Tm	Yb	Lu																																
Th	Pa	U	Np	Pu	Am	Cm	Bk	Cf	Es	Fm	Md	No	Lr																																

Fig. 1.1: MAX phase based periodic table. Reprinted from [5].

In 1960s, the MAX phase was first revealed by Nowotny *et al.* [1-4]. In the 1990s, Barsoum *et al.* [6, 7] renewed the attention by revealing their remarkable characteristics. They have remarkable mechanical strength, machinability, electronic conductivity, and thermal conductivity. They are also machinable, similar to metals,

have better mechanical properties at high temperatures, and are similar to ceramics in terms of oxidation and superior corrosion [8]. The MAX phase family has become a significant materials group from both the research and application points of view. Owing to the magnificent fusing of metallic and ceramic properties, the number of published articles is increasing day by day [9]. They are typically performed for automotive, electrical equipment, clinical, aircraft applications, etc. Due to their thickness, MAX phases are generally utilized as nano-laminates. Given its benefits in numerous industries, a thorough analysis of the MAX phase is necessary. A large number of MAX phases (more than 80) have been synthesized so far, most of which are 211 phases (58 prominent members) [10]. Based on the atoms in the unit cell, three categories of MAX phases are recognized. They are: M_2AX is referred to as the 211 phase, where $n = 1$; M_3AX_2 is referred to as the 312 phase, where $n = 2$ and M_4AX_3 is referred to as the 413 phase, where $n = 3$.

1.2 The Structure of Crystals for the MAX Phase

Fig. 1.2(i) shows the hexagonal unit cells [space group of $P6_3/mmc$] of the 211, 312, 413, and 514 MAX phases. There is a distinction between the three phases, and M layers in the unit cell separate the A layers to create these distinctions. A few of the hybrid MAX phases might also be made by combining the equivalent (211, 312, and 413) phases. The 713 and 523 phases are two other hybrid phases that have recently been synthesized and exhibit similar behavior. Two M layers comprise the 211 phase, three M layers comprise the 312 phase, four M layers comprise the 413 phase and five M layers comprise the 514 phase as illustrated in Fig. 1.2(i). As seen, the unit cell contains the M_6X octahedron interspersed involving two A layers. The binary carbides or nitrides, MX, and the octahedron M_6X in the unit cell are similar. The M(1) and M(2) sites, which are two M sites, are presented in the crystal structures of the 312 and 413 phases, respectively. M1 sites are contiguous to A layers, while M(2) sites are adjoining to X layers. Because of this, it was discovered that there are two atomic sites, X(1) and X(2), in the 413 phase, where X(1) and X(2) atoms build bonds with M(1) and M(2) atoms, respectively.

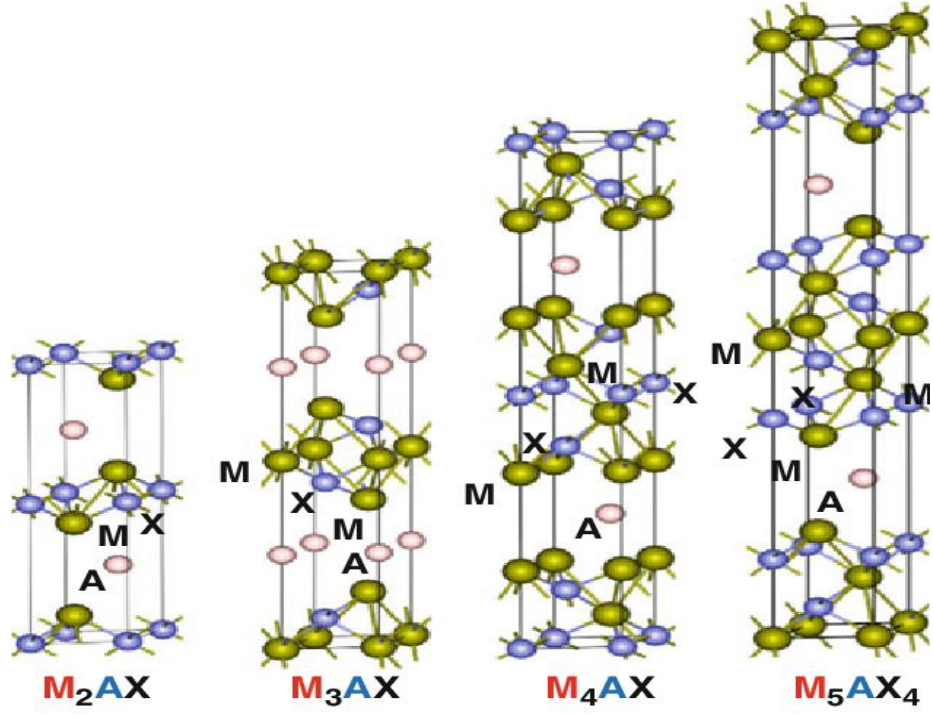


Fig. 1.2: (i) Crystal structure of $M_{n+1}AC_n$ phase [11].

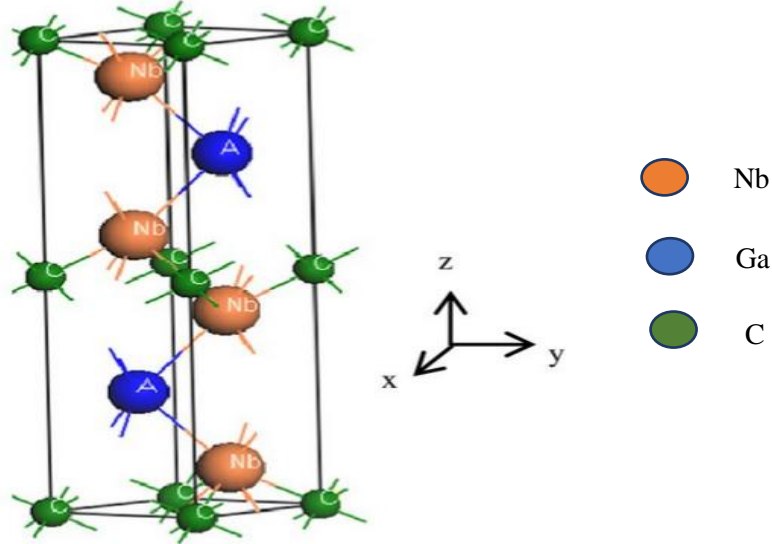


Fig. 1.2: (ii) the unit cell of Nb_2GaC .

The MX layers appear twinned because the A layers function as mirror planes. As shown in Fig. 1.2(i), the MAX phases have anisotropic structures. The c/a ratios for the 211, 312, and 413 phases are 4, 6, and 8, respectively. Because the MAX phases have a multilayer structure with layers in the nanoscale range, the structure is also

called "nano-laminated." Nb₂GaC, one of the targeted materials among the Nb₂AC (Ga, Ge, Tl, Zn) phases, is depicted in Fig. 1.2(ii), and its unit is comparable to that shown in the 211 MAX phase in Fig. 1.2 (i).

1.3 Structural Aspects

Knowing the unit cell and MAX phase crystallography provides a comprehensive understanding of crystal structure. The positions of the atoms in the crystal are depicted in a few illustrations.

1.3.1 Unit Cell

X atoms occupy the octahedral locations between the almost M closed-packed layers and layers of authentic A-group components, which along with the former, form the unique unit cell of the MAX phases. The M₆X octahedra are the same as those in the equivalent binary MX carbide rock salt configurations. Trigonal prisms, which are larger than octahedral sites and hence better suited to accept bigger A atoms, are where the A-group materials are found [12-15]. The A layer is separated from the two, three, and four M layers if n is 1, 2, and 3, respectively. There are two polymorphs, α and β , of the 312 and 413 MAX phases. Because of a variation in the A-element layers, the polymorphism of the 413 MAX phases differs from that seen in the 312 MAX phases. The atoms of M(2) and C(2) placements determine the distinction between α -413 and β -413. The following 413 phases usually crystallize in bulk form in the polymorph [16–18], while only Ta₄AlC₃ is present in the bulk of both polymorphs [19, 20]. The MAX phase members have two formula units in the unit cell. Each formula unit cell has four atoms.

1.3.2 Crystallography

The hexagonal system includes the elements used in the MAX phase. For the MAX phase, P6₃/mmc is used after Hermann-Mouguin as the space group, and the number of the space group is 194. The P6₃/mmc, which is Hermann-Mouguin notation, is described as follows:

- P denotes a primitive cell with only the eight corners' lattice points. It has no additional translation symmetry for the lattice points. No other base, body, or face-centered positions exist.
- The rotational and translational symmetry of the screw axis is 6_3 , where "6" denotes the 6-fold symmetry and the subscript "3" represents the translation's distance along the axis which is primary. The hexagonal system's primary direction, along the c-axis, is [0001]. The symbol n_r denotes a symmetry component with a rotation of $2\pi/n$ and a translation of a proportion (r/n) of unit cell length c is denoted by. In this way, 6_3 denotes a rotation of $2\pi / 6 = \pi / 3$ (60°) and a translation of $3/6$ along c , which is half of the lattice constant.
- The symbol mmc - denotes the mirror's and the glide plane's symmetry when viewed at right angles to the primary, secondary, and tertiary axes. Regarding the hexagonal system, [0001] direction is taken into consideration to be the primary direction along the c-axis, and $[10\bar{1}0]$ direction is taken into consideration to be the secondary direction. It is along the a axis, and $[11\bar{2}0]$ is considered the tertiary axis, it is the bisector of both the a and b axes. For both the (0001) and $(10\bar{1}0)$ planes, the "mm" denotes mirror symmetry, while the "c" stands for the glide plane that is at a right angle to $[11\bar{2}0]$ and has a glide vector of $c/2$. According to the value of n , which might be 1, 2, 3, or 4, the MAX phases are divided into various subgroups. The α and β phases are two distinct stacking layers that exist between the 312 and 413 phases.

1.4 Aims and Objectives of the Present Study

The aims and objectives of the present research are:

- The structural properties such as lattice constants, density and volume of Nb_2AC ($A = Ga, Ge, Tl, Zn$) will be calculated.
- To check the dynamical stability, phonon dispersion curves (PDC) and phonon density of states (PHDOS) of Nb_2AC ($A = Ga, Ge, Tl, Zn$) will be computed.

- The electronic properties such as electronic band structure and density of states will be calculated.
- The mechanical properties such as different elastic constants, elastic moduli, Hardness parameters, Pugh ratio, Poisson's ratio, mechanical anisotropy etc. will be investigated.
- The thermodynamic properties such as Debye temperature, minimum thermal conductivity, thermal expansion coefficient and melting temperature will be investigated.
- The important optical constants such as dielectric constant, refractive index, absorption coefficient, photoconductivity, reflectivity and loss function will also be investigated.

1.5 Outline of the Present Study

- Chapter one provides a general overview of the current investigation.
- Chapter two describes the literature review of the MAX phase.
- In chapter three, the methodology is presented, along with the theories related to properties.
- Chapter four presents the results and subsequent discussion of the present research.
- The important conclusions of the present study are drawn in chapter five.

References:

- [1] W. Jeitschko, H. Nowotny, F. Benesovsky, *Carbides of formula T_2MC* , J Less Common Met 7 (1964) 133-8.
- [2] H. Wolfsgruber, H. Nowotny, F. Benesovsky, *Die kristallstruktur von Ti_3GeC_2* , Monatsh Chem 98 (1967) 2403-5.
- [3] H. Nowotny, *Struktur chemieeiniger verbindungen der ubergangsmetale mit den elementen C, Si, Ge, Sn*, Prog Solid-State Chem 2 (1970) 27-70.
- [4] H. Nowotny, J. C. Schuster, *Structural chemistry of complex carbides and related compounds*, P. Rogl, J Solid State Chem 44 (1982) 126-33.
- [5] M. Sokol, V. Natu, S. Kota, M. W. Barsoum, *On the chemical diversity of the MAX phases*, Trends Chem. 1 (2019) 210-223.
- [6] M. W. Barsoum, T. El-Raghy, *Synthesis and characterization of a remarkable ceramic: Ti_3SiC_2* , J Am Ceram Soc 79 (1996) 1953-6.
- [7] M. W. Barsoum, *The $M_{n+1}AX_n$ phases: a new class of solids: thermodynamically stable nanolaminates*, Prog Solid-State Chem 28 (2000) 201-81.
- [8] M. W. Barsoum, *MAX phases: properties of machinable ternary carbides and nitrides*, WILEY VCH Verlag GmbH & Co. KGaA; (2013).
- [9] P. Chakraborty, A. Chakrabarty, A. Dutta, T. Saha-Das gupta, *Soft MAX phases with boron substitution: a computational prediction*, Phys. Rev. Mater. 2 (2018) 103605.
- [10] M. A. Hadi, *Superconducting phases in a remarkable class of metallic ceramics*, J. Phys. Chem. Solids 138 (2020) 109275.
- [11] T. Lookman, F. J. Alexander, K. Rajan, *Information Science for Materials Discovery and Design*, Springer Ser. Mater. Sci. 225 (2016) 187-212
- [12] W. Jeitschko, H. Nowotny, F. Benesovsky, *Ti_2AlN , eine stickstoffhaltige H-Phase*, Monatsh. Chem. 94 (1963) 1198.
- [13] W. Jeitschko, H. Nowotny, F. Benesovsky, *Die H-Phasen: Ti_2CdC , Ti_2GaC , Ti_2GaN , Ti_2InN , Zr_2InN und Nb_2GaC* , Monatsh. Chem. 95 (1964) 178.
- [14] W. Jeitschko, H. Nowotny, F. Benesovsky, *Kohlenstoffhaltige ternare Verbindungen ($V-Ge-C$, $Nb-Ga-C$, $Ta-Ga-C$, $Cr-Ga-C$ und $Cr-Ge-C$)*, Monatsh. Chem. 94 (1963) 844.

- [15] W. Jeitschko, H. Nowotny, F. Benesovsky, *Kohlenstoffhaltige ternäre Verbindungen (H-phase)*, Monatsh. Chem. 94 (1963) 672.
- [16] M. W. Barsoum, L. Farber, I. Levin, A. T. Procopio, T. El-Raghy, A. Berner, *High-resolution transmission electron microscopy of Ti_4AlN_3 , or $Ti_3Al_2N_2$ revisited*, J. Am. Ceram. Soc. 82 (1999) 2545.
- [17] J. Etzkorn, M. Ade, H. Hillebrecht, *V_2AlC , V_4AlC_{3-x} (x approximate to 0.31), and $V_{12}Al_3C_8$: synthesis, crystal growth, structure, and superstructure*, Inorg. Chem. 46 (2007) 7646.
- [18] C. J. Rawn, M. W. Barsoum, T. El-Raghy, A. T. Procopio, C. M. Hoffman, C. R. Hubbard, *Structure of Ti_4AlN_{3-x} : a layered $M_{n-1}AX_n$ nitride*, Mater. Res. Bull. 35 (2000) 1785.
- [19] P. Eklund, J. P. Palmquist, J. Höwing, D. H. Trinh, T. El-Raghy, H. Högberg, L. Hultman, *Ta_4AlC_3 : Phase determination, polymorphism and deformation*, Acta Materialia 55 (2007) 4723.
- [20] C. Hu, Z. Lin, L. He, Y. Bao, J. Wang, M. Li, Y. Zhou, *Physical and mechanical properties of bulk Ta_4AlC_3 ceramic prepared by an in situ reaction synthesis/hot-pressing method*, J. Am. Ceram. Soc. 90 (2007) 2542.

CHAPTER 2

LITERATURE REVIEW OF MAX PHASE

2.1 General

A review of the literary works can reveal the MAX phases' historical development. To give readers a thorough grasp of the MAX phase literature oversight, this chapter has been developed. The MAX phase has been extended as boride phases in the conventional structure, and borides formed in a separate space group with a slightly different structure. In order to study new useful MAX phase materials, the research has changed direction in various ways. In relation to our scientific endeavor, it also aids in our better understanding of the history of the C-containing MAX phase.

2.2 Historical Background

2.2.1 History of MAX Phases

The MAX phases are already readily available in a surprising number due to the extensive research on them. While many compounds have been studied theoretically, experimental studies have not been as thorough. The availability of compounds in the 211 phase is found to be significantly higher than in other phases. Use of C and N as X elements was confined for a long time [1, 2, 3], which has been extended recently where B also used as an X element. For the MAX phase materials the extension has opened a new platform, owing to the interesting properties and potential uses of B-containing compounds [4, 5]. Up to date, only few of the MAX phase borides have been synthesized so far in spite of a large number of predicted phases [6].

Rackl *et al.* [7, 8] synthesized the M_2SB ($M = Zr, Hf$ and Nb) phases. Solid-state techniques were used to create the MAX phase boride Nb_2SB and the solid solutions Nb_2SBx_{1-x} ($x = 0 - 1$), which were then examined via x-ray powder diffraction. All the calculations performed by first-principle calculations through the Vienna Ab

initio Simulation Package (VASP) code. First-principles calculations using density functional theory suggest the metallic state and a decrease in the electronic density of states in the boride at the level of Fermi energy. Ali *et al.* [9] were further investigated the M_2SB ($M = \text{Zr, Hf and Nb}$) phases, utilizing first-principle calculations.

Wang *et al.* [10] were successfully synthesized Ti_2InB_2 , which is one of the significant 212 MAX phase borides. At high temperatures, TiB is formed by the dealloying parent Ti_2InB_2 and high vacuum in order to remove the indium layer. They theoretically revealed that the TiB single-layer structure has greater potential as a Li/Na ion battery anode material than usual carbide MXenes like Ti_3C_2 . Pure TiB mono-layers have a significantly better capacity for storing ions (Li or Na) than Ti_3C_2 , a typical MXene, and have minimal energy barrier for Li and Na ion transport. These results also thoroughly further studied by Ali *et al.* [11].

The MAX phase attracted too little interest from the investigators or researchers, prior to the publication of Barsoum and El-Raghy's paper, in which they demonstrated that MAX phases exhibit properties of not only metallic but also ceramic compounds [4, 12]. In 2011 and 2012, a large number of 2D transition metals, both carbides and nitrides, were identified by the researchers [5, 6]. Throughout the midst of those years, a large number of newer MAX phases were synthesized. These are viewed as viable options for storing energy and are also utilized in a variety of modern technologies.

2.3 History of C-containing MAX Phases

A significant number of MAX phase carbides have already been synthesized and characterized, revealing their prospective applications. In parallel to the experimental study, a large number of computational approaches [13, 14] have also already been performed throughout the last decades. Nowotny and his associates researched numerous 211 phases throughout the course of sixty decades, for example, Ti_2AlC , and also two 312 phases, namely Ti_3SiC_2 and Ti_3GeC_2 [1]. Ti_3AlC_2

was identified to be a part of the 312 MAX phases by Schuster, a student of Nowotny's 20 years later [2].

The outcomes of a thorough computational study of the elastic properties of 240 elemental combinations of the M_2AX phase were studied by Cover *et al.* [15]. The results were performed the first-principles calculation through the Vienna Ab *initio* Simulation Package (VASP) code. They identified correlations revealing the role of the A elements and their interaction with the M elements. They identified that the W_2SnC phase shows the lowest C_{44} constant, suggesting that it would perform as efficiently as a dry lubricant in high-temperature.

By comparing the total energy of the various phases to that of the suitable competing phases, Keast *et al.* [16] used density-functional theory through the WIEN2K software package to confirm the stability of the various phases. They computed the total energies of competing phases to check the stability of five different schemes ($Cr_{n+1}-Al-C_n$, $Ti_{n+1}-Al-C_n$, $Ti_{n+1}-Si-N_n$, $Ti_{n+1}-Al-N_n$, and $Ti_{n+1}-Si-C_n$), where n is the positive integer with the value of 1~4). The findings also point to the possibility of producing metastable compounds of Ti_2SiC , Ti_2SiN , and Ti_3AlN_2 .

Aryal *et al.* [17] studied only electronic and elastic properties of 792 MAX phases, utilizing the Vienna Ab *initio* Simulation Package (VASP) code, which is based on density functional theory (DFT). The elastic constants computed for 792 crystals with $M = Sc, Ti, Zr, H, V, Nb, Ta, Cr, Mo$; $A = Al, Ga, In, Tl, Si, Ge, Sn, Pb, P, As, S$ and, $X = C$ or N , and $n = 1-4$ are computed. They additionally identified a number of new MAX phase theoretically unexplored, and thermodynamically stable MAX phases with remarkable mechanical properties. 665 phases were found to be thermodynamically and elastically stable.

The 10314 solid solutions and 216 possible M_2AX phases by computing formation energy were revealed by Ashton *et al.* [18]. To find several thermodynamically stable $M_{n+1}AX_n$ compounds where n belongs to 1, $M = V, Cr, Sc, Ti, Ta, Mo, Hf, Zr, Nb$; $A = P, S, Al, Si, As, Ga, Cd, In, Ge, Tl, Pb, Sn$; and X is C or N, they employed an investigation approach performed by density functional calculation through the Vienna Ab *initio* Simulation Package (VASP) package.

Khaledialidusti *et al.* [19] explored a large group of MAX phases where M is taken as Sc, Ti, Y, Zr, V, Cr, Nb, Hf, Ta, Mo, W; A is taken as P, S, Al, Si, Zn, Cu, Ga, As, Ge, Sn, Cd, In, Bi, Ir, Tl, Au, Pb; and revealed their possibility of exfoliation to produce 2D systems. According to their findings, it is possible to synthesis 466 MAX compounds, of which 136 MAX phases can be exfoliated to yield 26 MXenes. The DFT method was used for the entire calculations and it was performed using the Vienna Ab *initio* Simulation Package (VASP) code.

Nb₂AC (A = Al, Ge, Ga, Sn, In, As, P, S, and Cu) MAX phases were studied by Hadi *et al.* [20] to explore the elastic behavior and radiation tolerant behavior. Density functional theory (DFT), as applied by the CASTEP code, was used to accomplish the calculations. They demonstrated that Nb₂GeC is predicted to have a high elastic modulus while Nb₂InC will have a low anisotropy. It is anticipated that Nb₂GeC would be extremely ductile while Nb₂AlC will be more brittle. Nb₂SnC possess superior thermal shock resistance. Superconducting nature has been found in the Nb₂SnC, Nb₂InC, Nb₂AsC, and Nb₂SC phases [20] with the lowest superconducting temperature for Nb₂AsC [3].

Bouhemadou *et al.* [21, 22] performed first-principles calculations which implemented the Cambridge Serial Total Energy Package (CASTEP) code to study the structural and elastic properties of Nb₂InC and Nb₂GeC, besides electronic properties of Nb₂GeC. Nb₂GeC is an electrical conductor, as seen here by the band structures. The predicted phases C44's shear modulus reaches its maximum when the valence electron concentration is between 8.41 and 8.50, suggesting that the hardness may be attained when the valence electron concentration differs in this range.

Shein *et al.* [23] explored the structural, electrical, and elastic properties of M₂GaC (M = Mo, V, Nb). These properties were investigated using first principle calculations and it was implemented by the WIEN2K software package and Vienna Ab *initio* Simulation Package (VASP) code. They were able to carry out a thorough analysis of the declared properties of their researched materials according to the complementary of these two DFT-based programs. They demonstrated that the

anisotropic distortion of the crystal structure occurs as a result of M replacements in the series of M_2GaC phases. Among the M_2GaC phases that have been studied, Mo_2GaC possesses the largest bulk modulus but the shear modulus is smallest.

2.4 Conclusion and Impacts

In this study, we have chosen to explore Nb_2AC ($A = Ga, Ge, Tl, Zn$) carbides. Moreover, so far, we know only the electronic and mechanical characteristics of Nb_2AC ($A = Ga, Ge$) phases have been investigated, whereas, Nb_2AC ($A = Tl, Zn$) phases have been predicted to be stable via the calculation of formation energy [19], and the physical properties are not disclosed yet. Exploration of the physical properties of new materials carries the same significance as that of prediction of new materials: it is impossible to take any advantage of new materials unless their physical properties are brought out. Several essential physical aspects, mechanical anisotropy, important optical properties, Vickers hardness including Mulliken populations, along with the thermal properties of Nb_2AC ($A = Ga, Ge$) are still unexplored. Mulliken population analysis is important to prove the existence of the combination of the ceramic and metallic nature. Understanding the thermal properties is important to forecast their appropriateness for use in extreme conditions. The optical characteristics of standard MAX phase compounds are necessary to predict their possible applications, for instance, as coating materials to protect from solar heating. These are the motivations behind this study, which demonstrates the significance of in-depth research on MAX phase carbides Nb_2AC ($A = Ga, Ge, Tl, Zn$). Therefore, we aimed to perform a theoretical insight into the MAX phase carbides Nb_2AC ($A = Ga, Ge, Tl, Zn$) in which we will consider the first-time investigation of Nb_2AC ($A = Tl, Zn$) and some important unexplored properties of Nb_2AC ($A = Ga, Ge$) phases. Last of all, the calculated parameters of the titled phases are compared with those of the most known Nb-based phase, Nb_2AC ($A = P, In, Cd, Al$), to make this research a systematic one.

References:

- [1] H. Nowotny, *Struktur chemieeiniger verbindungen der ubergangsmetalemit den elementen C, Si, Ge, Sn*, Prog Solid-State Chem 2 (1970) 27-70.
- [2] J. C. Schuster, H. Nowotny, *Investigations of the ternary systems (Zr, Hf, Nb, Ta)-Al-C and studies on complex carbides*, Zeitsch. Met. 71 (1980) 341.
- [3] M. A. Hadi, *Superconducting phases in a remarkable class of metallic ceramics*, J. Phys. Chem. Solids 138 (2020) 109275.
- [4] M. W. Barsoum, L. Farber, L. Levin, A. Procopio, T. El-Raghy, A. Berner, *High-resolution transmission electron microscopy of Ti_4AlN_3 or $Ti_3Al_2N_2$ revisited*, J. Am. Ceram. Soc. 82 (1999) 2545.
- [5] M. Naguib, M. Kurtoglu, V. Presser, J. Lu, J. Niu, M. Heon, L. Hultman, Y. Gogotsi, M.W Barsoum, *Two-dimensional nano crystals produced by exfoliation of Ti_3AlC_2* , Adv. Matter. 23 (2011) 4248.
- [6] M. Naguib, O. Mashtalir, J. Carle, V. Presser, M. W. Barsoum, *Two-dimensional transition metal carbides*, ACS Nano, 6 (2012) 1322.
- [7] T. Rackl, D. Johrendt, *The MAX phase borides Zr_2SB and Hf_2SB* , Solid State Sci. 106 (2020) 106316.
- [8] T. Rackl, L. Eisenburger, R. Niklaus, D. Joherndt, *Syntheses and physical properties of the MAX phase boride Nb_2SB and the solid solutions $Nb_2SB_xC_{1-x}$ ($x = 0,1$)*, Phys. Rev. Mater. 3 (2019) 054001.
- [9] M. A. Ali, M. M. Hossain, M. M. Uddin, M. A. Hossain, A. K. M. A. Islam, S. H. Naqib, *Physical properties of new MAX phase borides M_2SB ($M = Zr, Hf$ and Nb) in comparison with conventional MAX phase carbides M_2SC ($M = Zr, Hf$ and Nb): Comprehensive insights*, J. Mater. Res. Technol. 11 (2021) 1000.
- [10] J. Wang, T. N. Ye, Y. Gong, J. Wu, N. Miao, T. Tada, H. Hosono, *Discovery of hexagonal ternary phase Ti_2InB_2 and its evolution to layered boride TiB* , Nat. Commun. 10 (2019) 1.
- [11] M. M. Ali, M. A. Hadi, I. Ahmed, A. F. M.Y. Haider, A. K. M. A. Islam, *Physical properties of a novel boron-based ternary compound Ti_2InB_2* , Mater. Today Commun. 25 (2020) 101600.

- [12] M. W. Barsoum, T. El-Raghy, *Synthesis and characterization of a remarkable ceramic: Ti_3SiC_2* , J Am Ceram Soc 79 (1996) 1953-6.
- [13] A. Jain, G. Hautier, C. J. Moore, S. P. Ong, C. C. Fischer, T. Mueller, K. A. Persson, G. Ceder, *A high-throughput infrastructure for density functional theory calculations*, Comput. Mater. Sci., 50 (2011) 2295-2310.
- [14] S. Curtarolo, G. Hart, M. B. Nardelli, N. Mingo, S. Sanvito, O. Levy, *The high-throughput highway to computational materials design*, Nature materials 12 (2013) 191-201.
- [15] M. F. Cover, O. Warschkow, M. M. M. Bilek, D. R. McKenzie, *A comprehensive survey of M_2AX phase elastic properties*, J. Phys. Condens. Matter 21 (2009) 305403.
- [16] V. J. Keast, S. Harris, D. K. Smith, *Prediction of the stability of the $Mn_{n+1}AX_n$ phases from first principles*, Phys. Rev. B, 80 (2009) 214113.
- [17] S. Aryal, R. Sakidja, M. W. Barsoum, W. Y. Ching, *A genomic approach to the stability, elastic, and electronic properties of the MAX phases*, physica status solidi (b), 251 (2014) 1480-1497.
- [18] M. Ashton, R. G. Hennig, S. R. Broderick, K. Rajan, S. B. Sinnott, *Computational discovery of stable M_2AX phases*, Phys. Rev. B, 94 (2016) 054116.
- [19] R. Khaledialidusti, M. Khazaei, S. Khazaei, K. Ohno, *High-throughput computational discovery of ternary-layered MAX phases and prediction of their exfoliation for formation of 2D MXenes*, Nanoscale 13 (2021) 7294-7307.
- [20] M. A. Hadi, S. R. G. Christopoulos, A. Chroneos, S. H. Naqib, A. K. M. A. Islam, *Elastic behaviour and radiation tolerance in Nb-based 211 MAX phases*, Mater. Today Communi. 25 (2020) 101499.
- [21] A. Bouhemadou, *Calculated structural and elastic properties of M_2InC ($M = Sc, Ti, V, Zr, Nb, Hf, Ta$)*, Mod. Phys. Let. B 22 (2008) 2063-2076.
- [22] A. Bouhemadou, *Calculated structural, electronic and elastic properties of M_2GeC ($M = Ti, V, Cr, Zr, Nb, Mo, Hf, Ta$ and W)*, Appl. Phys. A 96 (2009) 959-967.

[23] I. R. Shein, A. L. Ivanovskii, *Structural, elastic, electronic properties and Fermi surface for superconducting Mo₂GaC in comparison with V₂GaC and Nb₂GaC from first principles*, Physica C 470 (2010) 533-537.

CHAPTER-3

MATERIALS AND METHODOLOGY

To analyze materials, a variety of computational techniques are available. First-principles calculations are an essential tool that is particularly beneficial for phenomena determined by the atomic-scale characteristics of materials and materials in the solid state. Since no experimental parameters are employed as in numerical method, these computations are called "first-principles" or "*ab initio*" calculations, considering they are based on quantum mechanics' first principles. While it is almost impossible to unambiguously solve the key equations of quantum mechanics for many-body systems, assumptions, as well as reformulations, can be applied to get an output that converges to the Schrödinger equation's solution. Density functional theory is a significant first-principles approach to quantum mechanical simulation using electron density as a function. For the purpose of calculating the physical properties of Nb₂AC (A = Ga, Ge, Tl, and Zn), density functional theory has been developed using the CASTEP [1, 2] code. This chapter focuses on a brief overview of the tool and methodology utilized in this investigation.

3.1 CASTEP Code

The CASTEP (Cambridge Serial Total Energy Package) code for quantum-mechanics had been developed via first-principles theory, including density functional theory (DFT). Scientists at York's Universities, Durham, Cambridge, St. Andrews, and Rutherford Labs, have completely built the CASTEP code used in parallel calculations [2]. This tool can compute the properties of solids, such as the structural, thermal, optical, mechanical, and electrical properties. In addition, it is also employed to investigate a system's wave function as well as charge density mapping. This code can also be used to investigate the reactions of chemicals in bulk, surface diffusion procedures, etc. Much detail about CASTEP is available elsewhere [1, 2]. CASTEP uses the plane-wave pseudopotential relying on the DFT

approach. Computations become significantly more simplified by replacing the total potential, which considers both the system's core and valence electrons, with the more fundamentally beneficial possible term. A plane-wave basis set is used to accomplish the process of extending electron wave functions. Generalized gradient approximations (GGA) or the local density approximation (LDA) are used to compute electrons' exchange and correlation terms. The geometric optimizations of systems such as solids, surfaces, molecules, and interfaces are more effective when the above parameters are used. It is possible to determine the additional physical properties from the simulation results using the formalisms described in the next chapter.

3.2 Many-body Problems in Quantum Mechanics

A many-body system, initially at the atomic level, can be described using its electronic structure and its atomic configuration without the necessity to enter any exploratory variables. Here, we review key quantum mechanical concepts to establish the basis for the equations that must be resolved to explain materials.

3.2.1 Schrödinger Equation

For first-principles computations, the wave equation, which is Schrödinger's time-independent [3], is regarded as the fundamental equation whose solution can be utilized to predict the properties of materials. The following formula typically represents the time-independent equation:

$$H\Psi = E\Psi \quad (3.1)$$

Where H , Ψ , and E denote the Hamiltonian operator, many electrons wave function, and energy of the system, respectively. A system's Hamiltonian operator can be defined as follows if it has a finite number of electrons N_e , and nuclei N_n :

$$\begin{aligned}
H = & -\frac{1}{2} \sum_{i=1}^{N_e} \nabla_i^2 - \sum_{k=1}^{N_n} \frac{1}{2M_k} \nabla_k^2 - \sum_{i \neq k}^{N_e N_n} \frac{Z_k}{|r_i - r_k|} + \sum_{i \neq j}^{N_e N_e} \frac{1}{|r_i - r_j|} \\
& + \sum_{k \neq l}^{N_n N_n} \frac{Z_k Z_l}{|R_k - R_l|}
\end{aligned} \tag{3.2}$$

In the aforementioned equation, the first and second terms stand in for the kinetic energy of electrons and nuclei. The equation's third term gives the Coulomb's attraction between nuclei and electrons. Additionally, the fourth and fifth terms, respectively, indicate the Coulomb repulsion between electrons-electrons as well as between nuclei-nuclei.

3.2.2 Born-Oppenheimer Approximation

We can distinguish between the electronic or nuclear degrees of motion using the Born-Oppenheimer approximation [4]. Due to their mass, which is $\sim 10^3$ times more than that of electrons, nuclei can be regarded as static objects on that electronic timescale. Because of this, the contribution of nuclear kinetic energy to the system's overall energy can be disregarded. Therefore, in Eq. 3.2, the second term can be changed to zero. Due to the ability to distinguish between the movement of electrons and nuclei, different wave functions can solve the difficulties associated with nuclear and electronic components. The nuclei's Coulomb interaction is constant when the nuclei are considered motionless. As a result, while resolving the Schrödinger equation, the last part can be skipped and afterward added as a fixed value to its total energy. The Born-Oppenheimer approach makes a distinction between nuclear and electronic problems. Now that the Hamiltonian has been simplified in Eq. 3.2 by using the Born-Oppenheimer approximation, it can be written as:

$$H = -\sum_{i=1}^{N_e} \nabla_i^2 - \sum_{i \neq k}^{N_e N_n} \frac{Z_k}{|r_i - R_k|} + \sum_{i \neq j}^{N_e N_e} \frac{1}{|r_i - r_j|} + \sum_{k \neq l}^{N_n N_n} \frac{Z_k Z_l}{|R_k - R_l|} \tag{3.3}$$

3.3 Density Functional Theory

One of the established *ab initio* methodologies used as a substitute for the concept of electronic configuration computations is called density functional theory (DFT). The key component of this approach is the spatially varying electronic density rather than many-body wave functions. Before the development of the Hohenberg-Kohn theorems (H-K) [5], in 1927, Thomas and Fermi's DFT approach for quantum systems was deemed insufficiently correct and not a comprehensive theory. Kohn-Sham formalism added to the original theory's provisions. Functionality describes how atomic location affects electron density. Calculating the many-body system's physical characteristics via function is achievable. The scientific world has recently seen extensive usage of the DFT approach, especially during the 1990s, when effective applications of this technology have increased significantly. As a result of the details mentioned, the technique develops into the most successful and promising method for calculating the electronic structure of mechanisms. Using this method, it can calculate a wide range of physical characteristics, such as molecular structures, strengths, magnetic properties, etc. Density functional theory frequently termed the "theory of the moment," is now the condensed matter physics approach that is most widely accepted.

3.3.1 Hohenberg-Kohn Theorems

Density functional theory is greatly influenced by the theorems of Hohenberg-Kohn in order to perform many-body problems. With the use of these theorems, an additional system that is appropriate to solve can be used to replace the interrelated many-body system.

Theorem 1: The ground-state element density $n_0(r)$ to interact with particles, except a constant, can be used to determine a many-body system's external potential $V_{ext}(r)$. As a result, without considering the constant shifting of energies, the whole Hamiltonian could be ascertained by the ground state particle density. Following the principle, all of the many-body wave functions' states, including their ground

state as well as excited state, can be calculated. As a result, ground state density could be utilized for calculating a system's properties.

Theorem 2: The universal functional is influenced by external potentials; for example, the natural ground state energy of a system, which is limited by its ground state density $n_0(r)$, is the worldwide lowest value of something like the energy functional. The functional can, therefore, precisely calculate the energy or density of only the ground state.

3.3.2 Solution of Kohn-Sham Equation

According to the KS [6] equations, the independent-particle technique is used to determine the precise ground state density and energy. A reliable resolution for only the KS formula is necessary because of the connection between the efficient KS potential V_{KS} and the electron density $n(r)$. Fig. 3.3.2 illustrates the typical numerical method using self-consistent repetitions.

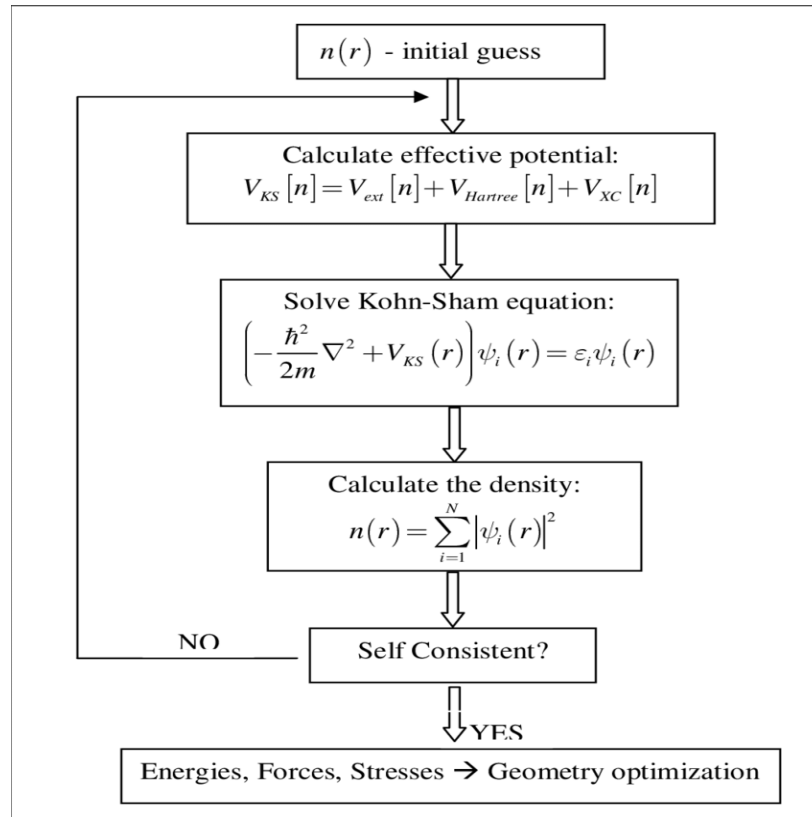


Fig. 3.3.2: Self-Consistent Kohn-Sham equation solution flow chart [7].

The procedure starts with a superposition with atomic electron densities, after which the efficient KS potential is calculated, and also the KS equation is solved using the Eigenvalues of single-particle and wave functions. A current electron density is computed using the wave function. Next, check the self-consistent requirement because this could have changed from the initial state depending on the total energy, electron density, applying force onto atoms, or a mix of these conditions. Whether the target of self-consistency cannot be achieved, the combined computed and formerly iterated electron densities are used to create a new electron density. When self-consistency is accomplished, a new iteration of the new electron density will begin. After getting the required self-consistency, the potential energy, stress, electron density of state, band structure, Eigenvalues, etc., are determined.

3.4 Pseudopotential

An approximate way to describe the complex system is with pseudo potential [8]. The Schrödinger equation substitutes this effective potential for the Coulomb potential. Hans Hellmann first proposed the concept of pseudopotential in the 1930s. In addition, because of this pseudopotential, the valence wave function is orthogonal for all core states.

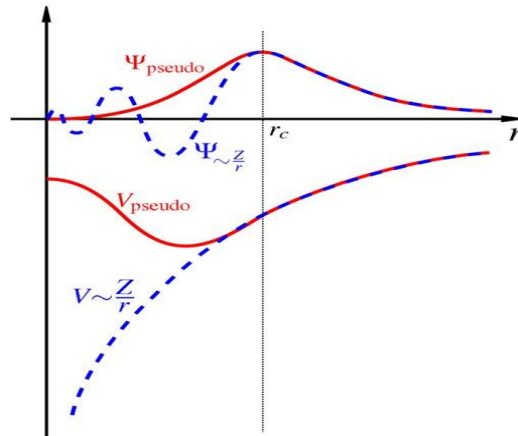


Fig. 3.4: All electrons (blue lines), pseudo-potentials (red lines), and the analogous wave functions are revealed schematically. The pseudopotentials and electron alignment are r_c [9].

The above effective potential takes the place of atomic electrons, and the pseudo wave function realizes defining valence electrons. The core electrons are left frozen mostly with nuclei in this method, which mainly deals with chemical valence electrons. Pseudopotential, as well as valence electron eigenstates, provide similar amplitude and energy outside of a chosen core cut-off radius, r_c . Pseudo-potentials are considered to be softer and to converge quickly because of their small cutoff radii. Pseudo-potential has two different varieties. Which are:

- a) Norm-conserving pseudopotential
- b) Ultra-soft pseudopotential

3.4.1 Norm-conserving Pseudopotential

Accurate computations of solid-state attributes are now possible because of Kleinman and Bylander's [10] advancement of the first-principles calculations of norm-conserving pseudopotential. The theoretical formulation of Kleinman-Bylander pseudopotentials is:

$$V_{KB} = V_{loc} + \sum \frac{|\psi_{lm} \delta V_l \rangle \langle \delta V_l \psi_{lm}|}{\langle \psi_{lm} | \delta V_l | \psi_{lm} \rangle} \quad (3.4)$$

Here, V_{loc} = arbitrary local potential, ψ_{lm} = pseudo-atom wave functions, and δV_l is explained by

$$\delta V_l = V_{l,non-local} - V_{local} \quad (3.5)$$

Therein $V_{l,non-local}$ is a non-local pseudopotentials l angular momentum element.

3.4.2 Ultra-soft Pseudopotential

By reducing the norm-conservation requirement, Vanderbilt [11] suggested a novel and radical technique for producing significantly smoother pseudopotentials in 1990. The pseudo-wave functions in the core region are permitted to be as smooth as is probable in this technique, significantly lowering the cutoff energy. On account of this, they are frequently referred to as ultrasoft pseudopotentials (USP). The introduction of a generalized orthonormality criterion technically accomplishes this. Recovering the entire electronic charge, electron density provided by the wave

function squared moduli must be increased inside this core region. As a result, the electron density is split into two parts: (1) a smooth portion that expands the entire unit cell and (2) a rigid portion that is confined in the core areas. Only the density contains the enhanced portion; the wave functions do not, dissimilar from techniques like LAPW, which analogously uses wave functions. In addition to being far smoother than norm-conserving potential (NCP), ultrasoft potentials also possess another benefit. The USP-generating algorithm guarantees good scattering qualities across a predetermined energy region, leading to stronger pseudopotential transferability and validity. The USP often includes multiple groups of active regions in every angular momentum channel and recognizes "shallow" core regions as valence. However, this also increases the potential's high precision and transferability at the cost of computational accuracy. Vanderbilt established an ultrasoft pseudopotential that is expressed as

$$V_{USP} = V_{loc}(r) + \sum_{l,m} D_{lm} |\beta_l\rangle\langle\beta_m| \quad (3.6)$$

With an ultrasoft pseudopotential, charge density is defined as

$$\rho(r) = \sum_{n,k} \phi_{nk}^*(r) \phi_{nk}(r) + \sum_{lm} P_{lm} Q_{lm}(r) \quad (3.7)$$

Where

$$D_{lm} = B_{lm} + \varepsilon_m Q_{lm} \quad (3.8)$$

$$P_{lm} = \sum_{n,k} \langle\beta_l|\phi_{nk}\rangle\langle\phi_{nk}|\beta_m\rangle \quad (3.9)$$

$$Q_{lm}(r) = \psi_l^*(r)\psi_m(r) - \phi_l^*(r)\phi_m(r) \quad (3.10)$$

First-row or transition metal systems may benefit from using Vanderbilt ultrasoft pseudopotentials, which have a detachable form suitable for solid-state computations involving plane waves.

3.5 Generalized Gradient Approximation (GGA)

The XC energy cannot be precisely estimated because of the LDA molecules' fixed electron density. To address this issue, GGA uses the electron density gradient. The enormous value of gradients in actual situations caused this approximation to

degrade and perform poorly in a specific situation considerably. Later, it was found that such enlargement was not required. In mathematics, it may be expressed as

$$E_{xc} = Exc[\rho(r), \nabla\rho(r)] \quad (3.11)$$

E_{xc} is the XC energy, and $\rho(r)$ is the electronic density in space. The effectiveness in LDA performance is significantly increased with the introduction of GGA. This method yields more accurate calculations of the material's structural and magnetic properties. During calculation, GGA considers an additional parameter in the space, although LDA only considers one. Perdew-Burke-Ernzerhof [12] type created the terminology GGA-PBE and Perdew-Burke-Ernzerhof for solids [13] type created the terminology GGA-PBEsol, which is used to investigate attributes more thoroughly. The PBE has been widely used for DFT calculations and MAX phases, whereas the PBEsol gives solids a more accurate lattice constant [14].

3.6 k-Point Sampling

The previously indicated finite set of k points samples the reciprocal space. In periodic solids, an infinite number of electrons can be accounted for by an infinite number of k-points. Monkhorst and Pack [15] established one of the most popular approaches for producing k-points. This pattern was gradually expanded to involve hexagonal systems and has a grid of k-points, including three axes of reciprocal space [16]. In this approach, the three variables q_1 , q_2 , and q_3 specify how many divisions will occur along each axis. The below series of numbers is produced by these integers' general form, q_i :

$$\Psi_{j,k}(r) = \sum_G c_{j,K+G} e^{i(k+G).r} \quad (3.12)$$

Within the range of 1 to q_i , the r 's value varies.

3.7 Theory of the Calculated Properties

The chapter explains how to compute the various Nb₂AC (A= Ga, Ge, Tl, Zn) MAX phase properties. The lattice parameters, unit cell volume, elastic constants, and bulk modulus are explored extensively in multiple theories. The Vickers hardness,

the total density of states, the partial density of states, and the electronic band structure were calculated understanding the bonding characteristics of the materials. Optical and thermodynamic properties are also studied to learn more about the nature of these materials.

3.7.1 Structure Relaxation

Cell parameter relaxation is required to achieve good stability. By ascertaining the structure's considerably lower energy, CASTEP carries out the structural relaxing procedure. The term "ground state energy" refers to this energy. The energy optimization process involves placing the atoms in patterns where the total inter-atomic force can be assumed to be nil (zero). The Schrödinger equation is used by CASTEP as part of the variational principle methodology. This model for identifying the lowest energy state is based on quantum mechanics. For instance, a process that iterates by assuming a first geometry would be complete whether the force exerted per each atom was less than a predetermined threshold or if the process was repeated to change the position vector for optimization.

3.7.2 Structural Parameters

The internal parameter of the hexagonal structure is Z_M , and the lattice parameters are a and c . The hexagonal ratio is often referred to as the c/a ratio. Equations are used to calculate the distortion parameter of octahedra [17] and the trigonal prism for the hexagonal scheme.

$$O_r = \frac{\sqrt{3}}{2\sqrt{4Z_M^2\left(\frac{c}{a}\right)^2 + \frac{1}{12}}} \quad (3.13)$$

O_r be the octahedral distortion parameter.

$$P_r = \frac{1}{\sqrt{(0.25 - Z_M^2)^2\left(\frac{c}{a}\right)^2 + \frac{1}{3}}} \quad (3.14)$$

P_r is the trigonal prism's distortion parameter.

3.7.3 Elastic Properties

The material's behavior is investigated by exerting stress, which is also directly relevant to the elastic constants. There are 27 varied materials along with 6×6 symmetrical matrices that can be combined to form the linear elastic constants, where σ and ε define stresses and strains using the equation $\sigma_{ij} = C_{ij}\varepsilon_j$ [18]. CASTEP has been equipped with a limited strain approach to investigate the elastic nature of materials. By employing the elastic constants C_{ij} , the Voigt [19] or Reuss [20] assumption is frequently employed to study the behavior of polycrystalline materials. Voigt presents the formula below, assuming a homogenous strain:

$$B_V = \frac{1}{9}[2(C_{11} + C_{12} + 4C_{13} + C_{33})] \quad (3.15)$$

$$G_V = \frac{1}{30}(C_{11} + C_{12} + 2C_{33} - 4C_{13} + 12C_{44} + 12C_{66}) \quad (3.16)$$

The Reuss approximation allows for the following expression of the bulk (B_R) and shear (G_R) moduli of stress:

$$B_R = \frac{(C_{11} + C_{12})C_{33} - 2C_{13}^2}{C_{11} + C_{12} + 2C_{33} - 4C_{13}} \quad (3.17)$$

$$G_R = \frac{5C_{44}C_{66}[(C_{11} + C_{12})C_{33} - 2C_{13}^2]}{2[3B_V C_{44}C_{66} + \{(C_{11} + C_{12})C_{33} - 2C_{13}^2\}(C_{44} + C_{66})]} \quad (3.18)$$

According to Hill [21], the Voigt and the Reuss values are both the upper and lower values for solids, and the bulk modulus (B) and shear modulus (G) performed the arithmetic means of these values. Consequently,

$$B = \frac{1}{2}(B_R + B_V); G = \frac{1}{2}(G_R + G_V) \quad (3.19)$$

Poisson's ratio (σ) and Young's modulus (Y) have been calculated by using the following relationships [22]:

$$Y = \frac{9BG}{3B + G}; \nu = \frac{3B - 2G}{2(3B + G)} \quad (3.20)$$

The ability of a substance to resist deformation under an applied force is known as hardness [23]. Dislocations [24] that significantly affect hardness are produced and

moved due to plastic deformation. In some cases, these parameters are used to predict the hardness of solids using the following formulae [25, 26]:

$$H_{Chen} = 2 \left[\left(\frac{G}{B} \right)^2 G \right]^{0.585} - 3 \quad (3.21)$$

$$\text{and } H_{miao} = \frac{(1-2\nu)E}{6(1+\nu)} \quad (3.22)$$

Non-metallic compound's hardness can be determined using the F. M. Gao formulation [27]. Based on Gou et al. [28], the formula, can also be used to determine the hardness of combined metal crystals for bonding with metals.

$$H_v^\mu = 740(P^\mu - P^{\mu'}) (v_b^\mu)^{-5/3} \quad (3.23)$$

Here, P^μ indicates μ type bond's Mulliken overlap population, $P^{\mu'}$ indicates metallic properties, and the volume of the μ -type bond is denoted by v_b^μ . Again,

$$P^{\mu'} = n_{free}/V; \quad (3.24)$$

where

$$n_{free} = \int_{E_F}^{E_p} N(E) dE \quad (3.25)$$

E_p indicates the energy of the pseudogap, and E_F indicates the energy of the Fermi level.

v_b^μ is calculated in the following way:

$$v_b^\mu = (d^\mu)^3 / \sum_v [(d^\mu)^3 N_b^v] \quad (3.26)$$

At last, the equation for Vickers hardness is as follows:

$$H_v = [\pi (H_v^\mu) n^\mu]^{1/3} \Sigma^{n^\mu}; \quad (3.27)$$

n^μ = μ -type bonds number.

3.7.4 Anisotropy Indices

Additional significant anisotropic indices have also been calculated. Using the following relationships, the three shear anisotropic factors [29], for instance, A_i ($i = 1, 2, 3$), are computed:

$$A_1 = \frac{1/6 (C_{11} + C_{12} + 2C_{33} - 4C_{13})}{C_{44}} \quad (3.28)$$

Shear anisotropy factors to the {100} plane are indicated in A_1 .

$$A_2 = \frac{2C_{44}}{C_{11} - C_{12}} \quad (3.29)$$

A_2 indicates for the {010} plane.

$$A_3 = A_1 \cdot A_2 = \frac{1/3 (C_{11} + C_{12} + 2C_{33} - 4C_{13})}{C_{11} - C_{12}} \quad (3.30)$$

A_2 refers to the {001} plane.

The elastic anisotropy for the bulk modulus (B_a, B_c) across both the a axis and c -axis are computed through the following relationships [30]:

$$B_a = a \frac{dp}{da} = \frac{A}{2+\alpha} \quad (3.31)$$

$$B_c = c \frac{dp}{dc} = \frac{B_a}{\alpha} \quad (3.32)$$

Where $A = 2(C_{11} + C_{12}) + 4C_{13}\alpha + C_{33}\alpha^2$; $\alpha = \frac{(C_{11}+C_{12})-2C_{13}}{C_{33}+C_{13}}$.

Additionally, using the following relation [31]:

$$\frac{k_c}{k_a} = C_{11} + C_{12} - 2C_{13}/(C_{33}-C_{13}) \quad (3.33)$$

The elastic anisotropy for the linear compressibility coefficients (k_c/k_a) ratio in the a along with c -directions, is computed.

The compressibility and shear modulus's percentage anisotropies were computed as follows [32]:

$$A_B = \frac{B_V - B_R}{B_V + B_R} \times 100\% \quad (3.34)$$

$$A_G = \frac{G_V - G_R}{G_V + G_R} \times 100\% \quad (3.35)$$

A_B and A_G correspond to the bulk and shear moduli percentage anisotropy factors, respectively.

We have calculated the universal anisotropy index A^U based on the Voigt, V (upper limit) and Reuss, R (lower limit) models using the following relation [33]:

$$A^U = 5 \frac{G_V}{G_R} + \frac{B_V}{B_R} - 6 \geq 0 \quad (3.36)$$

The elastic stiffness matrix was used to calculate bulk modulus (B), Young's modulus (Y), shear modulus (G), and Poisson ratio (σ) in 2D and 3D plots.

3.7.5 Electronic Band Structure

The enclosed pack of the energy levels in the condensed process forms energy bands or permitted bands. Bands could overlap in atomic orbitals, and if the energy range inside the bands is not fully utilized, a band gap can be discovered. The periodic system's electronic band structure is produced by diffracted electron waves, which are seen from the perspective of quantum mechanics. These (band and band gaps) are discovered via band theory by computing fundamental quantum mechanical wave functions for a particular molecule. The Bloch wave equation to the equation of Schrödinger for a single electron is,

$$\psi_{nk}(r) = e^{ikr} u_{nk}(r) \quad (3.37)$$

where the terms "wave vector" and "band index" separately refer to k and n . Every band in a molecule's $E_n(k)$ function specifies the dispersion connection for electrons inside that band. The 211 MAX phases are hexagonal, and Γ , H, K, Γ , M, and L are allocated for special high symmetry directions in the Brillouin zone.

3.7.6 Density of States

The QM model can estimate the density of states (DOS) for electrons, phonons, or photons. The DOS determines the amount of the condition at each energy gap at each energy level while the states are connected to electrons. Numerous states can obtain employment if the DOS is highly valued. Consequently, the DOS value zero has no occupied space that can be located. Mathematically, the density of states (DOS) can be expressed as,

$$N_n(E) = \int \frac{dk}{4\pi^3} \delta(E - E_n(k)) \quad (3.38)$$

Where the integral throughout the Brillouin Zone is calculated as well as $E_n(k)$ denotes the band dispersion. By adding together all the bands, the total density of states (DOS) has been determined,

$$N(E) = \int N_n(E) = \sum \int \frac{dk}{4\pi^3} \delta(E - E_n(k)) \quad (3.39)$$

In most cases, DOS is used for a quick visual assessment of the electronic structure. Understanding the valence bandwidth, the insulator's internal energy gap, and how changes in external pressure affect the electrical structure are all made easier with the assistance of DOS.

3.7.7 Optical Properties

It is essential to use the following equation to estimate all of the optical properties,

$$\varepsilon(\omega) = \varepsilon_1(\omega) + i\varepsilon_2(\omega). \quad (3.40)$$

Depending on the occupied and unoccupied electronic states of each the momentum matrices element, it is possible to state that $\varepsilon_2(\omega)$ is the imaginary portion of the related dielectric function and fully calculated by CASTEP using the formula below:

$$\varepsilon_2(\omega) = \frac{2e^2\pi}{\Omega\varepsilon_0} \sum_{k,v,c} |\psi_k^c| u \cdot r |\psi_k^v|^2 \delta(E_k^c - E_k^v - E) \quad (3.41)$$

Where the vector u designates how the incident electric field is polarized, ω represents the frequency of light, e stands for the electronic charge, ψ_k^c represents the conduction band wave function and ψ_k^v indicates that the valence band wave function. Applying the Kramers-Kronig transform, the imaginary part $\varepsilon_2(\omega)$ is used in order to obtain the real part (ε_1). The extinction coefficient (k), refractive index (n), absorption coefficient (α), photoconductivity (σ), reflectivity (R) and loss function (LF) are the other optical constants, and they are all provided by the following Equations [34-36]:

$$n(\omega) = \frac{1}{\sqrt{2}} \left[\sqrt{\{\varepsilon_1(\omega)\}^2 + \{\varepsilon_2(\omega)\}^2} + \varepsilon_1(\omega) \right]^{\frac{1}{2}} \quad (3.42)$$

$$k(\omega) = \frac{1}{\sqrt{2}} \left[\sqrt{\{\varepsilon_1(\omega)\}^2 + \{\varepsilon_2(\omega)\}^2} - \varepsilon_1(\omega) \right]^{\frac{1}{2}} \quad (3.43)$$

$$R(\omega) = \frac{(n-1)^2 + k^2}{(n+1)^2 + k^2} \quad (3.44)$$

$$\alpha(\omega) = \frac{2k\omega}{c} \quad (3.45)$$

$$L(\omega) = \text{Im} \left(\frac{-1}{\varepsilon(\omega)} \right) = \varepsilon_2(\omega) / [\{\varepsilon_1(\omega)\}^2 + \{\varepsilon_2(\omega)\}^2] \quad (3.46)$$

$$\sigma(\omega) = \sigma_1(\omega) + i\sigma_2(\omega) = -i \frac{\omega}{4\pi} [\varepsilon(\omega) - 1] \quad (3.47)$$

3.7.8 Thermal Properties

One of the most essential solids-specific parameters is the Debye temperature (Θ_D), is closely related to the material's bonding strength, melting temperature, thermal expansion, thermal conductivity, etc. The Θ_D of studied phases has been calculated using sound velocity following Anderson's method [37]. The relevant formulae are as follows:

$$\theta_D = h/k_B \left[\frac{(3n/4\pi)N_A\rho}{M} \right]^{1/3} v_m \quad (3.48)$$

where M = molar mass; n = the number of atoms in each molecule; ρ = mass density; h = Plank's constant; k_B = Boltzmann constant; N_A = Avogadro's number, and v_m = average sound velocity. In an isotropic material, the v_m can be computed from the longitudinal (v_l) and transverse (v_t) sound velocities using the given relationship:

$$v_m = [1/3 (1/v_l^3 + 2/v_t^3)]^{-1/3} \quad (3.49)$$

the v_l and v_t can be obtained from their relationships with the polycrystalline bulk modulus (B) and shear modulus (G):

$$v_l = [(3B + 4G)/3\rho]^{1/2} \quad (3.50)$$

$$v_t = [G/\rho]^{1/2} \quad (3.51)$$

Using the following equation [38], the K_{min} was calculated,

$$K_{min} = k_B v_m \left(\frac{M}{n\rho N_A} \right)^{-2/3} \quad (3.52)$$

where k_B = Boltzmann constant, v_m = average phonon velocity, N_A = Avogadro's number, and ρ = crystal's density, respectively.

An essential thermal parameter that helps to explain the anharmonic effects of lattice dynamics is the Grüneisen parameter (γ); lower anharmonic effects are expected for the solids used at high temperatures. To use the following equation [39] between γ and σ , the Grüneisen parameter (γ) is computed by using the Poisson's ratio:

$$\gamma = \frac{3}{2} \frac{(1 + \nu)}{(2 - 3\nu)} \quad (3.53)$$

The following equation [40] was used to get the melting temperature (T_m),

$$T_m = 354 + 1.5(2C_{11} + C_{33}) \quad (3.54)$$

References:

- [1] M. D. Segall, P. J. D. Lindan, M. J. Probert, C. J. Pickard, P. J. Hasnip, S. J. Clark, M. C. Payne, *First-principles simulation: ideas, illustrations and the CASTEP code*, J. Phys. Condens. Matter. 14 (2002) 2717.
- [2] S. J. Clark, M. D. Segall, C. J. Pickard, P. J. Hasnip, M. I. J. Probert, K. Refson, M. Payne, *First principles methods using CASTEP*, Zeitschrift Für Krist. Cryst. Mater. 220 (2005) 567.
- [3] E. Schrödinger, *Quantization as an eigenvalue problem*, Annalen der Physik. 79 (1926) 489.
- [4] M. Born, R. Oppenheimer, *The quantum theory of molecules*, Annalen der Physik. 84 (1927) 457.
- [5] P. Hohenberg, W. Kohn, *Inhomogeneous electron gas*, Phys. Rev. 136 (1964) 864.
- [6] W. Kohn, L. J. Sham, *Self-consistent equations including exchange and correlation effects*, Phys. Rev. 140 (1965) 1133.
- [7] A. I. Ciucivara, *Density functional studies of magnetic semiconductors and multiferroics*, (2007)
- [8] M. L. Cohen, V. Heine, *The fitting of pseudopotentials to experimental data and their subsequent application*, Solid Stat. Phys. 24 (1970) 37.
- [9] M. A. Hadi, *First-principles study of superconducting MAX phase*, (2015).
- [10] L. Kleinman, D. M. Bylander, *Efficacious Form for Model Pseudopotentials*, Phys. Rev. Lett. 48, 1425 (1982).
- [11] D. Vanderbilt, *Soft self-consistent pseudopotentials in a generalized eigenvalue formalism*, Phys. Rev. B, 41 (1990) 7892.
- [12] J. P. Perdew, K. Burke, M. Ernzerhof, *Generalized gradient approximation made simple*, Phys. Rev. Lett. 77 (1996) 3865.
- [13] J. P. Perdew, A. Ruzsinszky, G. I. Csonka, O. A. Vydrov, G. E. Scuseria, L. A. Constantin, Xiaolan Zhou, Kieron Burke, *Restoring the density-gradient expansion for exchange in solids and surfaces*, Phys. Rev. Lett. 100 (2008) 136406.
- [14] O. Beckstein, J. E. Klepeis, G. L. W. Hart, O. Pankratov, *First-principles elastic constants and electronic structure of α -Pt₂Si and PtSi*, Phys. Rev. B 63 (2001) 134112.

- [15] H. J. Monkhorst, J. D. Pack, *Special points for Brillouin-zone integrations*, Phys. Rev. B 13 (1976) 5188.
- [16] J. C. Phillips, L. Kleinman, *New method for calculating wave functions in crystals and molecules*, Phys. Rev. 116 (1959) 287.
- [17] M. B. Kanoun, S. Gourmi-said, M. Jaouen, *Steric effect on the M site of nanolaminate compounds M_2SnC ($M = Ti, Zr, Hf, \text{ and } Nb$)*, Phys. Condens. Matter 21 (2009) 045404.
- [18] N. W. Ashcroft, N. D. Mermin, *Electron dynamics in solids*, Saunders College: Philadelphia (1976).
- [19] W. Voigt, *Lehrbuch der kristallphysik*, Taubner, Leipzig, 1928.
- [20] A. Reuss, *Berechnung der fließgrenze von mischkristallen auf grund der plastizitäts bedingung für einkristalle*, Z. Angew. Math. Mech. 9 (1929) 49.
- [21] R. Hill, *The elastic behaviour of a crystalline aggregate*, Proc. Phys. Soc. A 65 (1952) 349.
- [22] E. Schreiber, O. L. Anderson, N. Soga, *Elastic constants and their measurements*, Mc Graw-Hill, New York, 1973.
- [23] Tse JS, *Intrinsic hardness of crystalline solids*, J. Superhard Materials, 32 (2010) 177.
- [24] J. Haines, J. M. Leger, G. Bocquillon, *Synthesis and Design of Superhard Materials*, Annu. Rev. Mater. Res. 31 (2001) 1.
- [25] X. Q. Chen, H. Niu, D. Li, Y. Li, *Modeling hardness of polycrystalline materials and bulk metallic glasses*, Intermetallics. 19 (2011) 1275–1281.
- [26] N. Miao, B. Sa, J. Zhou, Z. Sun, *Theoretical investigation on the transition-metal borides with Ta_3B_4 -type structure: A class of hard and refractory materials*, Comput. Mater. Sci. 50 (2011) 1559-1566.
- [27] F. M. Gao, *Theoretical model of intrinsic hardness*, Phys. Rev. B 73 (2006) 132104.
- [28] Y. H. Gou, L. Hou, J. W. Zhang, F.M. Gao, *First-principles study of structural, elastic, and electronic properties of chromium carbides*, Appl. Phys. Lett. 92 (2008) 0441909.
- [29] H. M. Ledbetter, *Elastic properties of zinc: a compilation and a review*, J. Phys. Chem. Ref. Data 6 (1977) 1181–1203.

- [30] A. K. M. A. Islam, A.S. Sikder, F. N. Islam, *NbB₂: a density functional study*, Phys. Lett. A 350 (2006) 288–292.
- [31] J. Wang, Y. Zhou, T. Liao, Z. Lin, *First-principles prediction of low shear-strain resistance of Al₃BC₃: a metal borocarbide containing short linear BC₂ units*, Appl. Phys. Lett. 89 (2006) 021917.
- [32] D. H. Chung, W.R. Buessem, In: F. W. Vahldiek, S. A. Mersol, editors. *Anisotropy in single crystal refractory compound*, Vol-2. New York: Plenum Press; 1968. P.
- [33] S. I. Ranganathan, M. Ostoja-Starzewski, *Universal elastic anisotropy index*, Phys. Rev. Lett. 101 (2008) 055504.
- [34] M. F. Li, *Physics of Semiconductor*, Science Press, Beijing, 1991.
- [35] R. C. Fang, *Solid Spectroscopy*, Chinese Science Technology University Press, Hefei, 2003.
- [36] Y. Zhang, W. M. Shen, *Basic of Solid Electronics*, Zhe Jiang University Press, Hangzhou, 2005.
- [37] O. L. Anderson, *A simplified method for calculating in the Debye temperature from elastic constants*, J. Phys. Chem. Solids 24 (1963) 909-917.
- [38] G. A. Slack, *The thermal conductivity of nonmetallic crystals*, Solid Stat. Phys. 34 (1979) 1–71.
- [39] V. N. Belomestnykh, E. P. Tesleva, *Interrelation between anharmonicity and lateral strain in quasi-isotropic polycrystalline solids*, Tech. Phys. 49 (2004) 1098–1100.
- [40] M. E. Fine, L. D. Brown, H. L. Marcus, *Elastic constants versus melting temperature in metals*, Scr. Metall. 18 (1984) 951–956.

CHAPTER-4

RESULTS AND DISCUSSION

4.1 Structural Properties and Phase Stability

4.1.1 Structural Properties

As shown in Fig. 4.1.1, the unit cell of Nb_2AC ($\text{A} = \text{Ga}, \text{Ge}, \text{Tl}, \text{Zn}$) compounds belong to the hexagonal system wherein $\text{P6}_3/\text{mmc}$ (No. 194) is the space group [1]. In the unit cell, there exist two formula units, and each formula unit cell has four atoms. The atomic positions in the unit cell are as follows: Nb atoms at $(1/3, 2/3, z_M)$, A atoms at $(2/3, 1/3, 1/4)$, and the C atoms at $(0, 0, 0)$. Additionally, z_M is an internal parameter; its value is listed in Table 4.1.1. Table 4.1.1 shows the lattice constants (a , c) for optimized cell, the hexagonal ratio (c/a) ratio and internal parameters of Nb_2AC ($\text{A} = \text{Ga}, \text{Ge}, \text{Tl}, \text{Zn}$) and Nb_2AC ($\text{A} = \text{P}, \text{In}, \text{Cd}, \text{Al}$), for comparing. The fundamental polyhedrons of Nb_2AC ($\text{A} = \text{Ga}, \text{Ge}, \text{Tl}, \text{Zn}, \text{P}, \text{In}, \text{Cd}, \text{Al}$) are studied using Hug's distortion indexes (DIs) [2, 3]. Two parameters - the distortion of octahedral (O_d) and trigonal prism (P_d) of the M_6X octahedrons and M_6A trigonal prisms, respectively are used to describe the distortions in the structure of the 211 MAX phases calculated using the 3.13 and 3.14 equations.

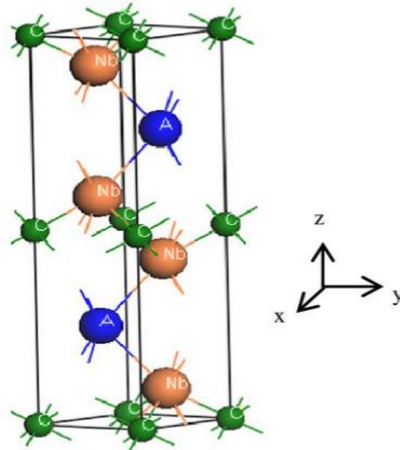


Fig. 4.1.1: The unit cell of Nb_2AC ($\text{A} = \text{Ga}, \text{Ge}, \text{Tl}, \text{Zn}$).

The polyhedron would be ideal when the octahedron and the trigonal parameters are equal to 1 [4]. The distortion of the polyhedron is measured by the deviation from 1, where a low distortion value indicates a more stable structure [4]. Table 4.1.1

Table 4.1.1: Calculated lattice constants (a and c), c/a ratio, internal parameter (Z_m), density (ρ), volume (\AA^3), distortion parameters of octahedra (O_d) and trigonal prism (P_d) of Nb_2AC (A= Ga, Ge, Tl, Zn), along with those of Nb_2AC (A = P, In, Cd, Al) MAX phases.

Phases	a (\AA)	c (\AA)	Z_m	c/a	Density (ρ)	Volume(\AA^3)	O_d	P_d	Ref.
Nb_2GaC	3.145	13.73	0.0896	4.366	7.59	^a 116.97	1.039	0.689	^a This
	3.115	13.51		4.337		^b 113.53	1.044	0.834	^b This
	3.143	13.64		4.340		116.66	*1.044	*0.834	[5]
	3.13	13.56		4.332		115.05	*1.046	*0.836	[1]
Nb_2GeC	3.244	12.69	0.095	3.914	7.76	115.75	1.086	0.904	^a This
	3.194	12.77		3.998		112.83	1.066	0.890	^b This
	3.255	12.59		3.868			*1.097	*0.912	[7]
	3.237	12.35		3.815			*1.109	*0.959	[6]
	3.228	12.76		3.953		115.10	*1.076	*0.898	[5]
Nb_2TlC	3.229	12.74	0.0795	3.944	10.18	131.11	1.254	0.891	^a This
	3.199	14.27		4.461		126.46	1.131	0.781	^b This
Nb_2ZnC	3.145	13.73	0.0875	4.366	7.43	117.58	1.060	0.829	^a This
	3.117	13.53		4.341		113.83	1.066	0.833	^b This
Nb_2PC	3.299	11.59	0.0999	3.515	8.28	109.33	1.149	0.978	^a This
	3.267	11.52		3.526		106.48	1.146	0.976	^b This
	3.292	11.578		3.517		108.68	*1.139	*0.978	[5]
	3.28	11.5		3.506		107.15	*1.152	*0.979	[1]
Nb_2InC	3.185	14.54	0.0821	4.563	11.49	127.69	1.103	0.799	^a This
	3.152	14.37		4.559		123.67	1.079	0.799	^b This
	3.186	14.528		4.560		127.72	*1.079	*0.799	[5]
	3.172	14.37		4.530		125.21	*1.085	*0.804	[10]
Nb_2CdC	3.172	14.68	0.0830	4.628	8.06	127.87	1.055	0.790	^a This
	3.140	14.45		4.602		123.37	1.060	0.794	^b This
Nb_2AlC	3.245	12.69	0.0897	3.911	6.34	115.74	1.142	0.902	^a This
	3.102	13.79		4.446		114.99	1.021	0.819	^b This
	3.12	13.93		4.463		117.41	*1.017	*0.817	[5]

^acalculated values using GGA PBE [8]; ^bcalculated values using GGA PBEsol [9], and *calculated values using reported data.

shows the value of the O_d and P_d of Nb_2AC (A= Ga, Ge, Tl, Zn, P, In, Cd, Al). Table 4.1.1 also contains the O_d and P_d of Nb_2AC (A= Ga, Ge, P, In, Al) as calculated from the reported lattice parameters. A very good consistency is observed for the

previously studied phases, indicating the reliability of our present calculations. The comparison is not possible for Nb₂AC (A= Tl, Zn, Cd) phases because of their first-time calculation. The accuracy of the present calculations is also revealed by the close agreement for the values of a and c [Table 4.1.1] of Nb₂AC (A= Ga, Ge, P, In, Al) phases with previously reported values [5, 6, 7].

4.1.2 The Dynamical Stability

Checking the titled phases' dynamical stability, we have computed the phonon dispersion curves (PDC) along with phonon density of states (PHDOS) of Nb₂AC (A= Ga, Ge, Tl, Zn), displayed in Fig. 4.1.2(a-d). The phonon frequency across the entire BZ is used to determine whether a compound is stable: positive frequencies indicate stability, whereas any negative frequencies show that the phases are unstable. As evident from Fig.4.1.2 (a-d), the studied phases are dynamically stable owing to the non-existence of the negative frequency. In addition, one can obtain some more information from the PDCs. In the unit cell, the PDCs have 24 vibrational modes caused by the eight atoms. There are only three acoustic modes, whereas the remaining 21 are known as optical modes. The dispersion curve for the lower three modes is of the form $\omega=vk$ at small k values, and it illustrates the sound wave's $\omega(k)$ relations. These modes are part of the acoustic branch. The optical branch is created by the upper vibrational modes. The optical phonons are produced due to the atom's out-of-phase oscillations caused by photon-induced excitation. Acoustic modes have zero frequency just at the G point. No phononic band gap is found due to the overlap of the optical branches and acoustic modes. Furthermore, the PHDOS is presented alongside the PDCs, wherein the PDC's flat modes lead the sharp peaks. Peaks are diminished when the dispersion changes, either upward or downward. We have presented only results for GGA PBEsol; GGA PBE results are not shown because of their similar nature.

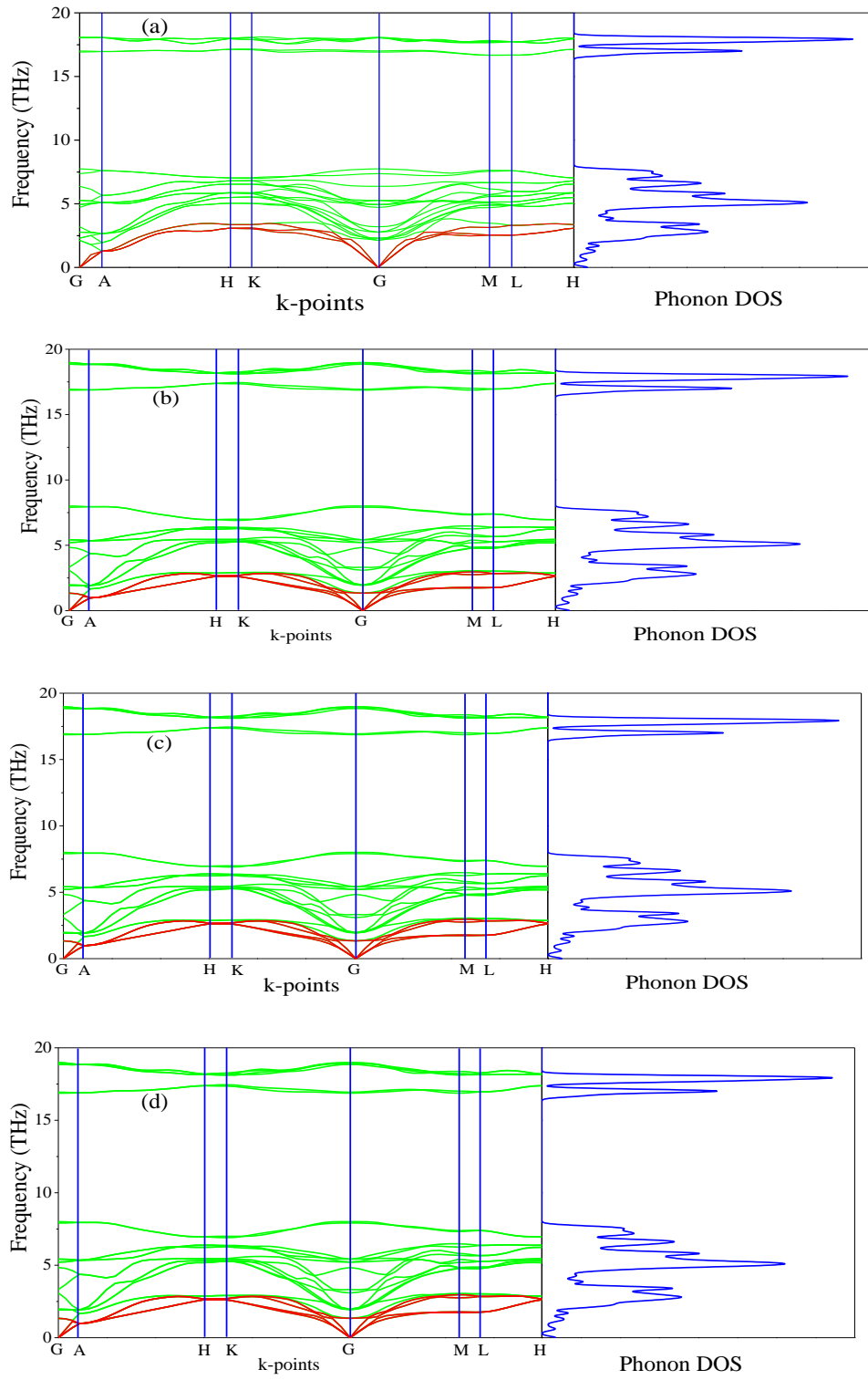


Fig. 4.1.2: Phonon dispersion curves along with phonon DOS of (a) Nb_2GaC , (b) Nb_2GeC , (c) Nb_2TiC , (d) Nb_2ZnC calculated using GGA PBEsol.

4.2 Mechanical Properties

4.2.1. Stiffness Constants and Elastic Moduli

We have calculated the elastic stiffness constants and the polycrystalline elastic moduli using the strain-stress method [11] to bring out the mechanical behavior of Nb₂AC (A= Ga, Ge, Tl, Zn, P, In, Cd, Al). Checking mechanical stability is a must for the solids before studying their mechanical properties. The Nb₂AC (A = Ga, Ge, Tl, Zn, P, In, Cd, Al) phases belong to the hexagonal system, which needs to satisfy the following requirements: $C_{11} > 0$, $C_{33} > 0$, $C_{44} > 0$, $C_{11} - C_{12} > 0$, $(C_{11} + C_{12})C_{33} - 2(C_{13})^2 > 0$ [12, 13]. We have calculated the elastic constants and presented them in Table 4.2.1, revealing that the requirements mentioned earlier have been satisfied by the selected carbides. Thus, Nb₂AC (A= Ga, Ge, Tl, Zn, P, In, Cd, Al) phases are mechanically stable. We may use the calculated stiffness constants to get some additional information. For instance, C_{11} and C_{33} determine the stiffness of the solid along the *a*-axis and *c*-axis when pressure is applied along [100] and [001] directions, respectively. Here, $C_{11} > C_{33}$ for Nb₂AC (A= Ga, Ge, Tl, Zn, P, In, Cd, Al) compounds, revealing the requirement of more pressure along the *a*-axis for deformation compared to the *c*-axis, whereas, for Nb₂PC $C_{33} > C_{11}$. Moreover, the inequality of C_{11} and C_{33} also indicates the anisotropic bonding strength. The hexagonal structure contains different atomic arrangements along the *a*- and *c*-axis, which is assumed responsible for the difference in bonding strength along the *a*- and *c*-axes. One of the stiffness constants, C_{44} , is considered the better hardness predictor [14] compared to other elastic constants. Thus, Nb₂PC is expected to be the hardest with the highest C_{44} (194 GPa), while Nb₂TlC is the softest with the lowest C_{44} (71 GPa). The C_{11} , C_{33} , and C_{44} of Nb₂AC (A= Ga, Ge, Tl, Zn, In, Cd) are lower than those of most known Nb-based Nb₂AlC phase, but the values are greater for Nb₂PC. Better visualization of the differences among values of the stiffness constants is done by presenting them in Fig.4.1.2 for GGA-PBEsol functional, where GGA-PBE also shows similar nature. Furthermore, the stiffness constants are used to predict the ductile/brittleness behavior of Nb₂AC (A= Ga, Ge, Tl, P, Zn, In, Cd, Al) phases by computing the Cauchy pressure (*CP*). The difference between C_{11} and C_{44} is defined as the *CP* [15]; a

negative and positive value represents the brittle and ductile nature, respectively. Negative and positive values also indicate the directional covalent and ionic bonds, respectively. As evident from Table 4.2.1, Nb₂GaC, Nb₂GeC, Nb₂PC, Nb₂InC, and Nb₂AlC have directional covalent bonds and behave as brittle solids. On the contrary, Nb₂TlC, Nb₂ZnC, and Nb₂CdC phases behave as ductile solids with a positive *CP*. Though most MAX phases are brittle, a few of them, such as Zr₃CdB₄, Ti₂CdC, and Ti₂ZnX (X = C, N), have already been reported as ductile [16, 17, 18].

Finally, calculating the polycrystalline elastic moduli using through the stiffness constants. In order to calculate the bulk modulus (*B*) and shear modulus (*G*), Hill's approximation [19] was applied, and it is the average of the Voight [20] and the Reuss [21] models calculated using 3.15-3.18 equations. *B_V* and *B_R* are expressed as the upper (Voight) and lower limit (Reuss) of *B*, respectively. Here, *G_V* and *G_R* are also expressed as the upper (Voight) and lower limit (Reuss) of *G*, respectively. The Poisson's ratio (*ν*) and Young's modulus (*Y*) are also computed from *B* and *G* by using 3.19 and 3.20 relations.

Table 4.2.1: Calculated stiffness constant (*C_{ij}*), bulk modulus (*B*), shear modulus (*G*), Young's modulus(*Y*), machinability index (*B/C₄₄*), Cauchy pressure (*CP*), Poisson's ratio (*ν*), and Pugh ratio (*G/B*) of Nb₂AC (A= Ga, Ge, Tl, Zn), along with those of Nb₂AC (A = P, In, Cd, Al) MAX phases.:

Parameters	Nb ₂ GaC	Nb ₂ GeC	Nb ₂ TlC	Nb ₂ ZnC	Nb ₂ PC	Nb ₂ InC	Nb ₂ CdC	Nb ₂ AlC	Ref.
<i>C</i> ₁₁ (GPa)	337	265	265	289	368	303	262	357	^a This
	363	306	283	294	394	331	282	368	^b This
	323	284			373	280		333	[5]
		308							[6]
<i>C</i> ₃₃ (GPa)	289	220	235	221	400	269	231	315	^a This
	313	295	258	225	423	295	258	314	^b This
	281	275			407	266		284	[5]
		306							[6]
<i>C</i> ₄₄ (GPa)	130	147	71	101	194	102	77	160	^a This
	141	151	86	113	212	112	89	164	^b This
	126	152			193	104		138	[5]
		177							[6]
<i>C</i> ₁₂ (GPa)	83	146	105	132	123	77	103	98	^a This

	92	137	106	137	132	85	123	84	^b This
	77	136			114	80		84	[5]
		133							[6]
C_{13} (GPa)	119	161	98	106	162	103	88	123	^a This
	131	161	118	122	179	112	102	119	^b This
	130	161			172	113		117	[5]
		168							[6]
CP (GPa)	-47	-1	34	31	-71	-25	26	-62	^a This
	-49	-14	20	24	-80	-27	34	-80	^b This
	*-49	*-16			*-79	*-24		*-54	[5]
		*-44							[6]
B (GPa)	178	184	152	163	225	160	146	190	^a This
	194	203	168	173	242	175	163	188	^b This
	178	195			230	160		176	[5]
		206							[6]
G (GPa)	119	76	75	85	148	102	79	133	^a This
	128	101	84	88	153	112	85	140	^b This
	114	101			150	96		122	[5]
		109							[6]
γ (GPa)	291	201	194	218	365	253	200	324	^a This
	314	261	215	225	379	277	216	337	^b This
	282	258			369	240		298	[5]
		279							[6]
ν	0.23	0.32	0.29	0.28	0.23	0.24	0.27	0.22	^a This
	0.23	0.29	0.29	0.28	0.24	0.23	0.28	0.20	^b This
	*0.24	*0.28			*0.23	*0.25		*0.22	[23]
		*0.28							[25]
G/B	0.67	0.41	0.49	0.52	0.65	0.63	0.54	0.70	^a This
	0.66	0.49	0.50	0.51	0.63	0.64	0.52	0.74	^b This
	*0.64	*0.52			*0.65	*0.60		*0.69	[5]
		*0.53							[6]
B/C_{44}	1.36	1.25	2.14	1.61	1.15	1.56	1.89	1.18	^a This
	1.38	1.34	1.95	1.53	1.14	1.56	1.83	1.15	^b This
	*1.41	*1.28			*1.19	*1.54		*1.28	[5]
		*1.16							[6]

^acalculated values using GGA PBE [8]; ^bcalculated values using GGA PBEsol [9], and
*calculated values using reported data.

As known, the pure deformations (volume and shape) are studied by the bulk modulus (mostly known for the study of elastic response against pressure) and the shear modulus (mostly known for the study of rigidity of solids against pressure). It is seen from Table 4.2.1 that Nb₂PC (Nb₂CdC) has the highest (lowest) resistance

against hydrostatic pressure, whereas the lowest resistance to plastic deformation is noted for Nb₂TiC among the studied compounds.

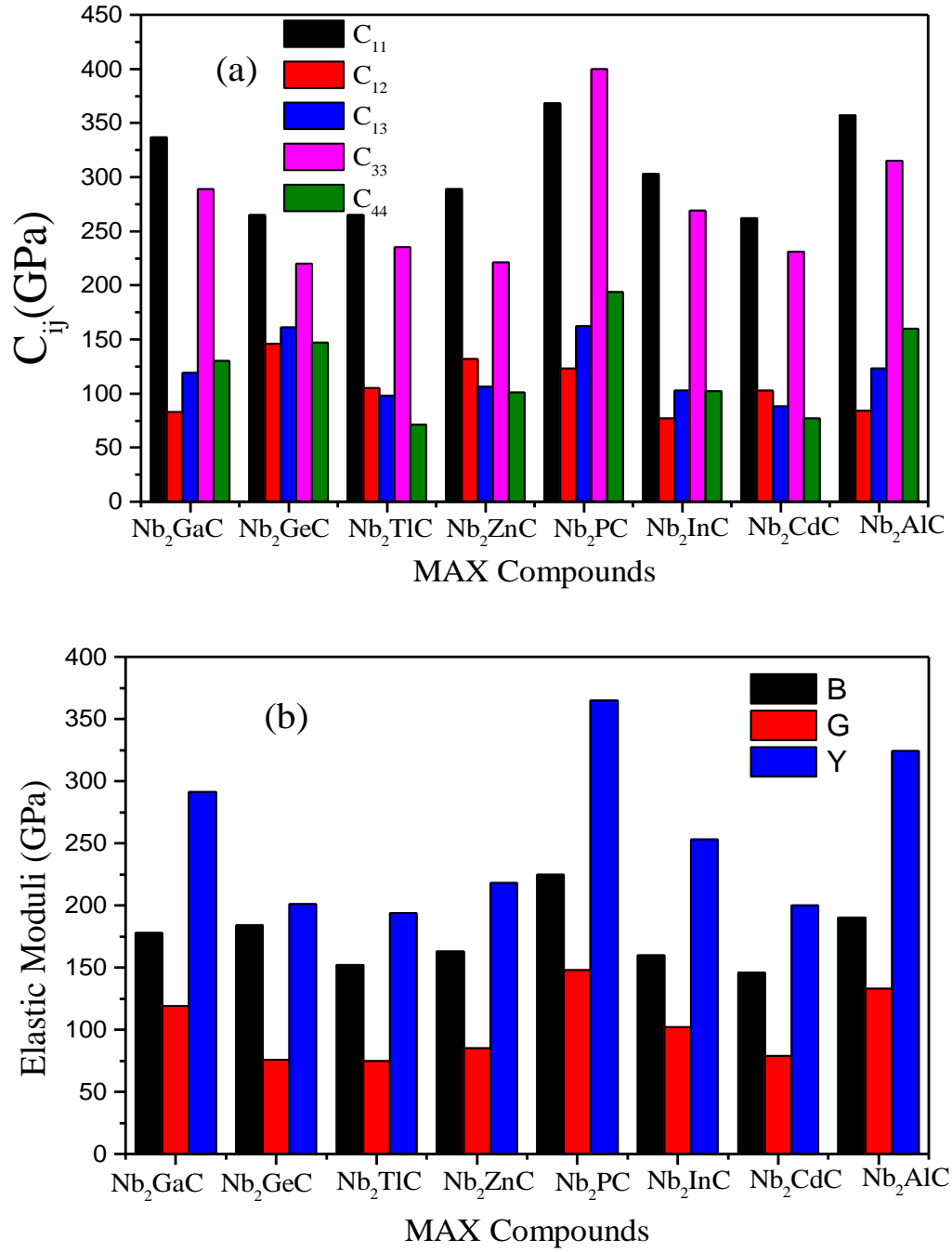


Fig.4.2.1: Comparison of (a) stiffness constants and (b) elastic moduli of Nb₂AC (A= Ga, Ge, Ti, Zn, P, In, Cd, Al) MAX phases calculated using GGA PBEsol.

However, According to the values of B (determined using GGA-PBEsol), the compounds can be ordered as follows: Nb₂PC > Nb₂GeC > Nb₂GaC > Nb₂AlC >

$\text{Nb}_2\text{InC} > \text{Nb}_2\text{ZnC} > \text{Nb}_2\text{TlC} > \text{Nb}_2\text{CdC}$, whereas the ranking for G will be as follows: $\text{Nb}_2\text{PC} > \text{Nb}_2\text{AlC} > \text{Nb}_2\text{GaC} > \text{Nb}_2\text{InC} > \text{Nb}_2\text{GeC} > \text{Nb}_2\text{ZnC} > \text{Nb}_2\text{CdC} > \text{Nb}_2\text{TlC}$.

For Young's modulus, Y is the measure of the stiffness of solids that relates the stiffness with the thermal shock resistance (inverse relationship) of solids. Therefore, a solid with a high Y value indicates high stiffness and low thermal shock resistance (TSR) [22]. The Y -based ranking of the phases also follows the G -based ranking. Table 2 implies that Nb_2TlC exhibits high TSR while Nb_2PC has the lowest TSR, followed by the Y -based reverse ranking among the herein-studied phases. Although these moduli do not indicate hardness, they are usually higher for harder materials [23]. Compared to Y , B , and G have a close relationship with the material's hardness. In some cases, these parameters are used to predict the hardness of solids by using the 3.21 and 3.22 formulae. Table 4.2.1 also includes the previously reported values [5]. As evident from Table 4.2.1, the obtained values are in good accord with reported values, ensuring the accuracy of the present calculation that helps other researchers to consider our calculated values as a reference for both application and research purposes.

4.2.2 The Brittleness of Nb_2AC ($A = \text{Ga, Ge, Tl, Zn, P, In, Cd, Al}$)

The remarkable combination of metal and ceramic characteristics is the most excellent feature of MAX phases [24]. They are machinable, just like metals, as stated in the preceding section, and brittle, just like ceramic materials. However, some are also ductile [18, 16, 25], making them more machinable and, consequently, more useful owing to easy shaping. By using the Pugh ratio (G/B) [26] and Poisson's ratio (ν) [27], the ductile/brittleness characteristics of Nb_2AC ($A = \text{Ga, Ge, Tl, Zn, P, In, Cd, Al}$) has been evaluated and presented in Table 4.2.1. Pugh proposed a critical value of G/B ratio (0.571) for ductile (less than 0.571) and brittle (greater than 0.571) classification, whereas ν used to separate the brittle (less than 0.26) and ductile (greater than 0.26) solids with a critical value of 0.26. As evident, Nb_2GaC , Nb_2PC , Nb_2InC , and Nb_2AlC are brittle, while Nb_2GeC , Nb_2TlC , Nb_2ZnC , and Nb_2CdC are ductile; outcomes are in good agreement with the CP outcomes presented above

and the previously reported results [5, 6]. The Machinability Index (MI) is commonly used in the tribological sector to forecast a solid's performance and is defined as the B/C_{44} ratio. The MI index has been presented in Table 4.2.1. The MI of Nb_2TiC , Nb_2ZnC , and Nb_2CdC is higher than that of other studied phases owing to their ductile nature. Though Nb_2GeC is ductile, its C_{44} is comparatively higher, which results in a lower MI value. Based on the values [Table 4.2.1], the titled phases are expected to be more machinable than the widely known Nb_2AlC phase except for Nb_2PC . The lowest MI is found for Nb_2PC , as expected, due to its highest C_{44} . In addition, a good relationship between machinability and ductility is observed, as expected. The MI values are also different for PBE and PBEsol functions because of the different values of B and C_{44} . However, the obtained values of MI are comparable with some other 211 MAX phases, like, Ti_2AlC , whose machinability index is 1.23 [28]. Though some 211 phase exhibits very high value of MI, such as W_2SnC (MI = 33.3) and Mo_2PbC (MI = 15.8) [29, 30], it should be noted that their C_{44} values are much lower W_2SnC (6 GPa) and Mo_2PbC (10 GPa) [30].

4.2.3 Theoretical Values of Vickers Hardness

Due to the atomic bonds present within the solids, the Vickers hardness is the solid's ability to resist deformation under extreme conditions. Different factors, such as the strength of the atomic bonds, atomic arrangement, the structure of the solids, crystal defects, etc. determine the hardness of solids. The Vickers hardness of the Nb_2AC ($A = Ga, Ge, Ti, Zn, P, In, Cd, Al$) MAX phases are calculated using Mulliken bond populations based on Gou *et al.* [31, 32], which is suitable mainly for partial metallic systems like MAX phases. The relevant hardness formula is using 3.23-3.25 equations. The volume of the μ -type bond is denoted by v_b^μ , which is calculated using 3.26. At last, the equation for Vickers hardness is using 3.27 equation. Table 4.2.3 shows the computed Vickers hardness of Nb_2AC ($A = Ga, Ge, Ti, Zn, P, In, Cd, Al$). As shown in Table 4.2.3, Nb_2PC has higher Vickers hardness than other studied compounds, wherein Nb_2TiC possesses the lowest value of H_v , in agreement with mechanical parameters such as C_{44} and G , which are assumed to be more related to

the hardness of solids. The H_v of Nb₂AC (A = Ga, Ge, Tl, Zn, In, Cd, Al) are comparable except for Nb₂PC, which has a much higher value of H_v . This can be explained based on the bond overlap population (P^μ). As seen in Table 4.2.3, the P^μ of Nb₂PC is 1.01 and 0.98 for C-Nb and P-Nb bonds, respectively, indicating that strong covalent bonding is found between Nb-C and Nb-P atoms. Whereas for Nb₂AC (A = Ga, Ge, Tl, Zn, In, Cd, Al), P^μ is found only for Nb-C atoms; no other significant covalent bond is noticed for these phases.

Table 4.2.3: Calculated Mulliken bond number n^μ , bond length d^μ , bond overlap population P^μ , metallic population $P^{\mu'}$, bond volume v_b^μ , bond hardness H_v^μ of μ -type bond and Vickers hardness H_v of Nb₂AC (A= Ga, Ge, Tl, Zn), along with those of Nb₂AC (A = P, In, Cd, Al) MAX phases:

Compounds	Bond	n^μ	d^μ (Å)	P^μ	$P^{\mu'}$	v_b^μ (Å ³)	H_v^μ (GPa)	H_v (GPa)	Ref.
Nb ₂ GaC	C-Nb	4	2.177	0.93	0.0223	0.0036	2.418	2.418	^a This
			2.167	0.93	0.0209	0.0037	2.55	2.55	^b This
Nb ₂ GeC	C-Nb	4	2.208	0.99	0.0443	0.0037	1.498	1.498	^a This
			2.183	1.02	0.0100	0.0038	2.86	2.86	^b This
Nb ₂ TlC	C-Nb	4	2.194	0.94	0.0358	0.0029	1.994	1.994	^a This
			2.176	0.96	0.0207	0.0031	2.19	2.19	^b This
Nb ₂ ZnC	C-Nb	4	2.177	0.92	0.0504	0.0036	2.297	2.297	^a This
			2.160	0.91	0.0741	0.0037	2.33	2.33	^b This
Nb ₂ PC	C-Nb	4	2.229	1.01	0.0195	0.0187	13.706	9.312	^a This
	P-Nb	4	2.580	0.98		0.0089	6.326		^a This
	C-Nb	4	2.211	1.00	0.0166	0.0200	14.56	10.02	^b This
	P-Nb	4	2.557	0.98		0.0096	6.89		^b This
Nb ₂ InC	C-Nb	4	2.193	0.96	0.0184	0.0031	2.160	2.160	^a This
			2.174	0.95	0.0105	0.0032	2.82	2.82	^b This
Nb ₂ CdC	C-Nb	4	2.177	0.99	0.0206	0.0031	2.224	2.224	^a This
			2.160	0.93	0.0648	0.0032	2.11	2.11	^b This
Nb ₂ AlC	C-Nb	4	2.165	0.98	0.0179	0.0037	2.63	2.63	^a This
			2.166	1.00	0.0112	0.0037	2.71	2.71	^b This

^acalculated values using GGA PBE [8]; ^bcalculated values using GGA PBEsol [9].

Thus, significant covalent bonding among Nb-C and Nb-P atoms is assumed responsible for such higher hardness. However, the variation in H_v of Nb₂AC (A =

Ga, Ge, Tl, Zn, In, Cd, Al) phases is due to the combined effect of the variation in bond population P^μ and bond length d^μ .

4.3. Electronic Properties, Mulliken Atomic and Bond Population Analysis

4.3.1 Electronic Properties

The electronic conductivity, contribution from different states, and nature of atomic bonding can be revealed by studying the electronic band structure, the total and partial density of states (DOS), and Mulliken's population analysis. We have calculated the electronic band structure to predict the metallic nature of the titled MAX compounds. Fig.4.3.1(i) (a-d) [calculated using PBEsol] show the calculated electronic band structure of Nb₂AC (A= Ga, Ge, Tl, Zn), in which the Fermi level (E_F) is represented by a horizontal dashed line. The green curves indicate the Fermi level crossing bands and blue curves denote the bands in the valence and conduction bands. As seen from Fig.4.3.1(i) (a-d), Due to the fact that the conduction and valence bands overlapped, there is no band gap at the Fermi level; thus, the Nb₂AC (A= Ga, Ge, Tl, Zn) phases are considered to be metallic solids. The path ways Γ -A, H-K, and M-L show the energy dispersion for the c -direction.

On the contrary, the pathways A-H, K- Γ , Γ - M, and L-H show energy dispersion in the basal planes. It has been seen from Fig.4.3.1(i) (a-d), that the energy dispersion is smaller in the c -direction than that of the basal plane (ab -plane), thus, the electronic conductivity in the basal plane is higher than that of c -direction [37]. The effective mass tensor is assumed to be higher in the c -direction than that of the basal plane, which is responsible for smaller dispersion in the c -direction [38]. Consequently, the anisotropic nature of electronic conductivity is observed in the herein-studied phases, a common feature of the MAX phases, including Nb₂AlC [6, 32] and Nb₂AC (A = P, In, Cd).

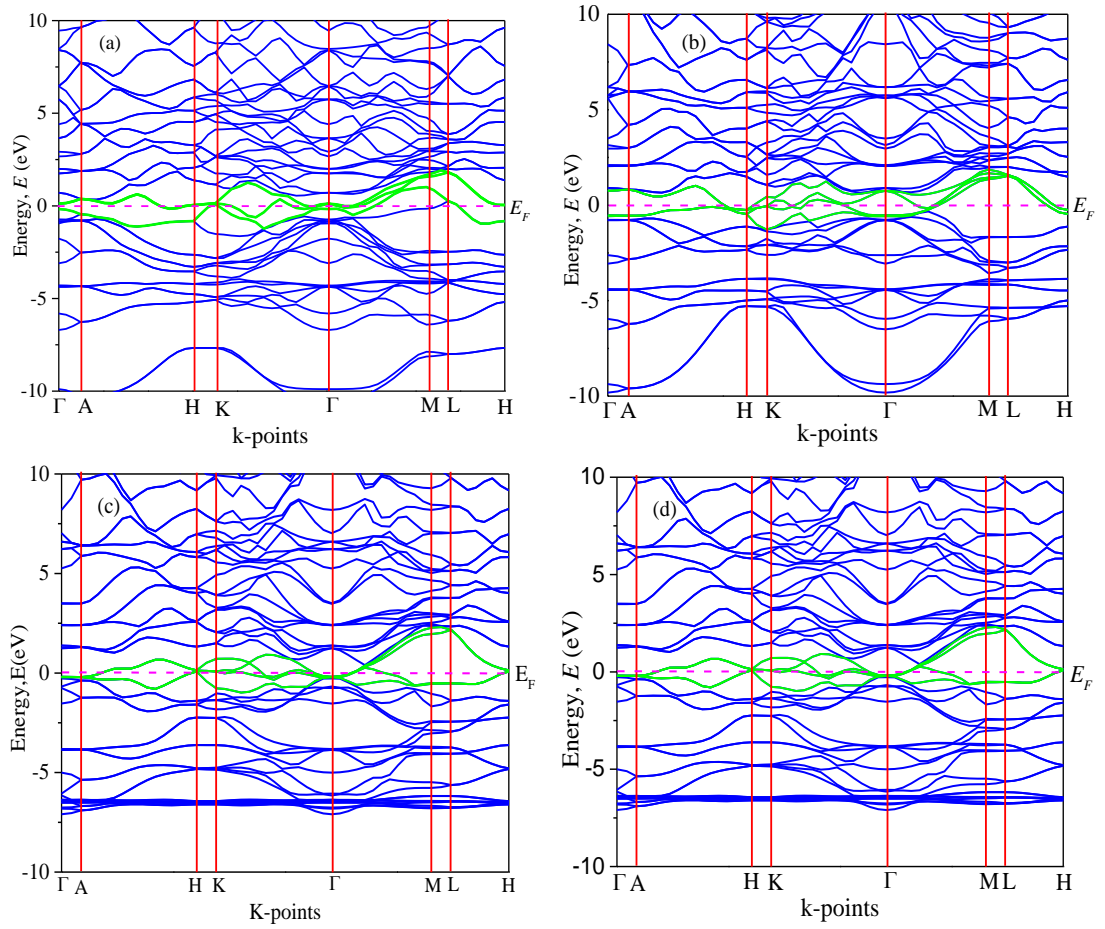


Fig.4.3.1 (i): Band Structure of (a) Nb₂GaC, (b) Nb₂GeC, (c) Nb₂TiC, (d) Nb₂ZnC calculated using GGA PBEsol.

We have also computed the total and partial density of states (DOS) of Nb₂AC (A= Ga, Ge, Ti, Zn), which are also shown in Fig. 4.3.1(ii) (a-d) [calculated using PBEsol]. E_F is the Fermi level, where the DOS values are 3.2, 3.3, 4.0, and 3.5 for Nb₂GaC, Nb₂GeC, Nb₂TiC, and Nb₂ZnC, respectively. The computed compound's DOSs of the studied phases are found to be similar to those of reported MAX phases [6, 32] and Nb₂AC (A = P, In, Cd, Al), which are presented here for comparison where their DOS values are 3.0, 3.1, 2.8, and 3.0. The partial density of states (PDOS) has also been calculated to understand better the chemical bonding of Nb₂AC (A= Ga, Ge, Ti, Zn). Fig.4.3.1(ii) (a-d) [calculated using PBEsol] show the PDOS for Nb₂AC. As seen, C-2s does not involve in the DOS at E_F . As a result, the conduction properties are not attributed to carbon. On the other hand, at the Fermi level, Nb-*d* electrons contribute

significantly to the DOS; therefore, the conduction properties ought to be involved in Nb.

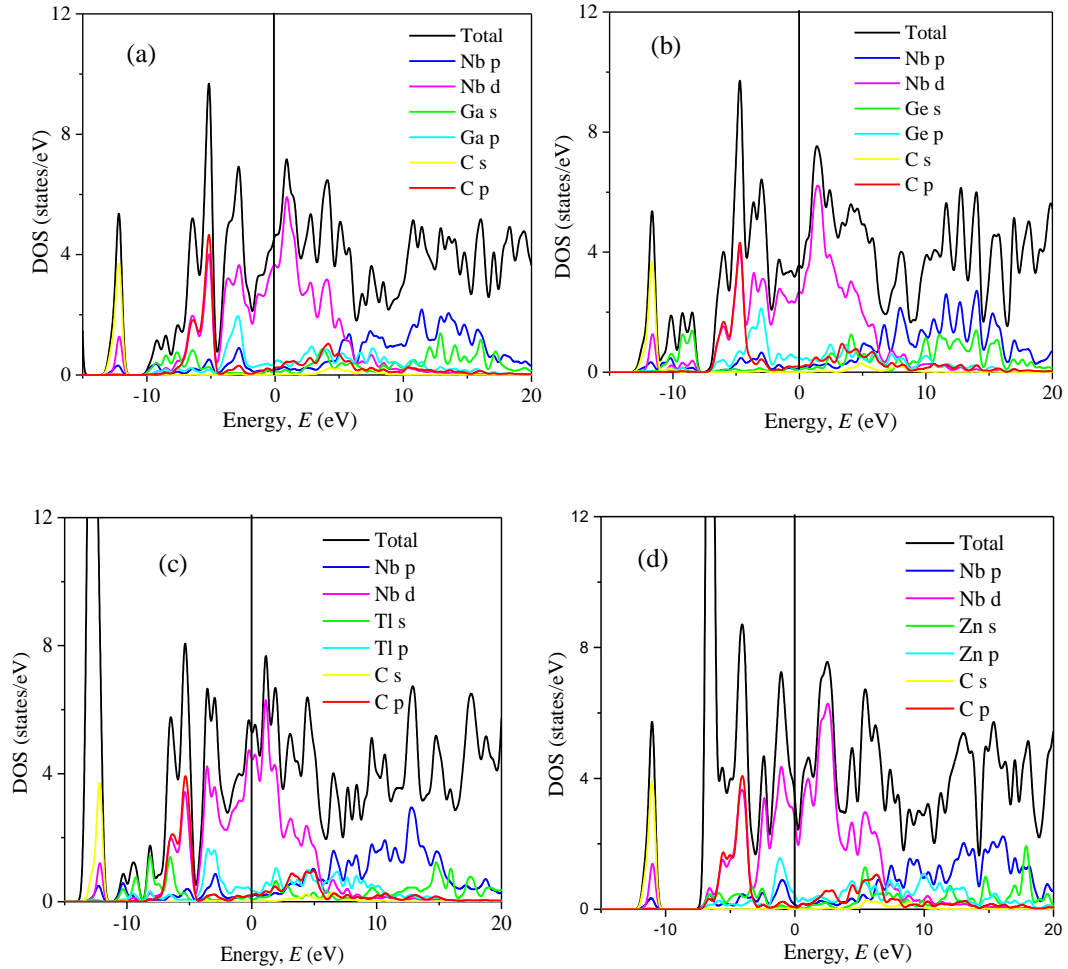


Fig.4.3.1 (ii): Total and partial DOS of (a) Nb₂GaC, (b) Nb₂GeC, (c) Nb₂TiC, (d) Nb₂ZnC calculated using GGA PBEsol.

The A-*p* (A = Ga, Ge, Ti, Zn) electrons are also involved in the conduction mechanism, with a much lower contribution level. C-*p* states also slightly contribute to the conduction properties. This outcome is in line with earlier MAX phase reporting [27]. The degenerate states concerning both lattice sites and angular momentum indicate that a covalent interaction exists between the atoms of the compounds. Hybridized states include C-*p*, Nb-*d*, and A (A= Ga, Ge, Ti, Zn) *p* and Nb *d* states. Moreover, some ionic characteristics can be anticipated because of the disparity in electro-negativity between the constituent atoms. There is a covalent-

ionic combination in the bonding character, which has been explained in section 4.3.2. When compared to Nb-*d* and A-*p* states, the hybridization peak of Nb-*d* and C-*p* lies in the lower energy side, as seen in the PDOS; consequently, covalent bonding due to hybridization between Nb-*d* and C-*p* states is stronger than that of Nb-*d* and A-*p* states (A = Ga, Ge, Tl, Zn). The peak position of hybridization between Nb-*X* and Nb and A states is also responsible for the variation in the hardness of the studied phases. For example, the hybridization among Nb-*d*, P-*p*, and C-*p* states is observed in the lowest energy side (below - 5 eV), which results in strong hybridization among them, and a higher bond overlap population is found, which results in the hardest phase of Nb₂PC among the considered phases. The same hybridization peak for other phases appears at an energy scale of above -5 eV. Equivalent outcomes for the MAX phases have also been reported [6, 32]. Additionally, the PDOS of Nb₂AC (A = P, In, Cd, Al) are similar to those of Nb₂AC (A = Ga, Ge, Tl, Zn).

4.3.2 Mulliken's Atomic and Bond Population Analysis

Studying the atomic population assist in understanding the charge transfer mechanism. The Mulliken's atomic populations are presented in Table 4.3.2(a) [calculated using GGA PBEsol] and Table 4.3.2(b) [calculated using GGA PBE]. As seen, C possesses a negative charge for each phase, whereas Nb and A (A = Ga, Ge, Tl, Zn, P, In, Cd, Al) have positive charges, which indicates that the charges are transferred from A (A = Ga, Ge, Tl, Zn) and Nb to the C atoms. The charge transfer mechanism in these phases indicates the existence of ionic bonding within them. The BOP (bond overlap population) study quantitatively provides bonding and anti-bonding strength [39]. A positive BOP stands for covalent bonds, and negative BOP value certifies the ionic bonds. As evident from Table 4.3.2(a) and 4.3.2(b), a strong covalent bond is formed between Nb and C atoms for each of the titled phases. For Nb₂PC, strong covalent bond is also expected to be formed in association with the Nb-C bonds, which is responsible for a much higher hardness value compared to other phases presented here. Thus, electronic charge transfer ensured the presence of ionic bonding. In contrast, the high positive value of BOP

revealed the existence of covalent bonding, a common characteristic of the MAX phase materials.

Table 4.3.2(a): Mulliken atomic and bond overlap population (BOP) calculated using GGA PBEsol of Nb₂AC (A= Ga, Ge, Tl, Zn), along with those of Nb₂AC (A = P, In, Cd, Al) MAX phases.

Phases	Atoms	<i>s</i>	<i>p</i>	<i>d</i>	Total	Charge(e)	Bond	Bond number <i>n</i> ^u	Bond overlap population <i>P</i> ^u	Ref.
Nb ₂ GaC	C	1.43	3.22	0.00	4.65	-0.65	C-Nb	4	0.93	This
	Ga	0.88	1.84	9.99	12.71	0.29				
	Nb	2.27	6.62	3.94	12.82	0.18				
Nb ₂ GeC	C	1.45	3.23	0.00	4.67	-0.67	C-Nb	4	1.02	This
	Ge	0.99	2.53	0.00	3.52	0.48				
	Nb	2.35	6.56	3.99	12.90	0.10				
Nb ₂ TlC	C	1.43	3.22	0.00	4.65	-0.65	C-Nb	4	0.96	This
	Tl	3.11	7.84	9.92	20.87	0.13				
	Nb	2.25	6.58	3.92	12.74	0.26				
Nb ₂ ZnC	C	1.43	3.23	0.00	4.66	-0.66	C-Nb	4	0.91	This
	Zn	0.53	1.32	9.93	11.78	0.22				
	Nb	2.28	6.63	3.87	12.78	0.22				
Nb ₂ PC	C	1.44	3.20	0.00	4.63	-0.63	C-Nb	4	1.00	This
	P	1.57	3.45	0.00	5.02	0.04	P-Nb	4	0.98	
	Nb	2.24	6.45	3.98	12.67	0.33				
Nb ₂ InC	C	1.43	3.22	0.00	4.65	-0.65	C-Nb	4	0.95	This
	In	0.99	1.81	9.97	12.77	0.23				
	Nb	2.22	6.63	3.94	12.79	0.21				
Nb ₂ CdC	C	1.43	3.23	0.00	4.66	-0.66	C-Nb	4	0.93	This
	Cd	0.55	1.28	9.91	11.73	0.27				
	Nb	2.29	6.65	3.87	12.81	0.19				
Nb ₂ AlC	C	1.45	3.22	0.00	4.67	-0.67	C-Nb	4	1.00	This
	Al	0.97	1.83	0.00	2.80	0.20				
	Nb	2.22	6.57	3.98	12.76	0.24				

Table 4.3.2(b): Mulliken atomic and bond overlap population (BOP) calculated using GGA PBE of Nb₂AC (A= Ga, Ge, Ti, Zn), along with those of Nb₂AC (A = P, In, Cd, Al) MAX phases.

Phases	Atoms	<i>s</i>	<i>p</i>	<i>d</i>	Total	Charge(e)	Bond	Bond number <i>n^u</i>	Bond overlap population <i>P^u</i>	Ref.
Nb ₂ GaC	C	1.44	3.23	0.00	4.67	-0.67	C-Nb	4	0.93	This
	Ga	0.87	1.84	9.99	12.70	0.30				
	Nb	2.27	6.63	3.92	12.82	0.18				
Nb ₂ GeC	C	1.44	3.22	0.00	4.66	-0.66	C-Nb	4	0.99	This
	Ge	1.01	2.54	10.00	13.55	0.45				
	Nb	2.33	6.61	3.96	12.89	0.11				
Nb ₂ TiC	C	1.45	3.24	0.00	4.69	-0.69	C-Nb	4	0.94	This
	Ti	1.04	1.79	10.02	12.85	0.15				
	Nb	2.25	6.55	3.93	12.73	0.27				
Nb ₂ ZnC	C	1.44	3.23	0.00	4.67	-0.67	C-Nb	4	0.92	This
	Zn	0.53	1.32	9.93	11.78	0.22				
	Nb	2.28	6.64	3.85	12.77	0.23				
Nb ₂ PC	C	1.45	3.21	0.00	4.66	-0.66	C-Nb	4	1.01	This
	P	1.58	3.48	0.00	5.06	-0.06	P-Nb	4	0.98	
	Nb	2.24	6.45	3.95	12.64	0.36				
Nb ₂ InC	C	1.44	3.22	0.00	4.66	-0.66	C-Nb	4	0.96	This
	In	0.98	1.81	9.97	12.77	0.23				
	Nb	2.23	6.64	3.92	12.79	0.21				
Nb ₂ CdC	C	1.45	3.24	0.00	4.70	-0.70	C-Nb	4	0.99	This
	Cd	0.56	1.27	9.92	11.75	0.25				
	Nb	2.28	6.63	3.87	12.78	0.22				
Nb ₂ AlC	C	1.42	3.19	0.00	4.61	-0.68	C-Nb	4	0.98	This
	Al	0.93	1.82	0.00	2.75	0.21				
	Nb	2.18	6.56	3.95	12.69	0.27				

4.4 Elastic Anisotropy

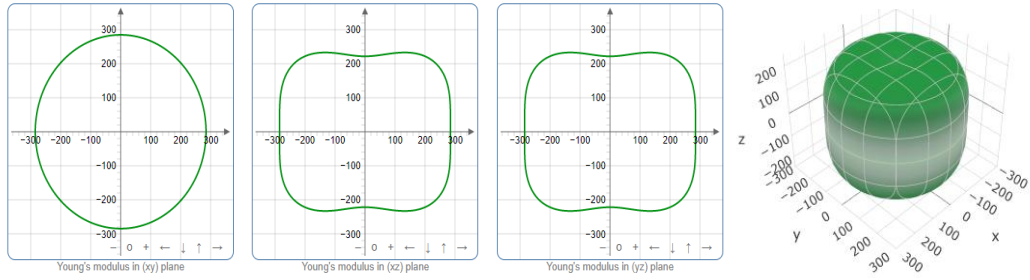
The study of the elastic anisotropy of the MAX phases is essential because of their potential use in practical applications. Some important physical processes, such as dislocation dynamics, plastic deformation, unusual phonon modes, crack behavior, etc., are caused through mechanical anisotropy in solids [36, 37]. Since the values of C_{11} and C_{33} are unequal [Table 4.2.1], other elastic moduli are calculated

using these constants. Thus anisotropic nature of the elastic properties is expected for these compounds. These facts encourage us to study the mechanical anisotropy of titled carbides in the 211 MAX phases. It is possible to demonstrate the level of anisotropy by plotting the elastic moduli in different directions. In this manner, we used the ELATE code [38] to compute the values of Young's modulus, compressibility, shear modulus, and Poisson's ratio, which are presented in Fig. 4.4(i) (a–d) for Nb₂GaC, 4.4. (ii) (a–d) for Nb₂GeC, 4.4. (iii) (a–d) for Nb₂TiC, 4.4. (iv) (a–d) for Nb₂ZnC. The 3D and 2D plots will help to explain the anisotropic nature. The isotropic nature of solids is represented by the sphere in 3D plots and the circle in 2D plots. In contrast, the anisotropy is indicated by a departure from a perfect circle or sphere, and the degree depends on the departure level. Young's modulus (Y) is anisotropic in the xz and yz planes but isotropic in the xy planes, as seen in Fig. 4.4(i) (a), 4.4(ii) (a), 4.4(iii) (a), 4.4(iv) (a). Y has minimum values at the vertical axis of the xz and yz planes and a maximum value at an intermediate angle of 45° of those axes. Fig. 4.4(i) (b), 4.4(ii) (b), 4.4(iii) (b), 4.4(iv) (b) depict the compressibility's (K), which exhibits a similar anisotropic character to that of Y . The compressibility (K) is isotropic in the xy plane whereas anisotropic in the xz and yz planes, where K has maximum values on the axes of the xz and yz planes and a minimum value at an angle of 45° to those axes. For the considered compounds presented in Fig. 4.4(i) (c), 4.4(ii) (c), 4.4(iii) (c), 4.4(iv) (c), the shear modulus (G) displays two surfaces for both 2D and 3D representations. The green line shows the minimum values for a 45° angle, while the blue line shows the maximum values for the same angle. In the xy and yz planes, G is maximum along both axes, with the minimum value found at an angle of 45° between the axes. In the xz plane, it is seen to be isotropic. In Fig. 4.4(i) (d), 4.4(ii) (d), 4.4(iii) (d), 4.4(iv) (d), a different anisotropic characteristic is seen for the Poisson's ratio. Like G , there are two surfaces for 2D and 3D representations, except Nb₂GeC. The blue line indicates maximum values at a 45° angle, whereas the green line indicates minimum values at the same angle for all compounds except Nb₂GeC. For Nb₂GeC, the green line indicates positive values where the values are maximum at 45° , and the red line indicates maximum negative values for the same

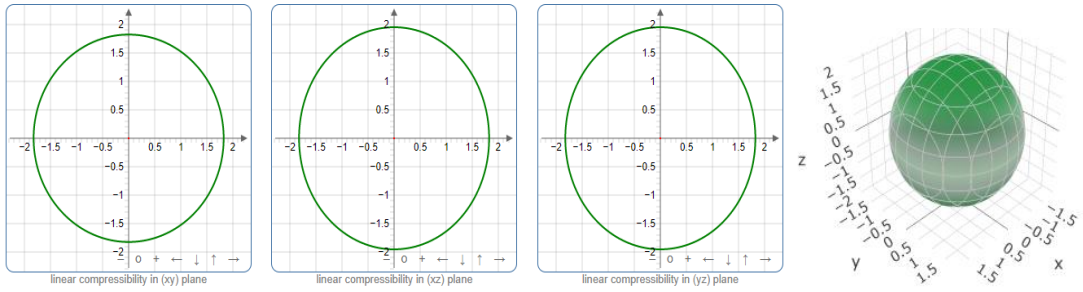
angle. The Poisson's ratio is also anisotropic, with the minimum values found within the vertical axes in the xz and yz planes. In contrast, the maximum values are found within the horizontal axes for both compounds. In the xy plane, Poisson's ratio is found to be isotropic.

Other important anisotropic indices have also been calculated. Using the 3.28-3.30 relationships, the three shear anisotropic factors, A_i ($i = 1, 2, 3$), are computed. Using the 3.31, 3.32 equations, the elastic anisotropy for the bulk modulus (B_a , B_c) across the a and c -axes are computed. Additionally, the elastic anisotropy for the ratio of the linear compressibility coefficients (k_c/k_a) [k_a for a and k_c for c -directions] is computed using the 3.33. Table 4.4(a) and Table 4.4(b) show the value of the obtained anisotropy factors. The values of $A_i = 1$ implies the isotropy, otherwise anisotropic nature; thus, the Nb_2AC ($A = Ga, Ge, Tl, Zn, P, In, Cd, Al$) compounds are anisotropic owing to their non-unit (1) value. The equality of k_c and k_a , and B_a and B_c , also implies the isotropic nature. These parameters also suggest the anisotropic nature of the titled compounds. Furthermore, the percentage anisotropies of compressibility and shear modulus were computed as 3.34 and 3.35 equations, certifying the anisotropic nature.

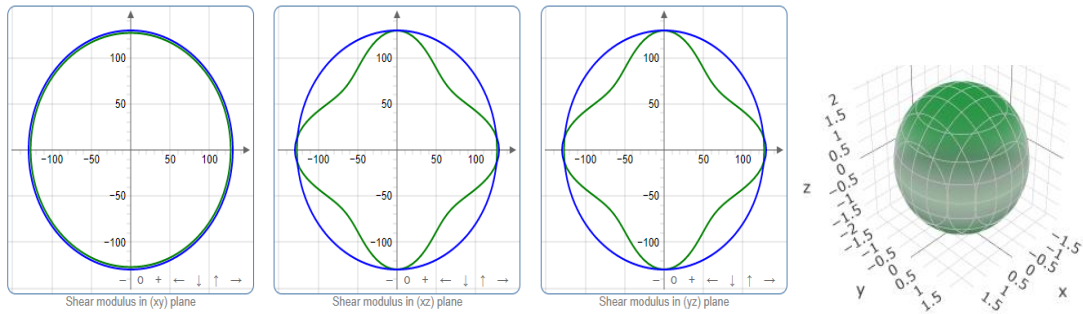
(a) Young's modulus



(b) Compressibility



(c) Shear modulus



(d) Poisson's ratio

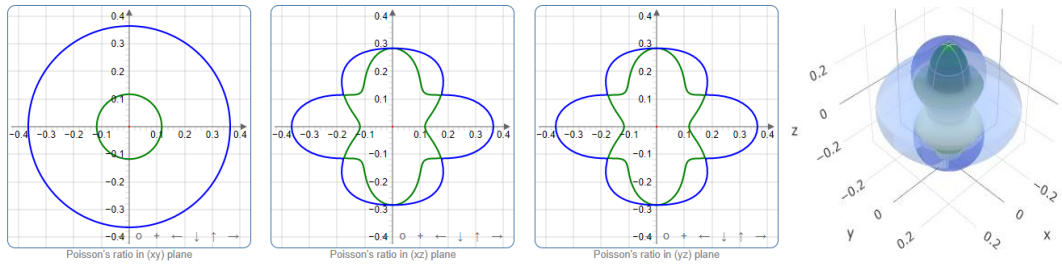
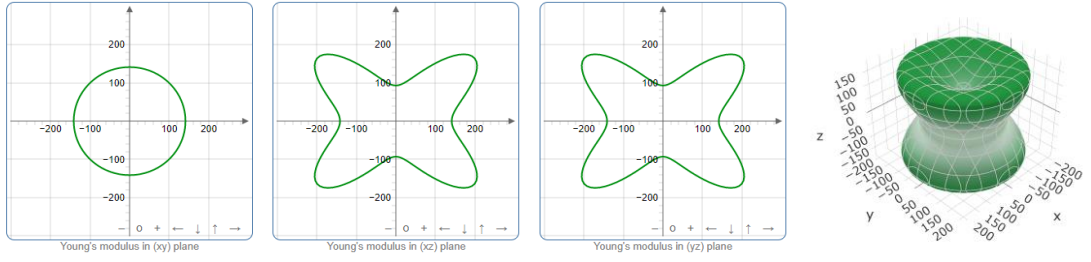
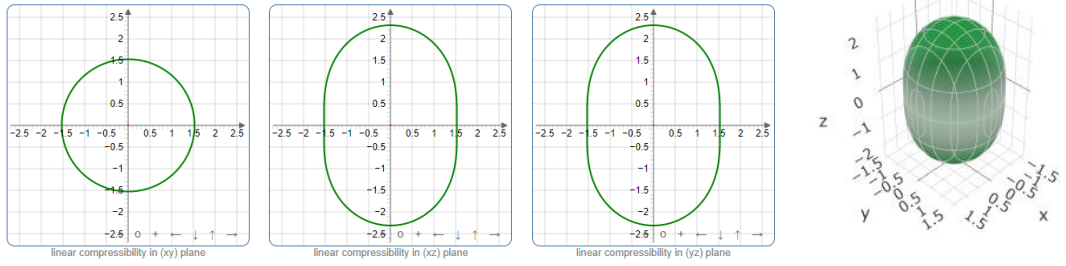


Fig. 4.4(i): The 2D and 3D plots of (a) Y , (b) K , (c) G and (d) ν of Nb_2GaC for GGA PBEsol.

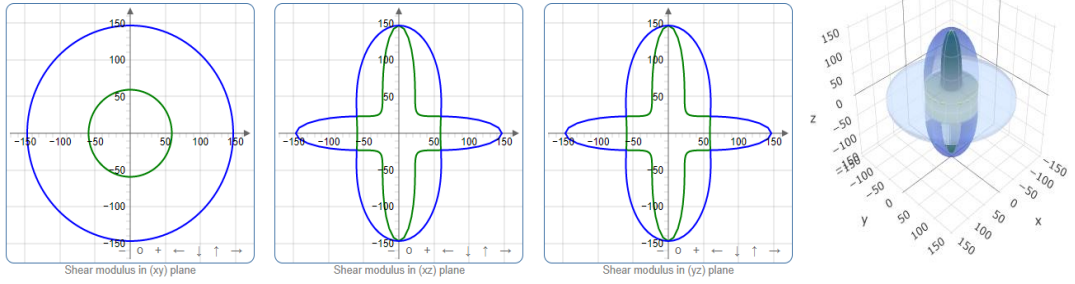
(a) Young's modulus



(b) Compressibility



(c) Shear modulus



(d) Poisson's ratio

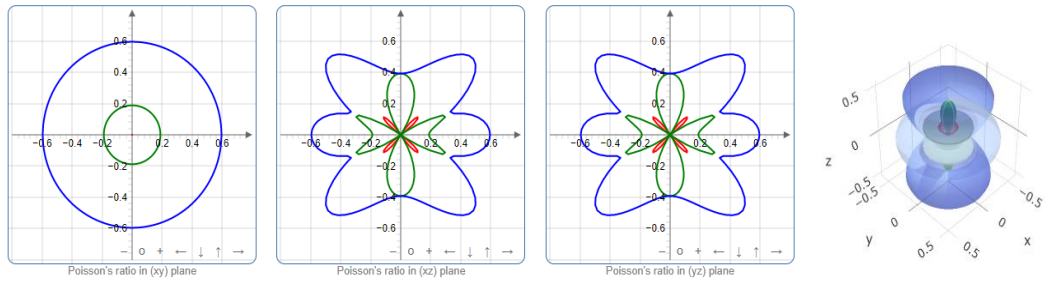
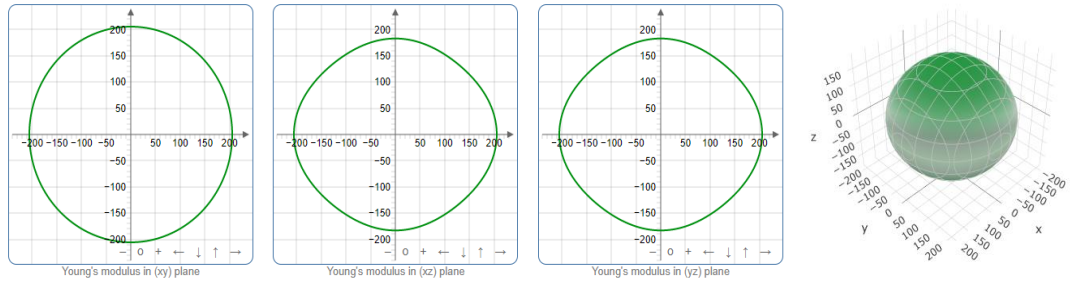
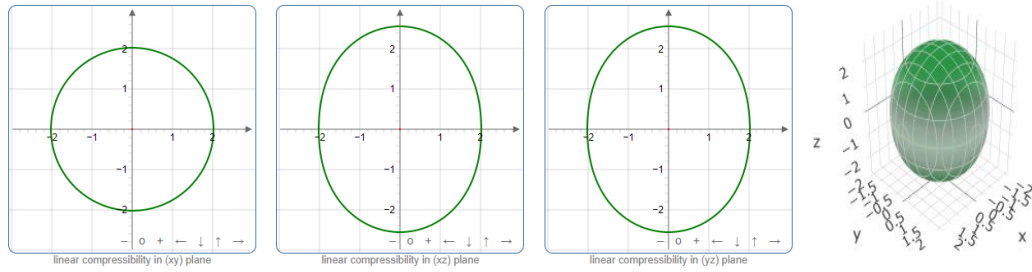


Fig. 4.4(ii): The 2D and 3D plots of (a) Y , (b) K , (c) G and (d) ν of Nb_2GeC for GGA PBEsol.

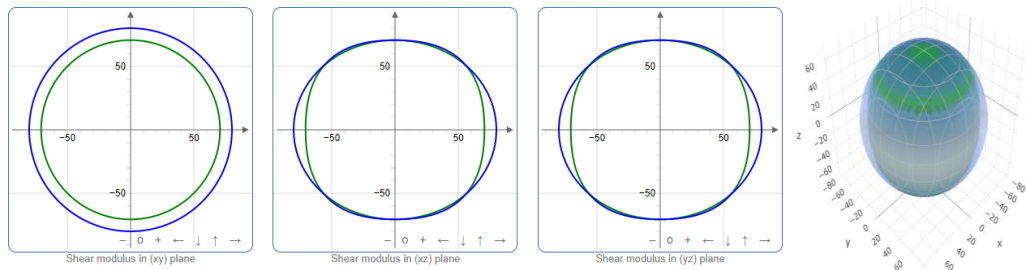
(a) Young's modulus



(b) Compressibility



(c) Shear modulus



(d) Poisson's ratio

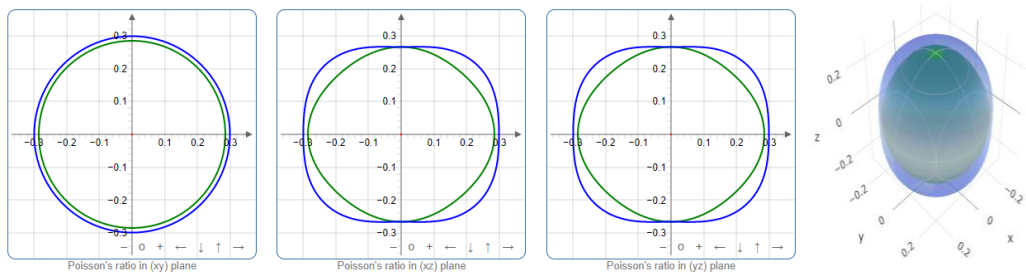
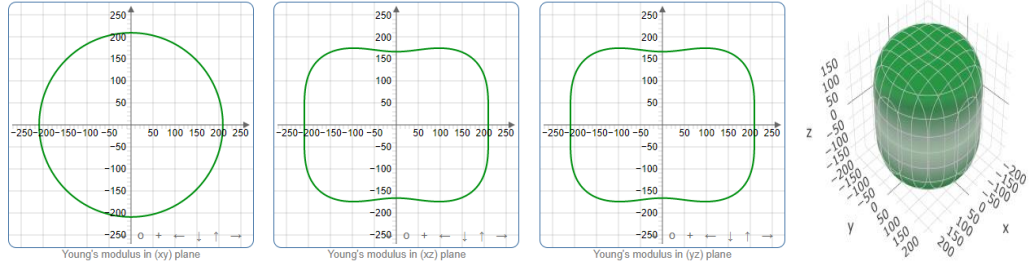
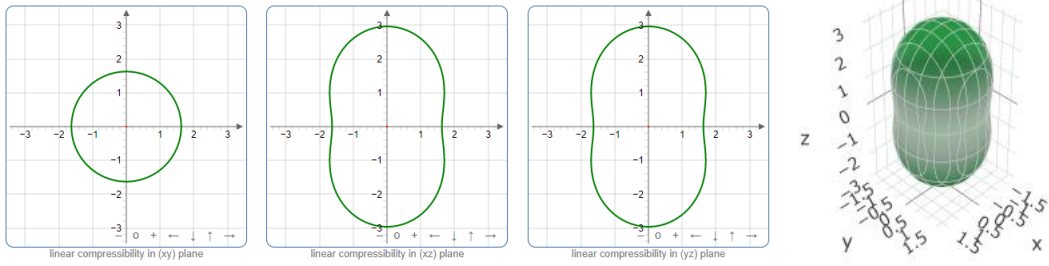


Fig. 4.4(iii): The 2D and 3D plots of (a) Y , (b) K , (c) G and (d) ν of Nb_2TIC for GGA PBEsol.

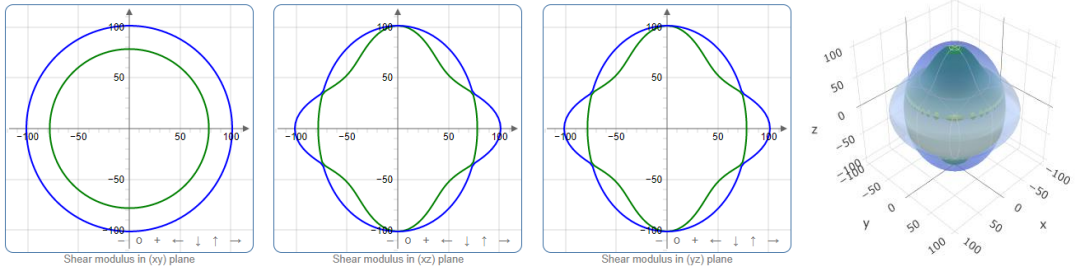
(a) Young's modulus



(b) Compressibility



(c) Shear modulus



(d) Poisson's ratio

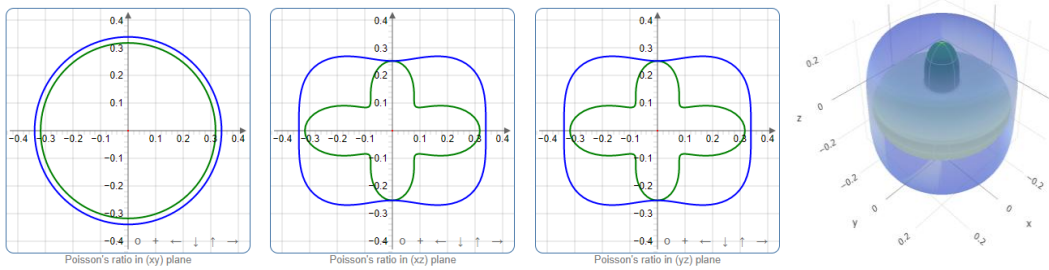


Fig. 4.4(iv): The 2D and 3D plots of (a) γ , (b) K , (c) G and (d) ν of Nb_2ZnC for GGA PBEsol.

Table 4.4. (a): Anisotropy factors $A_1, A_2, A_3, k_d/k_a, B_a, B_c$ percentage anisotropy factors A_G and A_B and universal anisotropic index A^u , calculated values using GGA PBEsol [9] of Nb₂AC (A= Ga, Ge, Tl, Zn), along with those of Nb₂AC (A = P, In, Cd, Al) MAX phases.

Phase	A_1	A_2	A_3	B_a	B_c	K_d/k_a	A_B	A_G	A^u	Ref.
Nb ₂ GaC	0.658	1.04	0.69	491.6	1130.9	1.06	0.001	0.013	0.130	This
	*0.59	*1.02	*0.59	*505.2	*1483.3	0.93	*0.001	*0.022	*0.224	[39]
Nb ₂ GeC	0.43	1.79	0.77	475.7	1792.8	0.90	0.003	0.057	0.607	This
	*0.36	*2.05	*0.73	*448.9	*1317.9	0.86	*0.004	*0.085	*0.932	[39]
	*0.36	*2.02	*0.72	*470.8	*2125.5	*0.76	*0.001	*0.084	*0.922	*[23]
Nb ₂ TlC	0.84	0.97	0.82	420.8	1034.1	1.09	0.002	0.003	0.031	This
Nb ₂ ZnC	0.58	1.44	0.83	468.8	869.9	1.82	0.012	0.027	0.296	This
Nb ₂ PC	0.52	1.62	0.83	563.7	2019.9	0.69	0.004	0.038	0.407	This
	*0.53	*1.49	*0.79	*520.2	*2105.9	0.61	*0.007	*0.033	*0.358	*[39]
Nb ₂ InC	0.83	0.91	0.76	448.7	951.1	1.05	0.006	0.005	0.051	This
	*0.71	*1.04	*0.73	*387.7	*1095.1	0.88	*0.005	*0.008	*0.095	[23]
Nb ₂ CdC	0.96	1.12	1.08	437.1	782.9	1.29	0.003	0.002	0.023	This
Nb ₂ AlC	0.61	1.16	0.71	487.5	986.4	1.09	0.003	0.016	0.165	This
	0.66	1.07	0.70	*438.9	*1042.5	0.95	0.006	0.012	0.129	[39]

*calculated values using reported data.

Table 4.4.(b): Anisotropy factors $A_1, A_2, A_3, k_d/k_a, B_a, B_c$ percentage anisotropy factors A_G and A_B and universal anisotropic index A^u , calculated using GGA PBE [8] of Nb₂AC (A= Ga, Ge, Tl, Zn), along with those of Nb₂AC (A = P, In, Cd, Al) MAX phases..

Phase	A_1	A_2	A_3	B_a	B_c	K_d/k_a	A_B	A_G	A^u	Ref.
Nb ₂ GaC	0.669	1.0236	0.685	453.71	1017.29	1.07	0.003	0.013	0.134	This
Nb ₂ GeC	0.2347	2.4706	0.5798	440.74	1886.74	1.51	0.003	0.016	1.846	This
Nb ₂ TlC	1.0516	0.8875	0.9333	513.49	982.77	1.27	0.002	0.002	0.024	This
Nb ₂ ZnC	0.7244	1.2866	0.9321	455.93	713.39	1.82	0.014	0.013	0.160	This
Nb ₂ PC	0.552	1.584	0.874	526.67	1773.29	0.70	0.002	0.032	0.328	This
Nb ₂ InC	0.827	0.903	0.747	440.46	941.15	1.05	0.003	0.005	0.050	This
Nb ₂ CdC	1.123	0.969	0.648	523.91	884.98	1.32	0.005	0.001	0.019	This
Nb ₂ AlC	0.618	1.236	0.764	491.06	1029.47	1.089	0.003	0.002	0.133	This

Finally, we have calculated the universal anisotropy index A^u based on the Voight, V (upper limit) and Reuss, R (lower limit) models by using the 3.36 relation. If the

value of A^u is zero, it implies isotropic behavior, whereas the non-zero value reveals anisotropic behavior. In summary, we have found the anisotropic nature of Nb₂AC (A = Ga, Ge, Tl, Zn, P, In, Cd, Al) compounds.

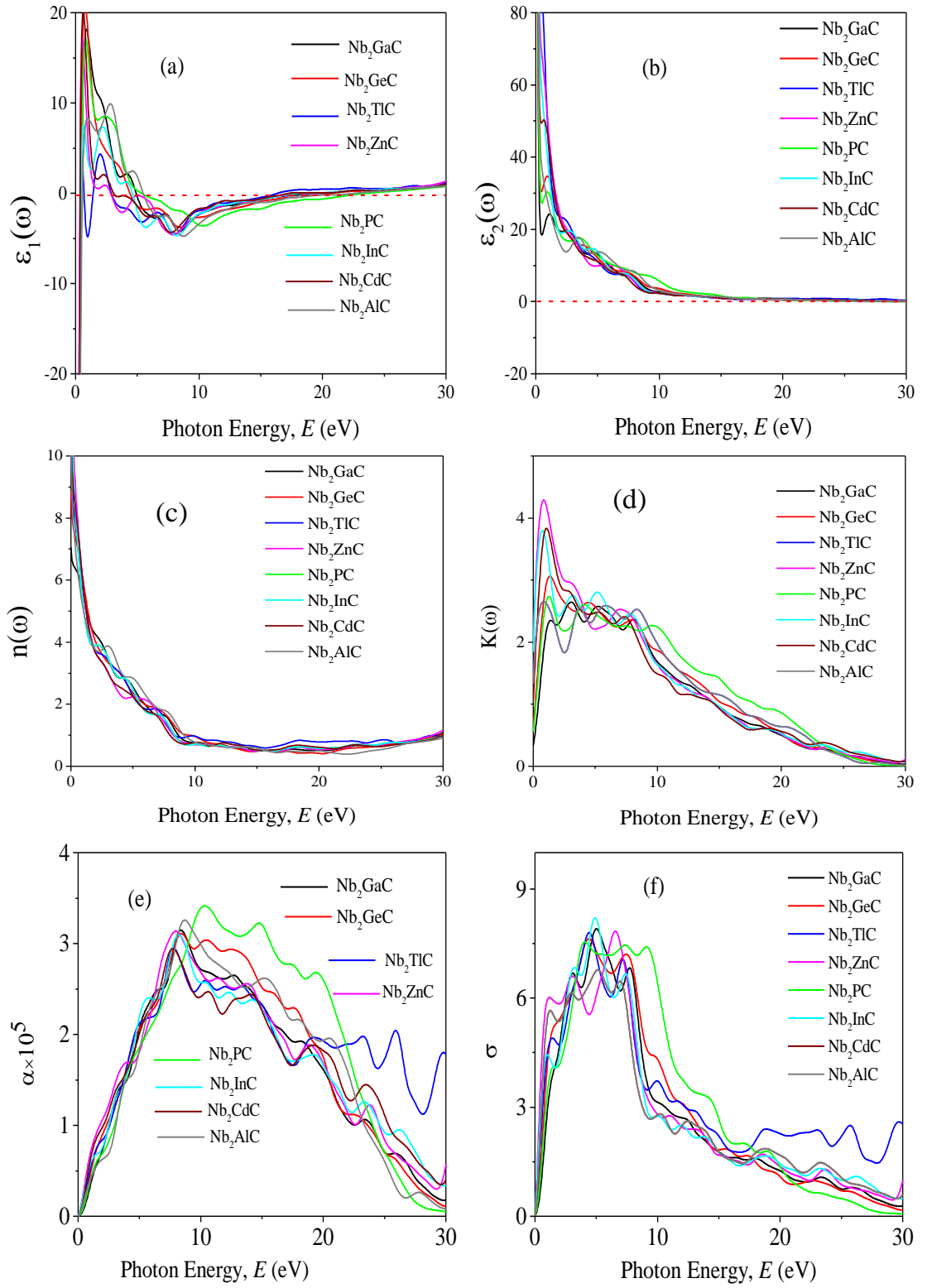
4.5 Optical Properties

The MAX phase materials have already been identified as prospective candidates for use as a coating layer to lessen solar heating [40]. They have also been used in other sectors, such as optical systems [40]. Therefore, it is also hoped that the studied carbides will be appropriate for the above-mentioned ones. We have computed a variety of optical constants in an approach to reveal the optical response of these carbides when electromagnetic radiation is incident upon them.

To estimate the optical properties, it is essential to use the equation 3.40-3.47. To study the dielectric function regarding metallic compounds, a drude correction must be made, which is often accomplished by first-principles calculations by including the plasma frequency and a broadening factor [41, 42]. Owing to the metallic nature of the studied carbides, a damping and plasma frequency of 0.05 eV and 3 eV, respectively, were used to enhance the computed spectra' lower energy side. Moreover, a Gaussian smearing value of 0.5 eV was also used to smear out the k-points around the Fermi level. The calculated optical constants of the titled phases are presented in Fig. 4.5, along with those of Nb₂AC (A = P, In, Cd, Al) for comparison. The real part $\epsilon_1(\omega)$ of the dielectric function, where the low energy peaks are attributed to electron intra-band transitions [43], is shown in Fig. 4.5(a). Because of the electron intra-band transitions, the assigned value for each peak is less than 1 eV. The materials exhibit Drude-like behavior, as indicated by the massive negative values of $\epsilon_1(\omega)$, whereas inter-band transitions occur at higher energies. Fig. 4.5(b) shows the imaginary part of the dielectric function $\epsilon_2(\omega)$. At around 16 eV, it has been seen that the values of $\epsilon_2(\omega)$ pass through zero from above. This is another example of the compound's metallic nature. A similar nature of the real and imaginary part of the dielectric function was reported for the most studied MAX phase, Ti₃SiC₂ [40], and widely used 211 MAX phase Ti₂AlC [44]. The

refractive index, $n(\omega)$, of Nb₂AC (A= Ga, Ge, Tl, Zn, P, In, Cd, Al) is depicted in Fig. 4.5(c). This significant optical constant contributes to the design of optical systems like photonic crystals and waveguides. As shown in Fig. 4.5(c), the static value of $n(\omega)$ for Nb₂AC (A = Ga, Ge, Tl, Zn, P, In, Cd, Al) are 7.0, 8.9, 9.4, 11, 8.3, 10.9, 9.5 and 8.9 respectively. Fig. 4.5(d) shows the extinction coefficient, $k(\omega)$, for the Nb₂AC (A= Ga, Ge, Tl, Zn, P, In, Cd, Al) MAX phases. The extinction coefficient, $k(\omega)$, is used for measuring the loss of electromagnetic radiation due to absorption and is found to vary similarly to $\varepsilon_2(\omega)$, like other MAX phases [42, 43]. In Fig. 4.5(e), the absorption coefficient of Nb₂AC (A= Ga, Ge, Tl, Zn, P, In, Cd, Al) Due to the researched compounds' metallic nature, MAX phases—where the spectra are seen increasing from zero photon energy—are illustrated. The spectra are seen to increase as incident energy increases. It showed the strongest absorption region in the spectral range of 7-10 eV; it decreases with a further increase in photon energy. Because of the high absorption coefficients in the high energy range (7-10eV), Nb₂AC (A = Ga, Ge, Tl, Zn, P, In, Cd, Al) MAX phases can be considered potential absorbing materials in this energy range. The photoconductivity of Nb₂AC (A= Ga, Ge, Tl, Zn, P, In, Cd, Al) is shown in Fig. 4.5(f), which is also found to initiate at the beginning from zero photon energy owing to the metallic behavior of the selected phases. The band structure and electronic DOS results are consistent with the photoconductivity and absorption coefficient results.

In order to reduce solar heating, MAX phases are applied as coating materials, one of their most significant applications. The reflectivity of the target materials has been investigated to disclose this possibility, shown in Fig. 4.5(g). It was reported by Li *et al.* [40, 45] that if a MAX compound has a reflectivity of 44% in the visible range, it will be able reducing solar heating. The reflectivity spectrum for Nb₂GaC begins with a value of 0.569 (56.9%), the minimum value among the studied phases. Nb₂TlC has the highest value, which is 0.982 (98.2%). For Ti₃SiC₂, the spectrum has an initial value of ~0.75 (75%), going down at around 1 eV and then remaining almost constant up to 6 eV, whereas it is for Nb₂AlC, it is started with



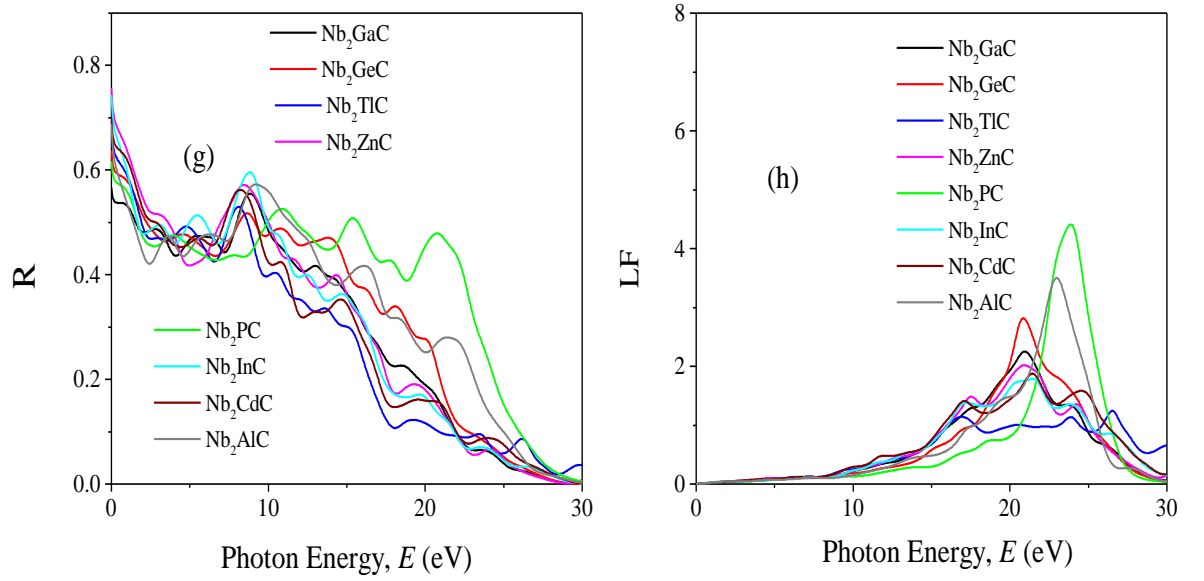


Fig. 4.5: (a) real part (ϵ_1) and (b) imaginary part (ϵ_2) of dielectric function (ϵ), (c) refractive index (n), (d) extinction coefficient (k), (e) absorption coefficient (α), (f) photoconductivity (σ), (g) reflectivity (R) and (h) loss function (LF) of Nb₂AC (A= Ga, Ge, Ti, Zn, P, In, Cd, Al) MAX phases as a function of photon energy calculated using GGA PBEsol.

an initial value of 0.68 (68%), which is down to below 44% at around 2.1 eV. Though Nb₂AC (A = Ga, Ge, P) has a lower initial value of R than Nb₂AlC, neither of these spectra is down to less than 44% up to the visible light range. However, each spectrum of the titled compounds exhibits average higher values (also higher than 44% up to visible light range) than that of Nb₂AlC. Thus, in comparison with Ti₃SiC₂ and Nb₂AlC, it can be concluded that for usage as cover materials to lessen solar heating, Nb₂AC (A= Ga, Ge, Ti, Zn, P, In, and Cd) compounds are suitable.

In the energy range of 5.5 to 11 eV, there are a few sharp peaks in the reflectivity spectra and around 30 eV, reflectivity finally approaches zero. When electrons move through materials, they lose their energy. An optical constant called the loss function is used to evaluate this type of energy loss. Fig. 4.5(h) displays the calculated loss functions for the aforementioned MAX phase compounds. The loss function's peak frequency is referred to as the plasma frequency (ω_p), which is seen at 20.89, 20.92, 16.38, 17.50, 23.91, 20.54, 17.21 and 23.11 for Nb₂GaC, Nb₂GeC,

Nb₂TiC, Nb₂ZnC, Nb₂PC, Nb₂InC, Nb₂CdC, and Nb₂AlC, respectively. In a loss function, this energy is determined by its characteristic frequency when $\varepsilon_1(\omega)$ and $\varepsilon_2(\omega)$ both pass through zero from below and above, respectively. Reflectivity also identifies the falling edges. This is the critical value ‘the plasma frequency’ establishes when the materials are transformed into transparent dielectric from the metallic system. We have also calculated the optical constant using GGA PBE, but shown due to similar nature.

4.6 Thermal Properties

MAX phases are excellent candidates for applications at high-temperature because of their excellent mechanical properties at high temperatures. Therefore, studying the basic parameters required to predict their application carries significant interest. The Debye temperature (Θ_D), Grüneisen parameter (γ), minimum thermal conductivity (K_{min}), melting temperature (T_m), etc., of the researched compounds, have been calculated for predicting their high-temperature applications.

The relevant formulae are calculated by using 3.48-3.51 equations. The calculated Θ_D of Nb₂AC (A = Ga, Ge, Ti, Zn, P, In, Cd, Al) is presented in Table 4.6(a) for GGA PBEsol and Table 4.6(b) for GGA PBE.

As shown in Table 4.6(a) and 4.6(b), Θ_D is highest for Nb₂PC and lowest for Nb₂TiC. The ranking of the compounds roughly followed the hardness-based ranking, which fairly agrees with the hardness and Debye temperature relationship [46]. The Θ_D of the titled compounds is lower than that of Nb₂AlC, except Nb₂PC. Recently, Hadi *et al.* [47] reported a MAX (V₂SnC) phase as TBC material with a Θ_D value of 472 K. Among the studied compounds, a much lower Θ_D is found for only Nb₂TiC (372 K) and Nb₂CdC (424 K); others have comparable or higher Θ_D than V₂SnC. In addition, the Θ_D of Y₄Al₂O₉, a well-known TBC material, is 564 K [49]. Thus, Θ_D of Nb₂AC (A = P, Al, Ga, Ge) phases [Table 4.6(a) and 4.6(b)] are comparable with that of Y₄Al₂O₉ [49].

Table 4.6(a): Calculated density (ρ), longitudinal, transverse, and average sound velocities (v_l , v_t , and v_m , respectively), Debye temperature (Θ_D), minimum thermal conductivity (K_{min}), and Grüneisen parameter (γ), calculated values using GGA PBEol [9] of Nb₂AC (A= Ga, Ge, Tl, Zn), along with those of Nb₂AC (A = P, In, Cd, Al) MAX phases.

Phases	ρ (g/cm ³)	v_l (m/s)	v_t (m/s)	v_m (m/s)	Θ_D (K)	K_{min} (W/mk)	γ	T_m (K)	Ref.
Nb ₂ GaC	7.59	6931	4106	4547	548	1.05	1.41	1913	This
Nb ₂ GeC	7.76	6596	3607	4022	485	0.93	1.71	1715	This
		6632	3695	4114	508	*0.95	*1.66	*1737	[6]
Nb ₂ TlC	10.18	5244	2872	3202	372	0.68	1.71	1590	This
Nb ₂ ZnC	7.43	6248	3440	3834	461	0.88	1.66	1574	This
Nb ₂ PC	8.28	7337	4297	4764	640	1.29	1.45	2171	This
Nb ₂ InC	11.49	5311	3121	3459	483	0.95	1.41	1790	This
Nb ₂ CdC	8.06	5855	3247	3616	424	0.79	1.65	1587	This
Nb ₂ AlC	6.34	7315	4405	4871	592	1.46	*1.37	1800	[47]

*calculated values using reported data.

Table 4.6(b): Calculated density (ρ), longitudinal, transverse, and average sound velocities (v_l , v_t , and v_m , respectively), Debye temperature (Θ_D), minimum thermal conductivity (K_{min}), and Grüneisen parameter (γ), calculated values using GGA PBE [8] of Nb₂AC (A= Ga, Ge, Tl, Zn), along with those of Nb₂AC (A = P, In, Cd, Al) MAX phases.

Phases	ρ (g/cm ³)	v_l (m/s)	v_t (m/s)	v_m (m/s)	Θ_D (K)	K_{min} (W/mk)	γ	T_m (K)	Ref.
Nb ₂ GaC	7.59	6660	3959	4031	533	0.91	1.41	1799	This
Nb ₂ GeC	7.76	6064	3129	3239	428	0.75	2.06	1479	This
Nb ₂ TlC	10.18	4975	2714	2794	354	0.59	1.71	1502	This
Nb ₂ ZnC	7.43	6098	3382	3480	457	0.79	1.66	1553	This
Nb ₂ PC	8.28	7140	4227	4682	736	1.81	1.41	2058	This
Nb ₂ InC	11.49	5074	2978	3301	492	1.15	1.45	1667	This
Nb ₂ CdC	8.06	5584	3130	3484	411	0.76	1.60	1487	This
Nb ₂ AlC	6.34	7612	4580	5065	612	1.42	2.45	1898	This

*calculated values using reported data.

The value of thermal conductivity that remains constant at high temperatures is referred to as the minimum thermal conductivity (K_{min}). As its name suggests, this conductivity is minimum owing to the breaking of the pairing of phonons at high temperatures. Calculation of minimum thermal conductivity is essential for predicting the use of solids at high temperatures. It has already been established that the MAX phases are suitable for high-temperature technology as a coating layer (TBC). Thus, the calculation of K_{min} is also required for the titled phases. We have calculated the K_{min} of Nb_2AC ($A = Ga, Ge, Ti, Zn, P, In, Cd, Al$) compounds by using the 3.52 equation, as listed in Table 4.6(a) and 4.6(b). The order of the value K_{min} is expected to be as follows: $Nb_2AlC > Nb_2PC > Nb_2GaC > Nb_2InC > Nb_2GeC > Nb_2ZnC > Nb_2CdC > Nb_2TiC$, i.e., the K_{min} of the studied compounds are lower than that of Nb_2AlC , indicating more suitability of the phases as smaller the K_{min} is, more suitable as TBC materials. It should be noted that the K_{min} of V_2SnC is $1.20 \text{ Wm}^{-1}\text{K}^{-1}$, and $Y_4Al_2O_9$ is $1.13 \text{ Wm}^{-1}\text{K}^{-1}$ [47, 50]. Thus, the K_{min} value is expected to suggest the studied compounds as suitable TBC materials.

An essential thermal parameter that helps to explain the anharmonic effects of lattice dynamics is the Grüneisen parameter (γ); lower anharmonic effects are expected for the solids used in high temperatures. Therefore, we have calculated γ of Nb_2AC ($A = Ga, Ge, Ti, Zn, P, In, Cd, Al$) compounds by using the 3.53 equation. According to Table 8, the obtained values of γ lie between 0.85 and 3.53, which is in line with what is predicted for the polycrystalline materials with v values in the range of 0.05-0.46 [51]. Besides, the low values of γ confirm the lower anharmonic effects in the selected compounds, like other MAX phase materials [52].

Finally, we calculated the melting temperature (T_m) of the studied compounds using through the 3.54 equation listed in Table 4.6(a) and 4.6(b). The melting temperature of the solids mainly depends on atomic bonding strength; the stronger the atomic bonding, the higher the T_m . Thus, a close relationship between T_m and Y is expected [47, 49], and the order of T_m for titled phases is found to be followed the Y -based ranking of the phases. It is seen from Table 4.6(a) and 4.6(b) that the T_m of Nb_2AC ($A = Ge, Ti, Zn, In, Cd$) is lower than that of the Nb_2AlC but still higher than

that of V_2SnC (1533 K) MAX phase, a known TBC material [47]. In addition, the T_m of Nb_2AC ($A = \text{Ga}, \text{P}$) is not only higher than that of Nb_2AlC [48] but also comparable to that of $\text{Y}_4\text{Al}_2\text{O}_9$ (2000 K). Though the T_m of Nb_2AC ($A = \text{Ge}, \text{Tl}, \text{Zn}, \text{In}, \text{Cd}$) is lower than $\text{Y}_4\text{Al}_2\text{O}_9$ (2000 K) but still reasonably high. Thus, based on the values of Θ_D , K_{min} , and T_m of the studied phases, in comparison with those of $\text{Y}_4\text{Al}_2\text{O}_9$ and some other MAX phases that have already been reported as TBC materials, we conclude that the titled phases can be considered as potential TBC materials.

References:

- [1] M. W. Barsoum, *The $M_{n+1}AX_n$ phases: a new class of solids: thermodynamically stable nanolaminates*, Prog Solid-State Chem 28 (2000) 201-81.
- [2] G. Hug, M. Jaouen, M. W. Barsoum, *X-ray absorption spectroscopy, EELS, and full-potential augmented plane wave study of the electronic structure of Ti_2Al_3 , Ti_2AlN , Nb_2AlC and $(Ti_{0.5}Nb_{0.5})_2AlC$* , Phys. Rev. B: Condens. Matter 71 (2005) 024105.
- [3] G. Hug, *Electronic structures of and composition gaps among the ternary carbides Ti_2MC* , Phys. Rev. B74 (2006) 184113.
- [4] M. B. Kanoun, S. Gourmi-said, M. Jaouen, *Steric effect on the M site of nanolaminate compounds M_2SnC ($M = Ti, Zr, Hf$ and Nb)*, Phys. Condens. Matter 21 (2009) 045404.
- [5] M. A. Hadi, S. R. G. Christopoulos, A. Chroneos, S. H. Naqib, A. K. M. A. Islam, *Elastic behaviour and radiation tolerance in Nb-based 211 MAX phases*, Mater. Today Communi.25 (2020) 101499.
- [6] A. Bouhemadou, *Calculated structural, electronic and elastic properties of M_2GeC ($M = Ti, V, Cr, Zr, Nb, Mo, Hf, Ta$ and W)*, Appl. Phys. A 96 (2009) 959-967.
- [7] I. R. Shein, A. L. Ivanovskii, *Structural, elastic, electronic properties and Fermi surface for superconducting Mo_2GaC in comparison with V_2GaC and Nb_2GaC from first principles*, Physica C 470 (2010) 533-537.
- [8] J. P. Perdew, K. Burke, M. Ernzerhof, *Generalized gradient approximation made simple*, Phys. Rev. Lett. 77 (1996) 3865.
- [9] J. P. Perdew, A. Ruzsinszky, G. I. Csonka, O. A. Vydrov, G. E. Scuseria, L. A. Constantin, X. Zhou, K. Burke, *Restoring the density-gradient expansion for exchange in solids and surfaces*, Phys. Rev. Lett. 100 (2008) 136406.
- [10] A.D. Bortolozzo, Z. Fisk, O.H. Sant' Anna, C.A.M. dos Santos, A. J. S. Machado, *Superconductivity in Nb_2InC* , Physica C 469 (2009) 57.
- [11] M. A. Ali, A. K. M. A. Islam, *$Sn_{1-x}Bi_xO_2$ and $Sn_{1-x}Ta_xO_2$ ($0 \leq x \leq 0.75$): A first-principles study*, Phys. B Condens. Matter. 407 (2012) 1020–1026.
- [12] M. Born, *On the stability of crystal lattices. I*, Math. Proc. Cambridge Philos. Soc. 36 (1940) 160–172.

- [13] Z. Sun, D. Music, R. Ahuja, J. M. Schneider, *Theoretical investigation of the bonding and elastic properties of nanolayered ternary nitrides*, Phys. Rev. B 71 (2005) 193402.
- [14] S. H. jhi, J. Ihm, S. G. Louie, M. L. Cohen, *Electronic mechanism of hardness enhancement in transition-metal carbonitrides*, Nature 399 (1999) 132-134.
- [15] D. G. Pettifor, *Theoretical predictions of structure and related properties of intermetallics*, J Mater. Sci. Tech. 8 (1992) 345-9.
- [16] M. W. Qureshi, M. A. Ali, X. Ma, *Screen the thermomechanical and optical properties of the new ductile 314 MAX phase boride Zr_3CdB_4 : A DFT insight*, J. Alloys Compd. 877 (2021) 160248.
- [17] M. Roknuzzaman, M. A. Hadi, M. J. Abden, M. T. Nasir, A. K. M. A. Islam, M. S. Ali, K. Ostrikov, S. H. Naqib, *Physical properties of predicted Ti_2CdN versus existing Ti_2CdC MAX phase: An ab initio study*, Comput. Mater. Sci. 113 (2016) 148–153.
- [18] M. W. Qureshi, M. A. Ali, X. Ma, G. Tang, M. U. Javed, D. Paudyal, *Verification of stability and unraveling the electronic and physical properties of bulk and (001)-surfaces of newly synthesized Ti_2ZnX ($X = C, N$) MAX phases*, Surf. And Interf. 31 (2022) 102032.
- [19] R. Hill, *The elastic behaviour of a crystalline aggregate*, Proc. Phys. Soc. Sect. A. 65 (1952) 349–354.
- [20] W. Voigt, *Lehrbuch der Kristallphysik* (Teubner, Leipzig, 1928).
- [21] A. Reuss, *Berechnung der fließgrenze von mischkristallen auf grund der plastizitätsbedingung für einkristalle*, ZAMM-J.Appl.Math.Mech./ Zeitschrift Für Angew. Math. Und Mech. 9 (1929) 49–58.
- [22] X. Wang, H. Xiang, X. Sun, J. Liu, F. Hou, Y. Zhou, *Mechanical properties and damage tolerance of bulk $Yb_3Al_5O_{12}$ ceramic*, J. Mater. Sci. Technol. 31 (2015) 369-374.
- [23] M. A. Ali, A. K. M. A. Islam, N. Jahan, S. Karimunnesa, *First-principles study of SnO under high pressure*, Int J Mod Phys B 30 (2016) 1650228.
- [24] M. Radovic, M. W. Barsoum, *MAX phases: Bridging the gap between metals and ceramics*, Am. Ceram. Soc. Bull. 92 (2013) 20–27.
- [25] M. Mebrek, A. Mokaddem, B. Doumi, A. Yakoubi, A. Mir, *A novel theoretical study of elastic and electronic properties of M_2CdC ($M = Zr, Hf, \text{ and } Ta$) MAX phases*, Acta Phys. Pol. A 133 (2018) 76–81.

- [26] S. F. Pugh, *Relations between the elastic moduli and the plastic properties of polycrystalline pure metals*, XCII. Philos. Mag. J. Sci. 45 (1954) 823–843.
- [27] M. Roknuzzaman, M. A. Hadi, M. A. Ali, M. M. Hossain, N. Jahan, M. M. Uddin, J. A. Alarco, K. Ostrikov, *First hafnium-based MAX phase in the 312 family, Hf_3AlC_2 : A first-principles study*, J. Alloys Compd. 727 (2017) 616–626.
- [28] I. R. Shein, A. L. Ivanovskii, *Graphene-like titanium carbides and nitrides $\text{Ti}_{n+1}\text{C}_n$, $\text{Ti}_{n+1}\text{N}_n$ ($n = 1, 2$, and 3) from de-intercalated MAX phases: First-principles probing of their structural, electronic properties and relative stability*, Comput. Mater. Sci. 65 (2012) 104.
- [29] I. R. Shein, A. L. Ivanovskii, *Elastic properties of superconducting MAX phases from first-principles calculations*, Phys. Status Solidi B 248 (2011) 228–232.
- [30] M. F. Cover, O. Warschkow, M. M. M. Bilek, D. R. McKenzie, *A comprehensive survey of M_2AX phase elastic properties*, J. Phys. Condens. Matter 21 (2009) 305403.
- [31] H. Gou, L. Hou, J. Zhang, F. Gao, *Pressure-induced incompressibility of ReC and effect of metallic bonding on its hardness*, Appl. Phys. Lett. 92 (2008) 2419.
- [32] P. Barua, M. M. Hossain, M. A. Ali, M. M. Uddin, S. H. Naqib, A. K. M. A. Islam, *Effects of transition metals on physical properties of M_2BC ($\text{M} = \text{V}, \text{Nb}, \text{Mo}$ and Ta): a DFT calculation*, J. Alloy. Compd. 770 (2018) 523–534.
- [33] Y. Zhou, Z. Sun, *Electronic structure and bonding properties of layered machinable and ceramics*, Phys. Rev. B - Condens. Matter Phys. 61 (2000) 12570–12573.
- [34] M. A. Ali, S. H. Naqib, *Recently synthesized $(\text{Ti}_{1-x}\text{Mo}_x)_2\text{AlC}$ ($0 \leq x \leq 0.20$) solid solutions: deciphering the structural, electronic, mechanical and thermodynamic properties via ab initio simulations*, RSC Adv. 10 (2020) 31535–31546.
- [35] A. Chowdhury, M. A. Ali, M. M. Hossain, S. H. Naqib, A. K. M. A. Islam, *Predicted MAX phase Sc_2InC : dynamical stability, vibrational and optical properties*, Phys. Stat. Sol. B 255 (2018) 1700235.
- [36] H.M. Ledbetter, A. Migliori, *A general elastic-anisotropy measure*, J. Appl. Phys. 100 (2006) 063516.
- [37] J. Chang, G. P. Zhao, X. L. Zhou, K. Liu, L. Y. Lu, *Structure and mechanical properties of tantalum mononitride under high pressure: a first-principles study*, J. Appl. Phys. 112 (2012) 083519.

- [38] R. Gaillac, P. Pullumbi, F. X. Coudert, *ELATE: an open-source online application for analysis and visualization of elastic tensors*, J. Phys. Condens. Matter 28 (2016) 275201.
- [39] M. A. Ali, M. A. Hossain, M. A. Rayhan, M. M. Hossain, M. M. Uddin, M. Roknuzzaman, K. Ostrikov, A. K. M. A. Islam, S. H. Naqib, *First-principles study of elastic, electronic, optical and thermoelectric properties of newly synthesized $K_2Cu_2GeS_4$ chalcogenide*, J. Alloys Compd. 781 (2018) 37–46.
- [40] S. Li, R. Ahuja, M. W. Barsoum, P. Jena, B. Johansson, *Optical properties of Ti_3SiC_2 and Ti_4AlN_3* , Appl. Phys. Lett. **92**, 221907 (2008).
- [41] M. T. Nasir, M. A. Hadi, M. A. Rayhan, M. A. Ali, M. M. Hossain, M. Roknuzzaman, *First-principles study of superconducting $ScRhP$ and $ScIrP$ pnictides*, Phys. Stat. Sol. B 254 (2017) 1700336.
- [42] F. Sultana, M. M. Uddin, M. A. Ali, M. M. Hossain, S. H. Naqib, A. K. M. A. Islam, *First principles study of M_2InC ($M = Zr, Hf$ and Ta) MAX phases: the effect of M atomic species*, Results Phys. 11 (2018) 869-76.
- [43] K. Akter, F. Parvin, M. A. Hadi, A. K. M. A. Islam, *Insights into the predicted Hf_2Sn in comparison with the synthesized MAX phase Hf_2SC : a comprehensive study*, Comput. Condens Matt. 24 (2020) e00485.
- [44] N. Haddad, E. G. Caurel, L. Hultman, M. W. Barsoum, G. Hug, *Dielectric Properties of Ti_2AlC and Ti_2AlN MAX Phases: The Conductivity Anisotropy*, J. Appl. Phys. 104 (2008) 023531.
- [45] M. A. Ali, M. W. Qureshi, *Newly synthesized MAX phase Zr_2SeC : DFT insights into physical properties towards possible applications*, RSC Adv. 11 (2021) 16892.
- [46] M. A. Ali, M. M. Hossain, M. M. Uddin, M. A. Hossain, A. K. M. A. Islam, S. H. Naqib, *Physical properties of new MAX phase borides M_2SB ($M = Zr, Hf$ and Nb) in comparison with conventional MAX phase carbides M_2SC ($M = Zr, Hf$ and Nb): Comprehensive insights*, j. Mater. Res. Tech. 11 (2021) 1000-1018.
- [47] M. A. Hadi, M. Dahlqvist, S. R. G. Christopoulos, S. H. Naqib, A. Chroneos, A. K. M. A. Islam, *Chemically stable new MAX phase V_2SnC : a damage and radiation tolerant TBC material*, RSC. Adv. 10 (2020) 43783-43798.

- [48] M. A. Hadi, N. Kelaidis, S. H. Naqib, A. K. M. A. Islam, A. Chroneos, R. V. Vovk, *Insights into the physical properties of a new 211 MAX phase Nb₂CuC*, J. Phys. Chem. Solids 149 (2020) 109759.
- [49] Y. Zhou, X. Lu, H. Xiang, Z. Feng, Z. Li, *Theoretical prediction on mechanical and thermal properties of a promising thermal barrier material: Y₄Al₂O₉*, J. Adv. Ceram. 4 (2015) 83-93.
- [50] G. A. Slack, *The thermal conductivity of nonmetallic crystals*, Solid Stat. Phys. 34 (1979) 1–71.
- [51] S. I. Mikitishin, *Interrelationship of Poisson's ratio with other characteristics of pure metals*, Sov. Mater. Sci. 18 (1982) 262–265.
- [52] V. N. Belomestnykh, E. P. Tesleva, *Interrelation between anharmonicity and lateral strain in quasi-isotropic polycrystalline solids*, Tech. Phys. 49 (2004) 1098–1100.

CHAPTER-5

KEY FINDINGS AND CONCLUSIONS

5.1 General

The first-principles computations were carried out to study the 211 MAX phase carbides: Nb₂AC (A = Ga, Ge, Ti, Zn), and we have compared our studied phases with other MAX phases which are Nb₂AC (A = P, In, Cd, Al). We have discovered some including observations regarding the Nb₂AC (A = Ga, Ge, Ti, Zn, P, In, Cd, Al) MAX phase carbides by investigating computationally derived constants.

5.2 Key Findings

The key findings can be summarized in the following points:

- ❖ In the case of lattice constants, an excellent consistency is observed for the previously studied phases, indicating the reliability of our present calculations. The distortion of the polyhedron is measured by the deviation from 1, where a low distortion value indicates a more stable structure.
- ❖ None existence of the negative frequency in phonon dispersion curves suggests that all title carbides are dynamically stable. The PHDOS is presented alongside the PDCs, wherein the PDC's flat modes lead the sharp peaks, and peaks are diminished when the dispersion changes, either upward or downward.
- ❖ The studied phases are mechanically stable compounds based on the computed elastic constants, C_{ij} . Moreover, the inequality of C_{11} and C_{33} also indicates the anisotropic bonding strength. Nb₂PC is expected to be the hardest with the highest C_{44} (194 GPa), while Nb₂TiC is the softest with the lowest C_{44} (71 GPa). Nb₂GaC, Nb₂GeC, Nb₂PC, Nb₂InC, and Nb₂AlC behave as brittle solids. On the contrary, Nb₂TiC, Nb₂ZnC, and Nb₂CdC phases behave as ductile solids. When compared to the other titled carbides MAX

phases, Nb₂PC has the largest bulk modulus (B), shear modulus (G), and Young elastic modulus (Y).

- ❖ The electronic band structure along with DOS confirm the metallic nature with a dominating contribution from Nb-3*d* states. Partial DOS discloses strong hybridization between Nb-*d* and C-2*p* states. Mulliken's population analysis reveals the existence of both ionic bonds and covalent bonds within the studied compounds.
- ❖ The calculated anisotropy indices values and 2D and 3D graphs of Young's modulus, compressibility, shear modulus, and Poisson's ratio demonstrate the anisotropic behavior of the titled compounds.
- ❖ The $\epsilon_1(\omega)$, $\epsilon_2(\omega)$, absorption spectra, and photoconductivity spectra confirmed the compound's metallic nature, consistent with band structure results. It is possible to utilize them as coating materials that diminish solar heating, as indicated by the reflectivity spectra. The low value of K_{min} and comparatively higher melting temperature with reasonable Debye temperature suggests the studied compounds as the TBC material.

Limitations of the Study

The calculation of the formation energy using competing phases and the study of 2D phases (MXene) were not considered. Future research may reveal important information for their applications in various sectors. In addition, study of boride MAX phases [substitution of C by B] may also exhibit better physical properties for diverse applications.

Practical Implication

The results found in this study are encouraging and hope to attract attention from the scientific community. We expect that the findings of this study will encourage further research into the synthesis of C-containing MAX phases and the physical

properties of the titled phases towards prospective applications in various future sectors.

Recommendation for Further Study

The potential of MXene and particular surfaces can suggest that the targeted phases have higher application possibilities.

See discussions, stats, and author profiles for this publication at: <https://www.researchgate.net/publication/368387866>

DFT insights into Nb-based 211 MAX phase carbides: Nb₂AC (A = Ga, Ge, Tl, Zn, P, In, and Cd)

Article in RSC Advances · February 2023

CITATIONS

0

READS

40

3 authors, including:



Nusrat Jahan

Chittagong University of Engineering & Technology

30 PUBLICATIONS 285 CITATIONS

[SEE PROFILE](#)



Md. Ashraf Ali

Chittagong University of Engineering & Technology

115 PUBLICATIONS 1,407 CITATIONS

[SEE PROFILE](#)

Some of the authors of this publication are also working on these related projects:



First principles study of 211 MAX phase carbides: Nb₂AC (A = P, Zn, Ga, Ge, Cd, In, Tl) [View project](#)



ReB₂C₂ (Re=Sc, Y, lanthanides and actinides) phases. [View project](#)


Cite this: *RSC Adv.*, 2023, 13, 5538

DFT insights into Nb-based 211 MAX phase carbides: Nb₂AC (A = Ga, Ge, Tl, Zn, P, In, and Cd)†

Prima Das, N. Jahan * and M. A. Ali *

In this study, we performed the first-principles calculations to study the 211 MAX phase carbides: Nb₂AC (A = Ga, Ge, Tl, Zn, P, In, Cd, and Al). The structural characteristics are in good agreement with those of the prior studies. The mechanical behavior has been explored by calculating the stiffness constants, elastic moduli, and Vickers hardness. The stiffness constants and phonon dispersion curves were used to check the structural stability of the selected compounds. 2D and 3D plotting of elastic moduli and calculated anisotropy indices disclosed the anisotropy of the elastic properties. We utilized the Mulliken atomic and bond overlap population to explain the mixture of ionic and covalent bonding among these carbides. The metallic behavior has been confirmed by calculating the band structure and density of states (DOS). Partial DOS was also used to discuss the bonding nature and strength among the different states. The optical properties of these phases have also been computed and analyzed to reveal possible relevance in diverse fields. The Debye temperature (Θ_D), Grüneisen parameter (γ), melting temperature (T_m), and minimum thermal conductivity (K_{min}) were studied to bring out their possible relevance in high-temperature technology. The outcomes of this research indicate that the titled carbides are suitable for use as solar radiation-protecting coating and thermal barrier coating (TBC) materials.

Received 23rd November 2022

Accepted 1st February 2023

DOI: 10.1039/d2ra07468k

rsc.li/rsc-advances

1 Introduction

Many ternary compounds such as carbides, nitrides, and borides have been included in the MAX phase materials family and can be expressed as M_{n+1}AX_n, where M belongs to the early transition metal group, A is the element that exists within the groups 12–16, and X can only be C, N, and B, and n is a positive integer with a value of 1–3.^{1–4} The MAX phase was first revealed in the 1960s by Nowotny *et al.*^{1–4} In the 1990s, Barsoum *et al.*^{5,6} renewed the interest by revealing their remarkable characteristics. They have remarkable mechanical strength, machinability, electronic conductivity, and thermal conductivity. They are also machinable, similar to metals, have better mechanical properties at high temperatures, and have superior corrosion and oxidation resistance including ceramics.⁷ The MAX phase family has become a significant materials group from both research and application points of view. Owing to the magnificent fusing of metallic and ceramic properties, the number of published articles is increasing day by day.⁸

Use of C and N as X elements was confined for a long time^{9–11} and has been extended recently, where B has been used as an X element. The extension has opened a new platform for the MAX phase materials, owing to the interesting properties and

potential applications of B and B-containing compounds.^{12,13} To date, only a few of the MAX phase borides have been synthesized so far in spite of a large number of predicted phases.¹⁴ On the contrary, a significant number of MAX phase carbides have already been synthesized and characterized, revealing their prospective applications. In parallel to the experimental study, a large number of computational approaches^{15,16} have also already been performed throughout the last decades. Cover *et al.*¹⁷ performed the first-principles calculation of the elastic properties of 240 elemental combinations, revealing the role of A elements and their interaction with M elements. Keast *et al.*¹⁸ computed the total energies of competing phases to check the stability of five different schemes (Cr_{n+1}-Al-C_n, Ti_{n+1}-Al-C_n, Ti_{n+1}-Si-N_n, Ti_{n+1}-Al-N_n, and Ti_{n+1}-Si-C_n, where n is a positive integer with a value of 1 ~ 4). Aryal *et al.*¹⁹ studied 792 MAX phases, and 665 phases were found to be thermodynamically and elastically stable. 10 314 solid solutions and 216 possible M₂AX phases were revealed by Ashton *et al.*²⁰ Khaledialidusti *et al.*²¹ explored a large group of MAX phases, where M is taken as Sc, Ti, Y, Zr, V, Cr, Nb, Hf, Ta, Mo, and W and A is taken as P, S, Al, Si, Zn, Cu, Ga, As, Ge, Sn, Cd, In, Bi, Ir, Tl, Au, and Pb, and revealed their possibility of exfoliation to produce 2D systems. More than 80 MAX phases have been synthesized, most of which are 211 phases (58 prominent members).²² These studies have inspired us to think about Nb-based 211 MAX phases.

Nb-based 211 MAX phases have also attracted attention in recent years. For example, Nb₂AC (A = Al, Ge, Ga, Sn, In, As, P, S, and Cu) MAX phases were studied by Hadi *et al.*²³ to explore the

Department of Physics, Chittagong University of Engineering and Technology (CUET), Chattogram-4349, Bangladesh. E-mail: nusrat83@cuet.ac.bd, dashrafphy31@cuet.ac.bd

† Electronic supplementary information (ESI) available. See DOI: <https://doi.org/10.1039/d2ra07468k>



elastic behavior and radiation tolerant behavior. Superconducting nature has been found in the Nb₂SnC, Nb₂InC, Nb₂AsC, and Nb₂SC phases²³ with the lowest superconducting temperature for Nb₂AsC.²² Bouhemadou *et al.*^{24,25} performed first-principles calculations to study the structural and elastic properties of Nb₂InC and Nb₂GeC. The Nb₂InC phase was first synthesized by Jeitschko *et al.*²⁶ Nb₂AlC has attracted much attention as a viable material because of its better mechanical and thermal properties.^{27,28} When compared with several MAX phases, it has been seen that Nb₂PC has higher elastic constants.¹⁷ The exfoliation possibility of Nb₂GaC and Nb₂InC into 2D MXene systems has been reported.²⁹ The electrochemical properties of Nb₂SnC have been investigated for use in a Li-ion electrolyte.³⁰ The noble transition metal Cu has also been selected as an A element in Nb₂CuC.³¹ Shein *et al.*³² explored the structural, electrical, and elastic properties of M₂GaC (M = Mo, V, and Nb). Cover *et al.*¹⁷ studied only the elastic and structural properties of Nb₂SiC, whereas some fundamental properties need to be investigated. Bouhemadou *et al.*³³ carried out a theoretical study to calculate the structural, elastic, electronic, and thermal properties of Nb₂SiC.

Moreover, so far, we know only the electronic and mechanical characteristics of Nb₂AC (A = Ga, Ge, P, and In) phases have been investigated, whereas Nb₂AC (A = Ti, Zn, and Cd) phases have been predicted to be stable *via* the calculation of formation energy,²¹ and the physical properties are not disclosed yet. Exploration of the physical properties of new materials carries the same significance as prediction of new materials: it is impossible to take any advantage of new materials unless their physical properties are brought out. Several essential physical aspects, important optical properties, mechanical anisotropy, Vickers hardness including Mulliken populations, and thermal properties of Nb₂AC (A = Ga, Ge, P, and In) are still unexplored. Mechanical anisotropy is critical for structural materials since it is linked to important mechanisms such as crack formation (and propagation), plastic deformation, and elastic instability, all of which limit their utility. The Vickers hardness describes the total strength properties of a solid's particular bonds. Mulliken population analysis is important to prove the existence of the combination of the ceramic and metallic nature. Understanding the thermal properties is important to forecast their appropriateness for use in extreme conditions. The optical characteristics of standard MAX phase compounds are necessary to predict their possible applications, for instance, as coating materials for protection from solar heating. These are the motivations behind this study, which demonstrates the significance of in-depth research on MAX phase carbides Nb₂AC (A = Ga, Ge, Ti, Zn, P, In, and Cd).

Therefore, we aimed to provide a theoretical insight into the MAX phase carbides Nb₂AC (A = Ga, Ge, Ti, Zn, P, In, and Cd), in which we will consider the first-time investigation of Nb₂AC (A = Ti, Zn, and Cd) and some important unexplored properties of Nb₂AC (A = Ga, Ge, P, and In) phases. Last of all, the calculated parameters of the titled phases are compared with those of the most known Nb-based phase, Nb₂AlC, to make this research a systematic one.

2 Computational methodology

The Nb₂AC (A = Ga, Ge, Ti, Zn, P, In, and Cd) carbides' physical properties have been calculated using the pseudopotential-based DFT, implemented in CASTEP (Cambridge Serial Total Energy Package).^{34,35} For the term of exchange-correlation, the GGA (generalized gradient approximation) of the PBE (Perdew–Burke–Ernzerhof)³⁶ and PBEsol (Perdew–Burke–Ernzerhof for solids)³⁷ were used. The PBE has been widely used for DFT calculations, whereas PBEsol gives a more accurate lattice constant for solids.³⁸ Recently, the effect of different functionals on the calculated values of the parameters has been reported, in which it is seen that the PBEsol gives more accurate results of the lattice parameters compared with other functionals for solids. The more accurate values of the lattice parameters give more accurate results, especially the mechanical behavior characterizing parameters. Thus, we have selected PBEsol in association with the mostly used GGA-PBE functional for this study.^{39,40} The electronic structure was optimized by density mixing, and the atomic configuration was relaxed using BFGS (Broyden Fletcher Goldfarb Shanno).⁴¹ The electronic orbitals of Nb- 4d⁴ 5s¹, C- 2s² 2p², Ga- 4s² 4p¹, Ge- 3d¹⁰ 4s² 4p², Ti- 3d² 4s² 4p¹, Zn- 3d¹⁰ 4s², P- 3s² 3p³, In- 4d¹⁰ 5s² 5p¹ and Cd- 4d¹⁰ 5s² were accomplished for pseudo-atomic calculations. The cutoff energy was set to 500 eV, and the convergence was assured using a *k*-point mesh of 9 × 9 × 2.⁴² The total energy self-consistent convergence was carried out using 5 × 10^{−6} eV per atom, with 0.01 eV Å as the maximum force on the atom. Again, 5 × 10^{−4} Å is used for an ionic displacement, which is the maximum range, with a maximum stress of 0.02 GPa. The phonon dispersion curves were calculated using the Density Functional Perturbation Theory (DFPT) linear-response method.⁴³ Most of our data have been compared to those of ref. 23 (and 25), where the calculations were performed using the following inputs: exchange-correlation – GGA-PBE (LDA-CA), cut-off energy- 550 (350) eV, *k*-points-10 × 10 × 2 (9 × 9 × 2).

3 Results and discussion

3.1 Structural properties and phase stability

3.1.1 Structural properties. As shown in Fig. 1, the unit cell of Nb₂AC (A = Ga, Ge, Ti, Zn, P, In, Cd, and Al) compounds belongs to the hexagonal system wherein the space group is *P6₃/mmc* (No. 194).⁶ Two formula units are there in the unit cell. Each formula unit cell has four atoms. The atomic positions in the unit cell are as follows: Nb atoms at (1/3, 2/3, *z_M*), A atoms at (2/3, 1/3, 1/4) and the C atoms at (0, 0, 0). Additionally, *z_M* is an internal parameter; its value is listed in Table 1.

Table 1 shows the lattice constants (*a*, *c*) for an optimized cell, internal parameters, and the hexagonal ratio (*c/a*) ratio of Nb₂AC (A = Ga, Ge, Ti, Zn, P, In, Cd, and Al). The fundamental polyhedrons of Nb₂AC (A = Ga, Ge, Ti, Zn, P, In, Cd, and Al) are studied using Hug's distortion indexes (DIs).^{44,45} Two parameters- the distortion of octahedral (*O_d*) and trigonal prism (*P_d*) of the M₆X octahedrons and M₆A trigonal prisms, respectively, are used to describe the distortions in the structure of the 211 MAX phases using the following equations:⁴⁶



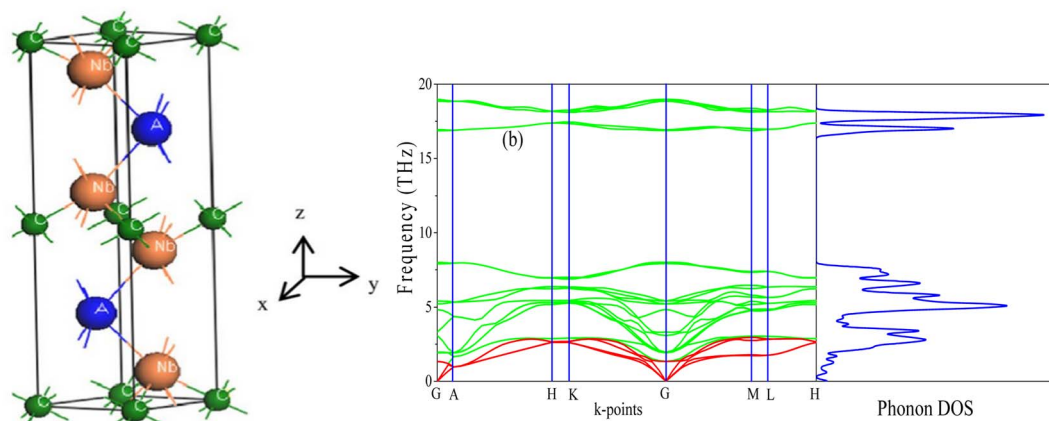


Fig. 1 (a) The unit cell of Nb₂AC (A = Ga, Ge, Tl, Zn, P, In, Cd, and Al); (b) phonon dispersion curve and DOS of Nb₂GaC calculated using GGA PBEsol.

Table 1 Calculated lattice parameters (*a* and *c*), *c/a* ratio, internal parameter (*Z_m*), density (*ρ*), volume (*V*), and distortion parameters of octahedral (*O_d*) and trigonal prisms (*P_d*) of Nb₂AC (A = Ga, Ge, Tl, Zn, P, In, Cd, and Al) MAX phases

Phases	<i>a</i> (Å)	<i>c</i> (Å)	<i>Z_m</i>	<i>c/a</i>	Density (<i>ρ</i>)	Volume (Å ³)	<i>O_d</i>	<i>P_d</i>	Ref.
Nb ₂ GaC	3.145	13.73	0.0896	4.366	7.59	^a 116.97	1.039	0.689	^a This
	3.115	13.51		4.337		^b 113.53	1.044	0.834	^b This
	3.143	13.64		4.340		116.66	*1.044	*0.834	23
	3.13	13.56		4.332		115.05	*1.046	*0.836	6
Nb ₂ GeC	3.244	12.69	0.095	3.914	7.76	115.75	1.086	0.904	^a This
	3.194	12.77		3.998		112.83	1.066	0.890	^b This
	3.255	12.59		3.868			*1.097	*0.912	32
	3.237	12.35		3.815			*1.109	*0.959	25
Nb ₂ TlC	3.228	12.76	0.0795	3.953	10.18	115.10	*1.076	*0.898	23
	3.229	12.74		3.944		131.11	1.254	0.891	^a This
	3.199	14.27		4.461		126.46	1.131	0.781	^b This
	3.145	13.73		4.366		117.58	1.060	0.829	^a This
Nb ₂ ZnC	3.117	13.53	0.0875	4.341	7.43	113.83	1.066	0.833	^b This
	3.299	11.59		3.515		109.33	1.149	0.978	^a This
	3.267	11.52		3.526		106.48	1.146	0.976	^b This
	3.292	11.578		3.517		108.68	*1.139	*0.978	23
Nb ₂ PC	3.28	11.5	0.0999	3.506	8.28	107.15	*1.152	*0.979	6
	3.185	14.54		4.563		127.69	1.103	0.799	^a This
	3.152	14.37		4.559		123.67	1.079	0.799	^b This
	3.186	14.528		4.560		127.72	*1.079	*0.799	23
Nb ₂ InC	3.172	14.37	0.0821	4.530	11.49	125.21	*1.085	*0.804	47
	3.172	14.68		4.628		127.87	1.055	0.790	^a This
	3.140	14.45		4.602		123.37	1.060	0.794	^b This
	3.245	12.69		3.911		115.74	1.142	0.902	^a This
Nb ₂ CdC	3.102	13.79	0.0830	4.446	6.34	114.99	1.021	0.819	^b This
	3.12	13.93		4.463		117.41	*1.017	*0.817	23
Nb ₂ AlC			0.0897						

^a Calculated values using GGA PBE.³⁶ ^b Calculated values using GGAPBEsol³⁷ and *calculated values using reported data.

$$O_d = \sqrt{3/2} \{4z_M^2(c/a)^2 + 1/12\}^{1/2}$$

$$P_d = 1/\{1/3 + (1/4 - z_M)^2(c/a)^2\}^{1/2}$$

The polyhedron would be ideal when both the octahedron and the trigonal parameters are equal to 1.⁴⁶ The distortion of the polyhedron is measured by the deviation from 1, where a low distortion value indicates a more stable structure.⁴⁶

Table 1 shows the value of the *O_d* and *P_d* of Nb₂AC (A = Ga, Ge, Tl, Zn, P, In, Cd, and Al). Table 1 also contains the *O_d* and *P_d* of Nb₂AC (A = Ga, Ge, P, In, and Al) as calculated from the reported lattice parameters. A very good consistency is observed for the previously studied phases, indicating the reliability of our present calculations. The comparison is not possible for Nb₂AC (A = Tl, Zn, and Cd) phases because of their first-time calculation. The accuracy of the present calculations is also revealed by the close agreement of the values of *a* and *c*



[Table 1] of Nb₂AC (A = Ga, Ge, P, In, and Al) phases with previously reported values.^{23,25,32}

3.1.2 The dynamical stability. To check the dynamical stability of the titled phases, we have computed the phonon dispersion curves (PDC) and phonon density of states (PHDOS) of Nb₂AC (A = Ga, Ge, Tl, Zn, P, In, and Cd), displayed in Fig. 1(b) for Nb₂GaC and Fig. S1(a–f) [in the ESI file†] for the rest of the six compounds. The phonon frequency across the entire BZ is used to determine whether a compound is stable or not: positive frequencies indicate stability, whereas any negative frequencies indicate the instability of the compounds. As evident from Fig. 1(b) and S1(a–f),† the studied phases are dynamically stable owing to the non-existence of the negative frequency. In addition, one can obtain some more information from the PDCs. The PDCs have 24 vibrational modes that are caused by the eight atoms in the unit cell. There are only three acoustic modes, whereas the rest 21 are called optical modes. The dispersion curve for the lower three modes is of the form $\omega = \nu k$ at small k values, and it illustrates the sound wave's $\omega(k)$ relations. These modes are the part of the acoustic branch. The upper vibrational modes create the optical branch. The optical phonons are produced due to the atom's out-of-phase oscillations caused by photon-induced excitation. Acoustic modes have zero frequency just at the G point. No phononic band gap is found due to the overlap of the optical branches and acoustic modes. Furthermore, the PHDOS is presented alongside the PDCs, wherein the PDC's flat modes lead the sharp peaks. Peaks are diminished when the dispersion changes, either upward or downward. We have presented only the results for GGA PBEsol; GGA PBE results are not shown because of similarity in nature (Fig. 2).

3.2 Mechanical properties

3.2.1 Stiffness constants and elastic moduli. We have calculated the elastic stiffness constants and the polycrystalline elastic moduli using the strain–stress method⁴⁸ to bring out the mechanical behavior of Nb₂AC (A = Ga, Ge, Tl, Zn, P, In, Cd, and Al). Checking mechanical stability is a must for solids before studying the mechanical properties. The Nb₂AC (A = Ga, Ge, Tl, Zn, P, In, Cd, and Al) phases belong to the hexagonal system,

which need to satisfy the following requirements: $C_{11} > 0$, $C_{33} > 0$, $C_{44} > 0$, $C_{11} - C_{12} > 0$, $(C_{11} + C_{12})C_{33} - 2(C_{13})^2 > 0$.^{49,50} We have calculated the elastic constants and presented them in Table 2, revealing that the requirements mentioned earlier have been satisfied by the selected carbides. Thus, Nb₂AC (A = Ga, Ge, Tl, Zn, P, In, Cd, and Al) phases are considered to be mechanically stable. We may use the calculated stiffness constants to get some additional information. For instance, C_{11} and C_{33} measure the stiffness of the solid along the a -axis and c -axis when pressure is applied along [100] and [001] directions, respectively. Here, $C_{11} > C_{33}$ for Nb₂AC (A = Ga, Ge, Tl, Zn, P, In, Cd, and Al) compounds, revealing the requirement of more pressure along the a -axis for deformation compared to the c -axis, whereas for Nb₂PC $C_{33} > C_{11}$. Moreover, the inequality of C_{11} and C_{33} also indicates the anisotropic bonding strength. The hexagonal structure contains different atomic arrangements along the a - and c -axis, which is assumed to be responsible for the difference in the bonding strength along the a - and c -axis. One of the stiffness constants, C_{44} , is considered to be a better hardness predictor⁵¹ in comparison with other elastic constants. Thus, Nb₂PC is expected to be the hardest one with the highest C_{44} (194 GPa), while Nb₂TlC is the softest one with the lowest C_{44} (71 GPa). The C_{11} , C_{33} , and C_{44} of Nb₂AC (A = Ga, Ge, Tl, Zn, In, and Cd) are lower than those of the most known Nb-based Nb₂AlC phase, but the values are greater for Nb₂PC. Better visualization of the differences among the values of the stiffness constants is done by presenting them in Fig. 2(a) for the GGA-PBEsol functional. Fig. S2(a)† shows the values calculated using GGA-PBE.

Furthermore, the stiffness constants are used to predict the ductile/brittle behavior of Nb₂AC (A = Ga, Ge, Tl, P, Zn, In, Cd, and Al) phases by computing the Cauchy pressure (CP). The difference between C_{11} and C_{44} is defined as the CP;⁵² a negative and positive value represents the brittle and ductile nature, respectively. Negative and positive values also indicate the directional covalent and ionic bonds, respectively. As evident from Table 2, Nb₂GaC, Nb₂GeC, Nb₂PC, Nb₂InC, and Nb₂AlC have directional covalent bonds and behave as brittle solids. On the contrary, Nb₂TlC, Nb₂ZnC, and Nb₂CdC phases behave as ductile solids with a positive CP. Though most MAX phases are brittle, a few of them, such as Zr₃CdB₄, Ti₂CdC,

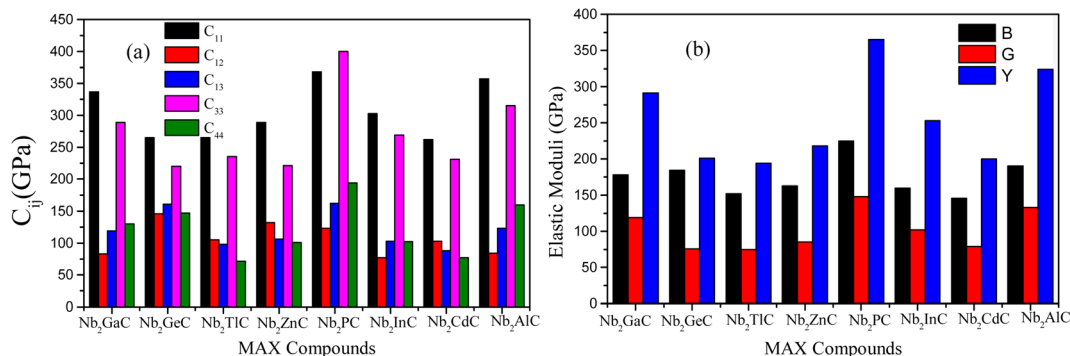


Fig. 2 Comparison of (a) stiffness constants and (b) elastic moduli of Nb₂AC (A = Ga, Ge, Tl, Zn, P, In, Cd, and Al) MAX phases calculated using GGA PBEsol.



Table 2 Calculated stiffness constant (C_{ij}), bulk modulus (B), shear modulus (G), Young's modulus (Y), machinability index (B/C_{44}), Cauchy pressure (CP), Poisson's ratio (ν), and Pugh ratio (G/B)

Parameters	Nb ₂ GaC	Nb ₂ GeC	Nb ₂ TiC	Nb ₂ ZnC	Nb ₂ PC	Nb ₂ InC	Nb ₂ CdC	Nb ₂ AlC	Ref.
C_{11} (GPa)	337	265	265	289	368	303	262	357	^a This
	363	306	283	294	394	331	282	368	^b This
	323	284			373	280		333	23
		308							25
C_{33} (GPa)	289	220	235	221	400	269	231	315	^a This
	313	295	258	225	423	295	258	314	^b This
	281	275			407	266		284	23
		306							25
C_{44} (GPa)	130	147	71	101	194	102	77	160	^a This
	141	151	86	113	212	112	89	164	^b This
	126	152			193	104		138	23
		177							25
C_{12} (GPa)	83	146	105	132	123	77	103	98	^a This
	92	137	106	137	132	85	123	84	^b This
	77	136			114	80		84	23
		133							25
C_{13} (GPa)	119	161	98	106	162	103	88	123	^a This
	131	161	118	122	179	112	102	119	^b This
	130	161			172	113		117	23
		168							25
CP (GPa)	−47	−1	34	31	−71	−25	26	−62	^a This
	−49	−14	20	24	−80	−27	34	−80	^b This
	*−49	*−16			*−79	*−24		*−54	23
		*−44							25
B (GPa)	178	184	152	163	225	160	146	190	^a This
	194	203	168	173	242	175	163	188	^b This
	178	195			230	160		176	23
		206							25
G (GPa)	119	76	75	85	148	102	79	133	^a This
	128	101	84	88	153	112	85	140	^b This
	114	101			150	96		122	23
		109							25
Y (GPa)	291	201	194	218	365	253	200	324	^a This
	314	261	215	225	379	277	216	337	^b This
	282	258			369	240		298	23
		279							25
ν	0.23	0.32	0.29	0.28	0.23	0.24	0.27	0.22	^a This
	0.23	0.29	0.29	0.28	0.24	0.23	0.28	0.20	^b This
	*0.24	*0.28			*0.23	*0.25		*0.22	23
		*0.28							25
G/B	0.67	0.41	0.49	0.52	0.65	0.63	0.54	0.70	^a This
	0.66	0.49	0.50	0.51	0.63	0.64	0.52	0.74	^b This
	*0.64	*0.52			*0.65	*0.60		*0.69	23
		*0.53							25
B/C_{44}	1.36	1.25	2.14	1.61	1.15	1.56	1.89	1.18	^a This
	1.38	1.34	1.95	1.53	1.14	1.56	1.83	1.15	^b This
	*1.41	*1.28			*1.19	*1.54		*1.28	23
		*1.16							25

^a Calculated values using GGA PBE.³⁶ ^b Calculated values using GGA PBEsol³⁷ and *calculated values using reported data.

and Ti₂ZnX (X = C and N), have already been reported to be ductile.^{53–55}

Finally, the stiffness constants were used to calculate the polycrystalline elastic moduli. Hill's approximation⁵⁶ was used to compute the bulk modulus (B) and shear modulus (G), which is the average of the Voigt⁵⁷ and the Reuss⁵⁸ models as follows: $[B = (B_V + B_R)/2]$; here, $B_V = [2(C_{11} + C_{12}) + C_{33} + 4C_{13}]/9$ and $B_R = C^2/M$, where $C^2 = C_{11} + C_{12}C_{33} - 2C_{13}^2$; $M = C_{11} + C_{12} + 2C_{33} - 4C_{13}$. B_V and B_R are expressed as the upper (Voigt) and lower

limit (Reuss) of B , respectively. Again, $[G = (G_V + G_R)/2]$; here, $G_V = [12C_{44} + 12C_{66}]/30$ and $G_R = (5/2)[C^2C_{44}C_{66}]/[3B_VC_{44}C_{66} + C^2(C_{44} + C_{66})]$, where $C_{66} = (C_{11} - C_{12})/2$. Here, like B , G_V and G_R are also expressed as the upper (Voigt) and lower limit (Reuss) of G , respectively. The Poisson's ratio (ν) and Young's modulus (Y) are also computed from B and G by using these relations: $Y = 9BG/(3B + G)$ and $\nu = (3B - Y)/(6B)$.^{59,60}

As known, the pure deformations (volume and shape) are studied by the bulk modulus (mostly known for the study of



elastic response against pressure) and the shear modulus (mostly known for the study of rigidity of solids against pressure). It is seen from Table 2 that Nb₂PC (Nb₂CdC) has the highest (lowest) resistance against hydrostatic pressure, whereas the lowest resistance to plastic deformation is noted for Nb₂TlC among the studied compounds. However, the compounds can be ranked based on the values of *B* (calculated using GGA-PBESol) as follows: Nb₂PC > Nb₂GeC > Nb₂GaC > Nb₂AlC > Nb₂InC > Nb₂ZnC > Nb₂TlC > Nb₂CdC, whereas the ranking for *G* will be as follows: Nb₂PC > Nb₂AlC > Nb₂GaC > Nb₂InC > Nb₂GeC > Nb₂ZnC > Nb₂CdC > Nb₂TlC. For Young's modulus, *Y* is the measure of the stiffness of solids that relates the stiffness with the thermal shock resistance (inverse relationship) of solids. Therefore, a solid with a high *Y* value indicates high stiffness and low thermal shock resistance (TSR).⁶¹ The *Y*-based ranking of the phases also follows the *G*-based ranking. Table 2 implies that Nb₂TlC exhibits high TSR, while Nb₂PC has the lowest TSR, followed by the *Y*-based reverse ranking among the herein-studied phases. Although these moduli do not indicate hardness, they are usually higher for harder materials.⁶² Compared to *Y*, *B* and *G* have a close relationship with the material's hardness. In some cases, these parameters are used to predict the hardness of solids using the following formulae: $H_{\text{Chen}} = 2 \left[\left(\frac{G}{B} \right)^2 G \right]^{0.585} - 3$,⁶³ and $H_{\text{miao}} = \frac{(1 - 2\nu)E}{6(1 + \nu)}$,⁶⁴ Table 2 also includes the previously reported values.²³ As evident from Table 2, the obtained values are in good accord with reported values, ensuring the accuracy of the present calculation that helps other researchers to consider our calculated values as a reference for both application and research purposes. A comparison of the elastic moduli for the studied compounds is shown in Fig. 2(b).

3.2.2 The brittleness of Nb₂AC (A = Ga, Ge, Tl, Zn, P, In, Cd, and Al). The remarkable combination of metal and ceramic characteristics is the most excellent feature of MAX phases.⁶⁵ They are machinable, just like metals, as stated in the preceding section, and brittle, just like ceramic materials. But, some of them are also ductile,^{53,55,66} making them more machinable and, consequently, more useful owing to easy shaping. By using the Pugh ratio (*G/B*)⁶⁷ and Poisson's ratio (*ν*),⁶⁸ the ductile/brittle characteristics of Nb₂AC (A = Ga, Ge, Tl, Zn, P, In, Cd, and Al) have been evaluated and are presented in Table 2. Pugh proposed a critical value of *G/B* ratio (0.571) for ductile (less than 0.571) and brittle (greater than 0.571) classification, whereas *ν* is used to separate the brittle (less than 0.26) and ductile (greater than 0.26) solids with a critical value of 0.26. As evident, Nb₂GaC, Nb₂PC, Nb₂InC, and Nb₂AlC are brittle, while Nb₂GeC, Nb₂TlC, Nb₂ZnC, and Nb₂CdC are ductile; the results are in good agreement with the CP results presented above and the previously reported results.^{23,25}

The Machinability Index (MI) is commonly used in the tribological sector to forecast a solid's performance and is defined as the *B/C*₄₄ ratio. The MI index is presented in Table 2. As evident, the MI of Nb₂TlC, Nb₂ZnC, and Nb₂CdC is higher than that of other studied phases owing to their ductile nature. Though Nb₂GeC is ductile, its *C*₄₄ is comparatively higher,

which results in a lower MI value. Based on the values [Table 2], the titled phases are expected to be more machinable than the widely known Nb₂AlC phase except for Nb₂PC. The lowest MI is found for Nb₂PC, as expected, due to its highest *C*₄₄. In addition, a good relationship between machinability and ductility is observed as expected. The MI values are also different for PBE and PBESol functions because of the different values of *B* and *C*₄₄. However, the obtained values of MI are comparable with those of some other 211 MAX phases, like Ti₂AlC, whose machinability index is 1.23.⁶⁹ Though some 211 phases exhibit a very high value of MI, such as W₂SnC (MI = 33.3) and Mo₂PbC (MI = 15.8),^{17,70} it should be noted that their *C*₄₄ values are much lower (W₂SnC, 6 GPa, and Mo₂PbC, 10 GPa).¹⁷

3.2.3 Theoretical values of Vickers hardness. The Vickers hardness, due to the atomic bonds present within the solids, is the solid's ability to resist deformation under extreme conditions. Different factors, such as the strength of the atomic bonds, atomic arrangement, the structure of the solids, crystal defects, *etc.*, determine the hardness of solids. The Vickers hardness of the Nb₂AC (A = Ga, Ge, Tl, Zn, P, In, Cd, and Al) MAX phases is calculated using Mulliken bond population based on Gou *et al.*,^{71,72} which is mostly suitable for partial metallic systems like MAX phases. The relevant hardness formula is $H_v^{\mu} = 740(P^{\mu} - P^{\mu'}) (v_b^{\mu})^{-5/3}$; here, P^{μ} indicates the μ type bond's Mulliken overlap population and $P^{\mu'} = n_{\text{free}}/v$; $n_{\text{free}} = \int_{E_p}^{E_F} N(E) dE$, E_p indicates the energy of the pseudogap and E_F indicates the energy of the Fermi level. The volume of the μ -type bond is denoted by v_b^{μ} , which is calculated in the following way: $v_b^{\mu} = (d\mu)^3 / \sum v[(d\mu)^3 N_b^{\mu}]$. At last, the equation for Vickers hardness is as follows: $H_v = [\prod \pi(H_v^{\mu}) n^{\mu}]^{1/\sum n^{\mu}}$; $n^{\mu} = \mu$ -type bond number. Table 3 shows the computed Vickers hardness of Nb₂AC (A = Ga, Ge, Tl, Zn, P, In, Cd, and Al). As shown in Table 3, Nb₂PC has higher Vickers hardness than other studied compounds, wherein Nb₂TlC possesses the lowest value of H_v , in agreement with mechanical parameters such as *C*₄₄ and *G*, which are assumed to be more related to the hardness of solids. The H_v values of Nb₂AC (A = Ga, Ge, Tl, Zn, In, Cd, and Al) are comparable with the exception of Nb₂PC, which has a much higher value of H_v . This can be explained on the basis of the bond overlap population (P^{μ}). As seen in Table 3, the P^{μ} of Nb₂PC is 1.01 and 0.98 for C–Nb and P–Nb bonds, respectively, which indicates that strong covalent bonding is found between both Nb–C and Nb–P atoms, whereas for Nb₂AC (A = Ga, Ge, Tl, Zn, In, Cd, and Al), P^{μ} is found only for Nb–C atoms, and no other significant covalent bond is noticed for these phases. Thus, both significant covalent bonding among Nb–C and Nb–P atoms is assumed to be responsible for such higher hardness. However, the variation in H_v of Nb₂AC (A = Ga, Ge, Tl, Zn, In, Cd, and Al) phases is due to the combined effect of the variation in both bond population P^{μ} and bond length d^{μ} .

3.3 Electronic properties, and Mulliken atomic and bond population analysis

3.3.1 Electronic properties. The electronic conductivity, contribution from different states, and nature of atomic



Table 3 Calculated Mulliken bond number n^μ , bond length d^μ , bond overlap population P^μ , metallic population $P^{\mu'}$, bond volume v_b^μ , bond hardness H_v^μ of the μ -type bond and Vickers hardness H_v

Compounds	Bond	n^μ	d^μ (Å)	P^μ	$P^{\mu'}$	v_b^μ (Å ³)	H_v^μ (GPa)	H_v (GPa)	Ref.
Nb ₂ GaC	C–Nb	4	2.177	0.93	0.0223	0.0036	2.418	2.418	^a This
			2.167	0.93	0.0209	0.0037	2.55	2.55	^b This
Nb ₂ GeC	C–Nb	4	2.208	0.99	0.0443	0.0037	1.498	1.498	^a This
			2.183	1.02	0.0100	0.0038	2.86	2.86	^b This
Nb ₂ TlC	C–Nb	4	2.194	0.94	0.0358	0.0029	1.994	1.994	^a This
			2.176	0.96	0.0207	0.0031	2.19	2.19	^b This
Nb ₂ ZnC	C–Nb	4	2.177	0.92	0.0504	0.0036	2.297	2.297	^a This
			2.160	0.91	0.0741	0.0037	2.33	2.33	^b This
Nb ₂ PC	C–Nb	4	2.229	1.01	0.0195	0.0187	13.706	9.312	^a This
	P–Nb	4	2.580	0.98		0.0089	6.326		^a This
	C–Nb	4	2.211	1.00	0.0166	0.0200	14.56	10.02	^b This
	P–Nb	4	2.557	0.98		0.0096	6.89		^b This
Nb ₂ InC	C–Nb	4	2.193	0.96	0.0184	0.0031	2.160	2.160	^a This
			2.174	0.95	0.0105	0.0032	2.82	2.82	^b This
Nb ₂ CdC	C–Nb	4	2.177	0.99	0.0206	0.0031	2.224	2.224	^a This
			2.160	0.93	0.0648	0.0032	2.11	2.11	^b This
Nb ₂ AlC	C–Nb	4	2.165	0.98	0.0179	0.0037	2.63	2.63	^a This
			2.166	1.00	0.0112	0.0037	2.71	2.71	^b This

^a Calculated values using GGA PBE.³⁶ ^b Calculated values using GGA PBEsol.³⁷

bonding can be revealed by studying the electronic band structure, total and partial density of states (DOS), and Mulliken's population analysis. We have calculated the electronic

band structure to predict the metallic nature of the titled MAX compounds. Fig. 3(a), (b) and S3† [calculated using PBEsol] show the calculated electronic band structure of Nb₂AC (A = Ga,

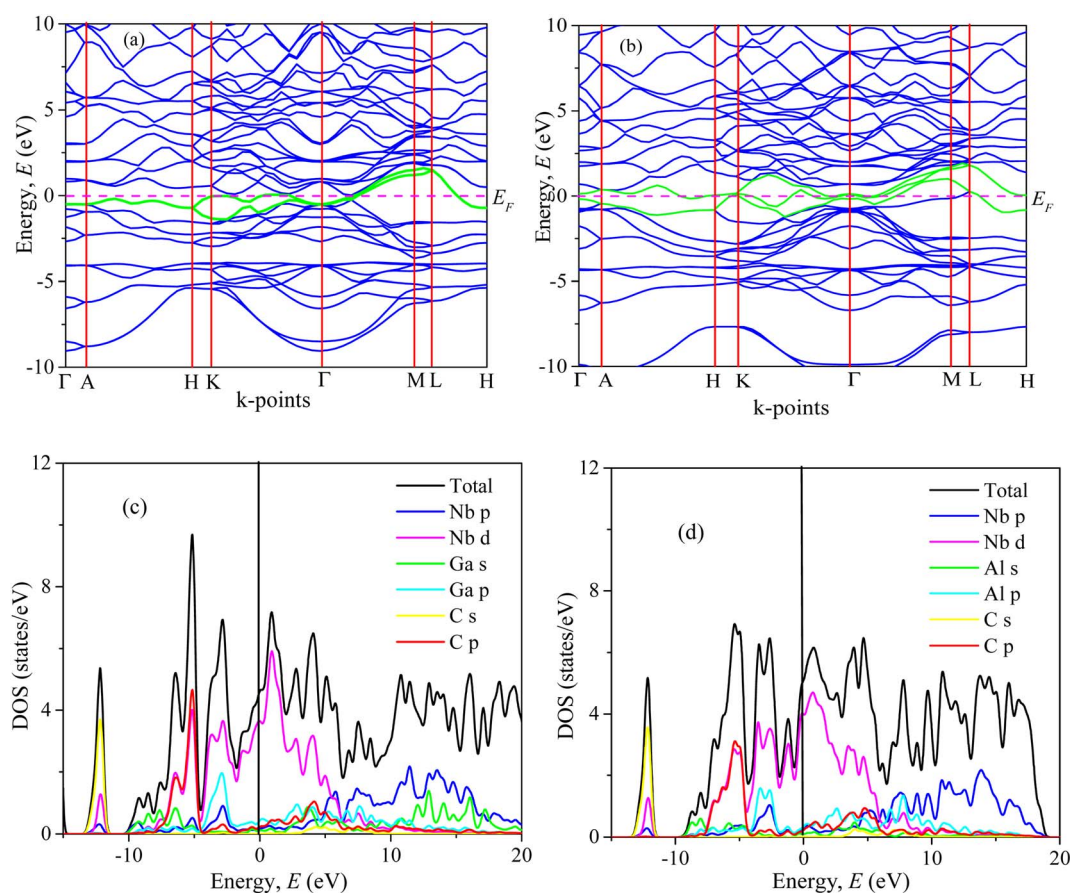


Fig. 3 Band structure, and total and partial DOS of (a, c) Nb₂GaC and (b, d) Nb₂AlC calculated using GGA PBEsol.



Ge, Tl, Zn, P, In, Cd, and Al), in which the Fermi level (E_F) is represented by a horizontal dashed line. The green curves indicate the Fermi level crossing bands and blue curves denote the bands in the valence and conduction bands. As seen from Fig. 3(a), (b) and S3(a)–(f)† due to the overlapping of the conduction and valence bands, there is no band gap at the Fermi level; thus, the Nb₂AC (A = Ga, Ge, Tl, Zn, P, In, Cd, and Al) phases are considered to be metallic solids. The pathways Γ -A, H-K, and M-L show the energy dispersion for the *c*-direction. On the other hand, the pathways A-H, K- Γ , Γ -M, and L-H show energy dispersion in the basal planes. It has been seen from Fig. 3(a), (b) and S3(a)–(f)† that the energy dispersion is smaller in the *c*-direction than that of the basal plane (*ab*-plane); thus, the electronic conductivity in the basal plane is higher than that of the *c*-direction.⁷³ The effective mass tensor is assumed to be higher in the *c*-direction than that of the basal plane, which is responsible for smaller dispersion in the *c*-direction.⁷⁴ Consequently, the anisotropic nature of electronic conductivity is observed in the herein-studied phases, a common feature of the MAX phases, including Nb₂AlC.^{25,72}

We have also computed the total and partial density of states (DOS) of Nb₂AC (A = Ga, Ge, Tl, Zn, P, In, Cd, and Al), which are also shown in Fig. 3(c), (d) and S4(a)–(f)† [calculated using PBEsol]. Here, E_F is the Fermi level, where the DOS values are 3.2, 3.3, 4.0, 3.5, 3.0, 3.1, 2.8, and 3.0 for Nb₂GaC, Nb₂GeC, Nb₂TlC, Nb₂ZnC, Nb₂PC, Nb₂InC, Nb₂CdC, and Nb₂AlC, respectively. The computed compound's DOSs of the studied phases are found to be similar to those of reported MAX phases^{25,72} and Nb₂AlC, which is presented here for comparison.

We have also computed the partial density of states (PDOS) to understand better the chemical bonding of Nb₂AC (A = Ga, Ge, Tl, Zn, P, In, Cd, and Al). Fig. 3(c), (d), and S4(a)–(f)† [calculated using PBEsol] show the PDOS for Nb₂AC. As seen, C-2s is not involved in the DOS at E_F . As a result, the conduction properties are not attributed to carbon. On the other hand, at the Fermi level, Nb-d electrons contribute significantly to the DOS; therefore, the conduction properties ought to be involved in Nb. The A-p (A = Ga, Ge, Tl, Zn, P, In, and Cd) electrons are also involved in the conduction mechanism, with a much lower level of contribution. C-p states also slightly contribute to the conduction properties. This outcome is in line with an earlier MAX phase reported.⁶⁸ The degenerate states concerning both lattice sites and angular momentum indicate that a covalent interaction exists between the atoms of the compounds. Hybridized states include C-p and Nb-d and A (A = Ga, Ge, Tl, Zn, P, In, Cd, and Al) p and Nb d states. Moreover, some ionic characteristics can be anticipated because of the disparity in electro-negativity between the constituent atoms. There is a covalent–ionic combination in the bonding character, which has been explained in Section 3.3.2. When compared to Nb-d and A-p states, the hybridization peak of Nb-d and C-p lies in the lower energy side, as seen in the PDOS; consequently, covalent bonding due to hybridization between Nb-d and C-p states is stronger than that of Nb-d and A p states (A = Ga, Ge, Tl, Zn, P, In, and Cd). The peak position of hybridization between Nb-X and Nb and A states is also responsible for the variation in the hardness of the

studied phases. For example, the hybridization among Nb-d, P-p and C-p states is observed in the lowest energy side (below -5 eV), which results in strong hybridization among them, and a higher bond overlap population is found, which results in the hardest phase of Nb₂PC among the considered phases. The same hybridization peak for other phases is found to appear at an energy scale of above -5 eV. Similar results are also reported for the MAX phases.^{25,72} Additionally, we demonstrated the PDOS of Nb₂AlC, which is similar to those of Nb₂AC (A = Ga, Ge, Tl, Zn, P, In, Cd, and Al).

3.3.2 Mulliken's atomic and bond population analysis. The charge transfer mechanism can be understood by analyzing the atomic population. Mulliken's atomic populations are presented in Table 4 [calculated using GGA PBEsol] and Table S1† [calculated using GGA PBE]. As seen, C possesses a negative charge for each phase, whereas Nb and A (A = Ga, Ge, Tl, Zn, P, In, Cd, and Al) have positive charges, which indicates that the charges are transferred from A (A = Ga, Ge, Tl, and Zn) and Nb to the C atoms. The charge transfer mechanism in these phases indicates the existence of ionic bonding within them. The BOP (bond overlap population) study quantitatively provides bonding and anti-bonding strength.⁷⁵ A positive BOP stands for covalent bonds, and a negative BOP value certifies ionic bonds. As evident from Table 4, a strong covalent bond is formed between Nb and C atoms for each of the titled phases. For Nb₂PC, a strong covalent bond is also expected to be formed in association with the Nb–C bonds, which is responsible for a much higher hardness value compared to other phases presented here. Thus, electronic charge transfer ensured the presence of ionic bonding. In contrast, the high positive value of BOP revealed the existence of covalent bonding, a common characteristic of the MAX phase materials.

3.4 The elastic anisotropy

The study of the elastic anisotropy of the MAX phases is essential because of their potential use in practical applications. Some important physical processes, such as plastic deformation, unusual phonon modes, dislocation dynamics, crack behavior, *etc.*, are caused by mechanical anisotropy in solids.^{76,77} Since the values of C_{11} and C_{33} are unequal [Table 2], other elastic moduli are calculated using these elastic constants. Thus anisotropic nature of the elastic properties is expected for these compounds. These facts encourage us to study the mechanical anisotropy of the titled carbides in the 211 MAX phases. It is possible to demonstrate the level of anisotropy by plotting the elastic moduli in different directions. In this manner, we used the ELATE code⁷⁸ to compute the values of Young's modulus, compressibility, shear modulus, and Poisson's ratio, which are presented in Fig. 4(a–d) for Nb₂GaC, 5(a–d) for Nb₂AlC, S5(a–d) for Nb₂GeC, S6(a–d) for Nb₂TlC, S7(a–d) for Nb₂ZnC, S8(a–d) for Nb₂PC, S9(a–d) for Nb₂InC and S10(a–d)† for Nb₂CdC. The 3D and 2D plots will help to explain the anisotropic nature. The isotropic nature of solids is represented by the sphere in 3D plots and the circle in 2D plots. In contrast, the anisotropy is indicated by a departure from a perfect circle or sphere, and the degree depends on the



Table 4 Mulliken atomic and bond overlap population (BOP) calculated using GGA PBEsol

Phases	Atoms	s	p	d	Total	Charge (e)	Bond	Bond number n^{μ}	Bond overlap population P^{μ}
Nb ₂ GaC	C	1.43	3.22	0.00	4.65	−0.65	C–Nb	4	0.93
	Ga	0.88	1.84	9.99	12.71	0.29			
	Nb	2.27	6.62	3.94	12.82	0.18			
Nb ₂ GeC	C	1.45	3.23	0.00	4.67	−0.67	C–Nb	4	1.02
	Ge	0.99	2.53	0.00	3.52	0.48			
	Nb	2.35	6.56	3.99	12.90	0.10			
Nb ₂ TlC	C	1.43	3.22	0.00	4.65	−0.65	C–Nb	4	0.96
	Tl	3.11	7.84	9.92	20.87	0.13			
	Nb	2.25	6.58	3.92	12.74	0.26			
Nb ₂ ZnC	C	1.43	3.23	0.00	4.66	−0.66	C–Nb	4	0.91
	Zn	0.53	1.32	9.93	11.78	0.22			
	Nb	2.28	6.63	3.87	12.78	0.22			
Nb ₂ PC	C	1.44	3.20	0.00	4.63	−0.63	C–Nb	4	1.00
	P	1.57	3.45	0.00	5.02	0.04	P–Nb	4	0.98
	Nb	2.24	6.45	3.98	12.67	0.33			
Nb ₂ InC	C	1.43	3.22	0.00	4.65	−0.65	C–Nb	4	0.95
	In	0.99	1.81	9.97	12.77	0.23			
	Nb	2.22	6.63	3.94	12.79	0.21			
Nb ₂ CdC	C	1.43	3.23	0.00	4.66	−0.66	C–Nb	4	0.93
	Cd	0.55	1.28	9.91	11.73	0.27			
	Nb	2.29	6.65	3.87	12.81	0.19			
Nb ₂ AlC	C	1.45	3.22	0.00	4.67	−0.67	C–Nb	4	1.00
	Al	0.97	1.83	0.00	2.80	0.20			
	Nb	2.22	6.57	3.98	12.76	0.24			

departure level. Young's modulus (Y) is anisotropic in the xz and yz planes but isotropic in the xy planes, as seen in Fig. 4(a), 5(a), S5(a), S6(a), S7(a), S8(a), S9(a), and S10(a).[†] Y has minimum values at the vertical axis of the xz and yz planes and a maximum value at an intermediate angle of 45° of those axes. Fig. 4(b), 5(b), S5(b), S6(b), S7(b), S8(b), S9(b), and S10(b)[†] depict the compressibility (K), which exhibits a similar anisotropic character to Y . The compressibility (K) is isotropic in the xy plane but anisotropic in the xz and yz planes, where K has maximum values on the axes of the xz and yz planes and a minimum value at an angle of 45° to those axes. For the considered compounds presented in Fig. 4(c), 5(c), S5(c), S6(c), S7(c), S8(c), S9(c), and S10(c),[†] the shear modulus (G) displays two surfaces for both 2D and 3D representations. The green line shows the minimum values for a 45° angle, while the blue line shows the maximum values for the same angle. In the xy and yz planes, G is maximum along both axes, with the minimum value found at an angle of 45° between the axes. In the xy plane, it is seen to be isotropic. In Fig. 4(d), 5(d), S5(d), S6(d), S7(d), S8(d), S9(d), and S10(d),[†] a different anisotropic characteristic is seen for Poisson's ratio. Like G , there are two surfaces for both 2D and 3D representations, except Nb₂GeC. The blue line indicates maximum values at a 45° angle, whereas the green line indicates minimum values at the same angle for all compounds except Nb₂GeC. For Nb₂GeC, the green line indicates positive values, where the values are maximum at an angle of 45° , and the red line indicates maximum negative values for the same angle. Poisson's ratio is also shown to be anisotropic, with the minimum values found within the vertical axes in the xz and yz planes. In contrast, the maximum values are found within the horizontal axes for both

compounds. In the xy plane, Poisson's ratio is found to be isotropic.

Other important anisotropic indices have also been calculated. Using the following relationships, the three shear anisotropic factors A_i ($i = 1, 2$, and 3) are computed:

$$A_1 = \frac{\frac{1}{6}(C_{11} + C_{12} + 2C_{33} - 4C_{13})}{C_{44}}, A_2 = \frac{2C_{44}}{C_{11} - C_{12}}, \text{ and } A_3 = A_1.$$

$$A_2 = \frac{\frac{1}{3}(C_{11} + C_{12} + 2C_{33} - 4C_{13})}{C_{11} - C_{12}},^{79} \text{ for the } \{100\}, \{011\}, \text{ and } \{001\}, \text{ respectively. Using the following relations, the elastic anisotropy for the bulk modulus } (B_a \text{ and } B_c) \text{ across both the } a \text{ and } c\text{-axes is computed:}^{80} B_a = a \frac{dp}{da} = \frac{A}{2 + \alpha} \text{ and } B_c = c \frac{dp}{dc} = \frac{B_a}{\alpha}, \text{ where } A = 2(C_{11} + C_{12}) + 4C_{13\alpha} + C_{33}\alpha^2, \text{ where } \alpha = \frac{(C_{11} + C_{12}) - 2C_{11}}{C_{33} + C_{13}}. \text{ Additionally, the elastic anisotropy for the ratio of the linear compressibility coefficients } (k_c/k_a) [k_a \text{ for } a \text{ and } k_c \text{ for } c\text{-directions}] \text{ is computed using the following relation:}^{81} \frac{k_c}{k_a} = C_{11} + C_{12} - 2C_{13}/(C_{33} - C_{13}). \text{ Table 5 and S2}^\dagger \text{ show the value of the obtained anisotropy factors. The value of } A_i = 1 \text{ implies isotropy, otherwise anisotropic nature; thus, the Nb}_2\text{AC (A = Ga, Ge, Tl, Zn, P, In, Cd, and Al) compounds are anisotropic owing to their non-unit (1) value. The equality of } k_c \text{ and } k_a, \text{ and } B_a \text{ and } B_c \text{ also implies the isotropic nature. As evident, these parameters also suggest the anisotropic nature of the studied compounds. Furthermore, the percentage anisotropies of compressibility and shear modulus were computed as follows:}^{82}$$



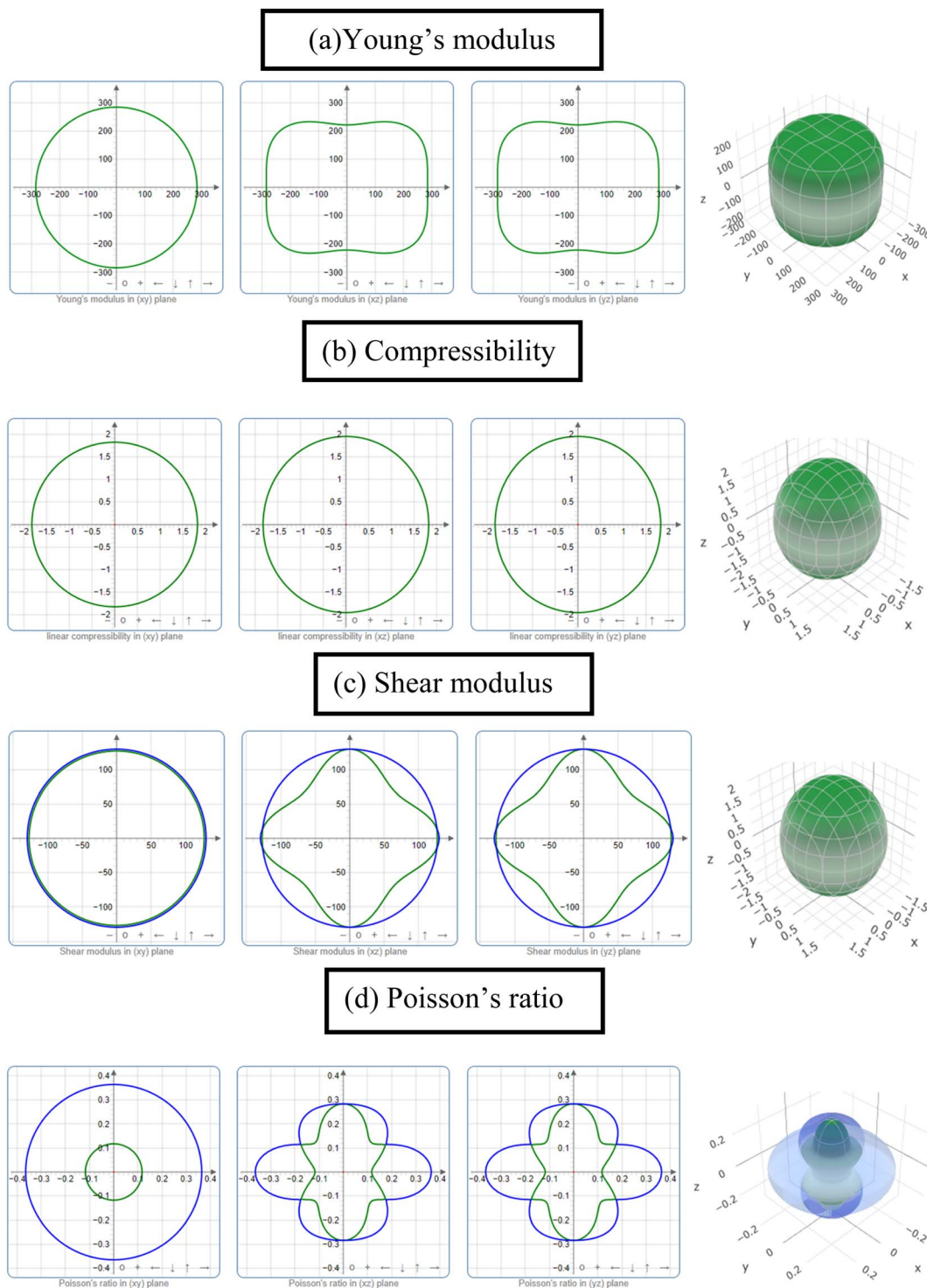


Fig. 4 The 2D and 3D plots of (a) Y , (b) K , (c) G and (d) ν of Nb_2GaC for GGA PBEsol.

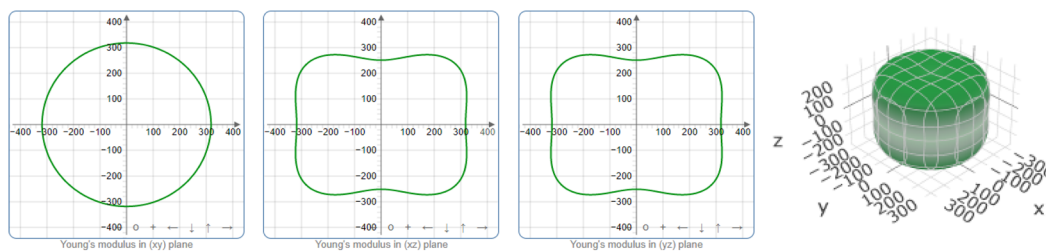
$A_B = \frac{B_V - B_R}{B_V + B_R} \times 100\%$ and $A_G = \frac{G_V - G_R}{G_V + G_R} \times 100\%$, also certifying the anisotropic nature.

Finally, we have calculated the universal anisotropy index A^U based on the Voigt, V (upper limit), and Reuss, R (lower limit), models using the following relation:⁸³ $A^U = 5 \frac{G_V}{G_R} + \frac{B_V}{B_R} - 6 \geq 0$.

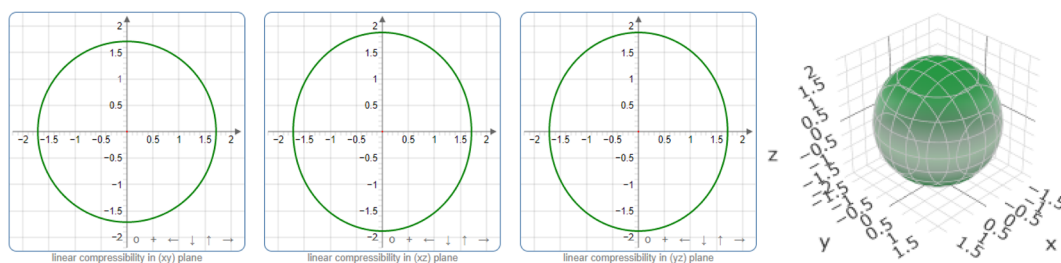
If the value of A^U is zero, it implies isotropic behavior, whereas a non-zero value reveals anisotropic behavior; the non-zero values of A^U reveal the anisotropic behavior of the studied compounds. In summary, we have found the anisotropic nature of Nb_2AC ($A = \text{Ga, Ge, Tl, Zn, P, In, Cd, and Al}$) compounds.



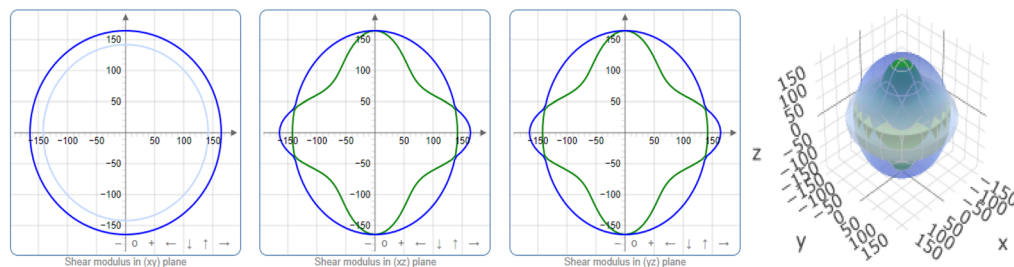
(a) Young's modulus



(b) Compressibility



(c) Shear modulus



(d) Poisson's ratio

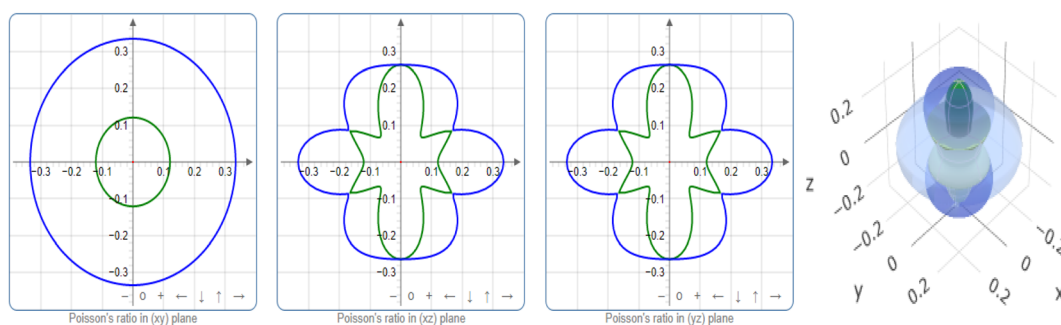


Fig. 5 The 2D and 3D plots of (a) Y , (b) K , (c) G and (d) ν of Nb_2AlC for GGA PBEsol.

3.5 Optical properties

The MAX phase materials have already been identified as prospective candidates for use as a coating layer to lessen

solar heating.⁸⁴ They have also been used in other sectors, such as optical systems.⁸⁴ Therefore, it is also hoped that the studied carbides will also be appropriate for the above mentioned ones. We have computed a variety of optical



Table 5 Anisotropy factors A_1 , A_2 , A_3 , k_c/k_a , B_a , and B_c , percentage anisotropy factors A_G and A_B and universal anisotropic index A^u , calculated values using GGA PBESOL^{37 a}

Phase	A_1	A_2	A_3	B_a	B_c	K_c/k_a	A_B	A_G	A^u	Ref.
Nb ₂ GaC	0.658	1.041	0.685	491.61	1130.96	1.06	0.001	0.013	0.130	This
	*0.585	*1.024	*0.599	*505.19	*1483.25	0.93	*0.001	*0.022	*0.224	23
Nb ₂ GeC	0.429	1.787	0.767	475.71	1792.77	0.90	0.003	0.057	0.607	This
	*0.358	*2.054	*0.734	*448.88	*1317.91	0.86	*0.004	*0.085	*0.932	23
	*0.359	*2.023	*0.723	*470.79	*2125.46	*0.76	*0.001	*0.084	*0.922	*25
Nb ₂ TlC	0.839	0.972	0.816	420.78	1034.08	1.09	0.002	0.003	0.031	This
Nb ₂ ZnC	0.579	1.439	0.833	468.84	869.98	1.82	0.012	0.027	0.296	This
Nb ₂ PC	0.515	1.618	0.833	563.72	2019.99	0.69	0.004	0.038	0.407	This
	*0.529	*1.490	*0.789	*520.15	*2105.85	0.61	*0.007	*0.033	*0.358	*23
Nb ₂ InC	0.830	0.911	0.756	448.67	951.08	1.05	0.006	0.005	0.051	This
	*0.705	*1.037	*0.731	*387.65	*1095.07	0.88	*0.005	*0.008	*0.095	25
Nb ₂ CdC	0.960	1.119	1.074	437.09	782.85	1.29	0.003	0.002	0.023	This
Nb ₂ AlC	0.614	1.155	0.709	487.51	986.40	1.09	0.003	0.016	0.165	This
	0.656	1.074	0.704	*438.87	*1042.45	0.95	0.006	0.012	0.129	23

^a *Calculated values using reported data.

constants in an approach to reveal the optical response of these carbides when electromagnetic radiation is incident upon them.

To estimate the optical properties, it is essential to use the equation $\varepsilon(\omega) = \varepsilon_1(\omega) + i\varepsilon_2(\omega)$. Based on the electronic states of each momentum matrix element's occupied and unoccupied states, it is possible to state that $\varepsilon_2(\omega)$ is the imaginary portion of the related dielectric function and fully calculated by CASTEP using the formula below:

$$\varepsilon_2(\omega) = \frac{2e^2\pi}{\Omega\varepsilon_0} \sum_{k,v,c} |\psi_k^c| u \cdot r |\psi_k^v|^2 \delta(E_k^c - E_k^v - E)$$

where the vector u designates how the incident electric field is polarized, ω represents the frequency of light, e stands for the electronic charge, ψ_k^c represents the conduction band wave function and ψ_k^v indicates the valence band wave function. By using the Kramers-Kronig transform, the real part (ε_1) is obtained from the imaginary part $\varepsilon_2(\omega)$. The refractive index (n), extinction coefficient (k), absorption coefficient (α), reflectivity (R), photoconductivity (σ) and loss function (LF) were calculated by the following equations:^{85–87}

$$n(\omega) = \frac{1}{\sqrt{2}} \left[\sqrt{\{\varepsilon_1(\omega)\}^2 + \{\varepsilon_2(\omega)\}^2} + \varepsilon_1(\omega) \right]^{1/2}$$

$$k(\omega) = \frac{1}{\sqrt{2}} \left[\sqrt{\{\varepsilon_1(\omega)\}^2 + \{\varepsilon_2(\omega)\}^2} - \varepsilon_1(\omega) \right]^{1/2}$$

$$R(\omega) = \frac{(n-1)^2 + k^2}{(n+1)^2 + k^2}$$

$$\alpha(\omega) = \frac{2k\omega}{c}$$

$$L(\omega) = \text{Im} \left(\frac{-1}{\varepsilon(\omega)} \right) = \varepsilon_2(\omega) / [\{\varepsilon_1(\omega)\}^2 + \{\varepsilon_2(\omega)\}^2]$$

$$\sigma(\omega) = \sigma_1(\omega) + i\sigma_2(\omega) = -i \frac{\omega}{4\pi} [\varepsilon(\omega) - 1]$$

A Drude correction must be made for the study of the dielectric function of metallic materials, which is usually done by adding the plasma frequency and a broadening factor during first-principles calculations.^{88,89} Because of the metallic nature of the studied carbides, a damping of 0.05 eV and plasma frequency of 3 eV were used to enhance the computed spectra lower energy side. Moreover, a Gaussian smearing value of 0.5 eV was also used to smear out the k -points around the Fermi level. The calculated optical constants of the titled phases are presented in Fig. 6, along with those of Nb₂AlC for comparison. The real part $\varepsilon_2(\omega)$ of the dielectric function, where the low energy peaks are attributed to electron intra-band transitions,⁹⁰ is shown in Fig. 6(a). Because of the electron intra-band transitions, the assigned value for each peak is less than 1 eV. The materials exhibit Drude-like behavior, as indicated by the massive negative values of $\varepsilon_1(\omega)$, whereas inter-band transitions occur at higher energies. Fig. 6(b) shows the imaginary part of the dielectric function $\varepsilon_2(\omega)$. At around 16 eV, it has been seen that the values of $\varepsilon_2(\omega)$ pass through zero from above. This is another example of the compound's metallic nature. A similar nature of the real and imaginary parts of the dielectric function was reported for the most studied MAX phase Ti₃SiC₂ (ref. 84) and widely used 211 MAX phase Ti₂AlC.⁹¹ The refractive index, $n(\omega)$, of Nb₂AC (A = Ga, Ge, Tl, Zn, P, In, Cd, and Al) is depicted in Fig. 6(c). This significant optical constant contributes to the design of optical systems like photonic crystals and wave guides. As shown in Fig. 6(c), the static value of $n(0)$ for Nb₂AC (A = Ga, Ge, Tl, Zn, P, In, Cd, and Al) is 7.0, 8.9, 9.4, 11, 8.3, 10.9, 9.5 and 8.9, respectively. Fig. 6(d) shows the extinction coefficient, $k(\omega)$, for the Nb₂AC (A = Ga, Ge, Tl, Zn, P, In, Cd, and Al)



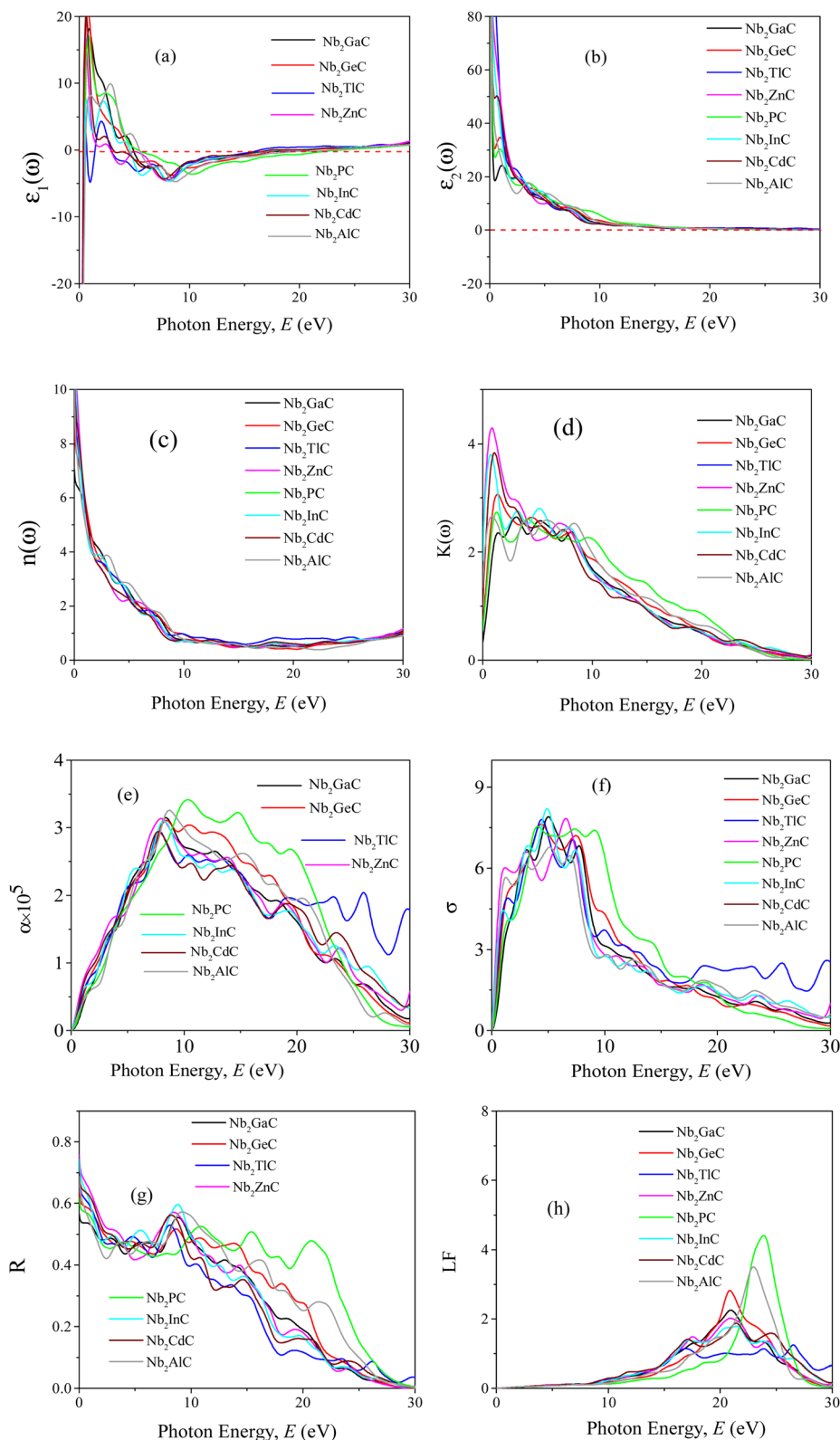


Fig. 6 (a) Real part (ϵ_1) and (b) imaginary part (ϵ_2) of dielectric function (ϵ), (c) refractive index (n), (d) extinction coefficient (k), (e) absorption coefficient (α), (f) photoconductivity (σ), (g) reflectivity (R), and (h) loss function (LF) of Nb_2AX ($A = \text{Ga, Ge, Ti, Zn, P, In, Cd, and Al}$) MAX phases as a function of photon energy calculated using GGA PBEsol.



MAX phases. The extinction coefficient, $k(\omega)$, is used for measuring the loss of electromagnetic radiation due to absorption and is found to vary similarly to $\varepsilon_2(\omega)$, like other MAX phases.^{89,90} In Fig. 6(e), the absorption coefficient of Nb₂AC (A = Ga, Ge, Ti, Zn, P, In, Cd, and Al) MAX phases is illustrated, where the spectra are shown to increase from zero photon energy due to the metallic behavior of the researched compounds. The spectra are seen to increase as incident energy increases. It showed the strongest absorption region in the spectral range of 7–10 eV; it decreases with a further increase in photon energy. Because of the high absorption coefficients in the high energy range (7–10 eV), Nb₂AC (A = Ga, Ge, Ti, Zn, P, In, Cd, and Al) MAX phases can be considered potential absorbing materials in this energy range. The photoconductivity of Nb₂AC (A = Ga, Ge, Ti, Zn, P, In, Cd, and Al) is shown in Fig. 6(f), which is also found to start at the beginning from zero photon energy because of the metallic behavior of the selected phases. The band structure and electronic DOS results are well consistent with the absorption coefficient and photoconductivity results.

MAX phases are used as coating materials to reduce solar heating, which is one of their most significant applications. The reflectivity of the target materials has been investigated to disclose this possibility, shown in Fig. 6(g). It was reported by Li *et al.*^{84,92} that if a MAX compound has a reflectivity of 44% in the visible range, it will be able to reduce solar heating. The reflectivity spectrum for Nb₂GaC begins with a value of 0.569 (56.9%), the minimum value among the studied phases. Nb₂TiC has the highest value, which is 0.982 (98.2%). For Ti₃SiC₂, the spectrum has an initial value of ~0.75 (75%), going down at around 1 eV, and then remaining almost constant up to 6 eV, whereas for Nb₂AlC, it starts with an initial value of 0.68 (68%), which is down to below 44% at around 2.1 eV. Though Nb₂AC (A = Ga, Ge, and P) has a lower initial value of R than Nb₂AlC, neither of their spectra are down to less than 44% up to the visible light range. However, each spectrum of the titled compounds exhibits average higher values (also higher than 44% up to the visible light range) than that of Nb₂AlC. Thus, in comparison with Ti₃SiC₂ and Nb₂AlC, it can be concluded that Nb₂AC (A = Ga, Ge, Ti, Zn, P, In, and Cd) compounds are candidates for use as cover materials to lessen solar heating. In the energy range of 5.5 to 11 eV, there are a few sharp peaks in the reflectivity spectra, and around 30 eV, reflectivity finally approaches zero.

When electrons move through materials, they lose their energy. An optical constant called the loss function is used to evaluate this type of energy loss. Fig. 6(h) displays the calculated loss functions for the aforementioned MAX phase compounds. The loss function's peak frequency is referred to as the plasma frequency (ω_p), which is observed at 20.89, 20.92, 16.38, 17.50, 23.91, 20.54, 17.21 and 23.11 for Nb₂GaC, Nb₂GeC, Nb₂TiC, Nb₂ZnC, Nb₂PC, Nb₂InC, Nb₂CdC, and Nb₂AlC, respectively. In a loss function, this energy is determined by its characteristic frequency when $\varepsilon_1(\omega)$ and $\varepsilon_2(\omega)$ both pass through zero from below and above, respectively. Reflectivity also identifies the falling edges. This is the critical value that is established by the plasma frequency when the materials are transformed into transparent dielectrics from the metallic system. We have also

calculated the optical constant using GGA PBE, but not been shown due to their similar nature.

3.6 Thermal properties

MAX phases are excellent candidates for applications at high-temperature because of their excellent mechanical properties at high temperatures. Therefore, the study of the basic parameters required to predict their application carries significant interest. The Debye temperature (Θ_D), minimum thermal conductivity (K_{\min}), Grüneisen parameter (γ), melting temperature (T_m), *etc.* of the researched compounds have been calculated for predicting their high temperature applications.

The Debye temperature (Θ_D), one of the key characteristic parameters of solids, is closely related to the material's bonding strength, melting temperature, thermal expansion, thermal conductivity, *etc.* The Θ_D of studied phases has been calculated using sound velocity following Anderson's method.⁹³ The relevant formulae are as follows:

$$\Theta_D = \frac{h}{k_B} \left[\left(\frac{3n}{4\pi} \right) N_A \rho / M \right]^{1/3} v_m;$$

where M is the molar mass; n is the number of atoms in the molecules; ρ is the mass density; h is Planck's constant; k_B is the Boltzmann constant; N_A is Avogadro's number; and v_m is the average sound velocity. In an isotropic material, the v_m can be computed from the longitudinal sound velocities (v_l) and transverse sound velocities (v_t) using the given relationship:

$$v_m = \left[\frac{1}{3} \left(\frac{1}{v_l^3} + \frac{2}{v_t^3} \right) \right]^{-1/3};$$
 v_l and v_t can be obtained from their relationships with the polycrystalline bulk modulus (B) and shear modulus (G): $v_l = [(3B + 4G)/3\rho]^{1/2}$ and $v_t = [G/\rho]^{1/2}$. The calculated Θ_D of Nb₂AC (A = Ga, Ge, Ti, Zn, P, In, Cd, and Al) is presented in Table 6 for GGA PBESol and Table S3† for GGA PBE.

As shown in Table 6, Θ_D is highest for Nb₂PC and lowest for Nb₂TiC. The ranking of the compounds roughly followed the hardness-based ranking, which fairly agrees with the hardness and Debye temperature relationship.⁹⁵ The Θ_D of the titled compounds is lower than that of Nb₂AlC, except Nb₂PC. Recently, Hadi *et al.*⁹⁶ reported a MAX (V₂SnC) phase as a TBC material with a Θ_D value of 472 K. Among the studied compounds, a much lower Θ_D is found for only Nb₂TiC (372 K) and Nb₂CdC (424 K); others have Θ_D either comparable to or higher than that of V₂SnC. In addition, the Θ_D of Y₄Al₂O₉, a well-known TBC material, is 564 K.⁹⁷ Thus, Θ_D values of Nb₂AC (A = P, Al, Ga, and Ge) phases [Table 6] are comparable with that of Y₄Al₂O₉.⁹⁷

The minimum thermal conductivity (K_{\min}) is defined as the constant value of thermal conductivity at high temperature. As its name suggests, this conductivity is minimum owing to the breaking of the pairing of phonons at high temperature. Calculation of minimum thermal conductivity is essential for predicting the use of solids at high temperature. It has already been established that the MAX phases are suitable for use in high temperature technology as a coating layer (TBC). Thus, calculation of K_{\min} is also required for the titled phases. We



Table 6 Calculated density (ρ), longitudinal, transverse and average sound velocities (v_l , v_t , and v_m , respectively), Debye temperature (Θ_D), minimum thermal conductivity (K_{\min}) and Grüneisen parameter (γ) of Nb₂AC (A = Ga, Ge, Tl, Zn, P, In, Cd, and Al)^a

Phases	ρ (g cm ⁻³)	v_l (m s ⁻¹)	v_t (m s ⁻¹)	v_m (m s ⁻¹)	Θ_D (K)	K_{\min} (W mK ⁻¹)	γ	T_m (K)	Ref.
Nb ₂ GaC	7.59	6931	4106	4547	548	1.05	1.41	1913	This
Nb ₂ GeC	7.76	6596	3607	4022	485	0.93	1.71	1715	This
		6632	3695	4114	508	*0.95	*1.66	*1737	25
Nb ₂ TlC	10.18	5244	2872	3202	372	0.68	1.71	1590	This
Nb ₂ ZnC	7.43	6248	3440	3834	461	0.88	1.66	1574	This
Nb ₂ PC	8.28	7337	4297	4764	640	1.29	1.45	2171	This
Nb ₂ InC	11.49	5311	3121	3459	483	0.95	1.41	1790	This
Nb ₂ CdC	8.06	5855	3247	3616	424	0.79	1.65	1587	This
Nb ₂ AlC	6.34	7315	4405	4871	592	1.46	*1.37	1800	94

^a Calculated values using GGA PBESOL³⁷ and *calculated values using reported data.

have calculated the K_{\min} of Nb₂AC (A = Ga, Ge, Tl, Zn, P, In, Cd, and Al) compounds using the following equation:⁹⁸

$$K_{\min} = k_B v_m \left(\frac{M}{n \rho N_A} \right)^{-2/3}, \text{ where } k_B \text{ is the Boltzmann constant,}$$

v_m is the average phonon velocity, N_A is Avogadro's number, and ρ is the crystal's density, respectively, as listed in Table 6. The order of the K_{\min} value is expected to be as follows: Nb₂AlC > Nb₂PC > Nb₂GaC > Nb₂InC > Nb₂GeC > Nb₂ZnC > Nb₂CdC > Nb₂TlC; that is, the K_{\min} values of the studied compounds are lower than that of Nb₂AlC, indicating more suitability of the phases as the smaller the K_{\min} is, the more suitable as TBC materials. It should be noted that the K_{\min} of V₂SnC is 1.20 Wm⁻¹ K⁻¹ and Y₄Al₂O₉ is 1.13 Wm⁻¹ K⁻¹.^{96,98} Thus, it is expected that the K_{\min} value suggests the studied compounds as suitable TBC materials.

An essential thermal parameter that helps to explain the anharmonic effects of lattice dynamics is the Grüneisen parameter (γ); lower anharmonic effects are expected for the solids used at high temperature. Therefore, we have calculated γ of Nb₂AC (A = Ga, Ge, Tl, Zn, P, In, Cd, and Al) compounds using the following equation:⁹⁹ $\gamma = \frac{3}{2} \frac{(1 + \nu)}{(2 - 3\nu)}$. According to

Table 6, the obtained values of γ are lying in between 0.85 and 3.53, which is in line with what is predicted for the polycrystalline materials with ν values in the range of 0.05–0.46.¹⁰⁰ Besides, the low values of γ confirm the lower anharmonic effects in the selected compounds, like other MAX phase materials.⁹⁹

Finally, we have calculated the melting temperature (T_m) of the studied compounds using the following equation:

$$T_m = 354 + \frac{4.5(C_{11} + C_{33})}{3},^{101} \text{ and listed it in Table 6. The}$$

melting temperature of the solids mainly depends on atomic bonding strength; the stronger the atomic bonding, the higher the T_m . Thus, a close relationship between T_m and γ is expected,^{94,97} and the order of T_m for the titled phases is found to be following the γ -based ranking of the phases. It is seen from Table 6 that T_m of Nb₂AC (A = Ge, Tl, Zn, In, and Cd) is lower than that of the Nb₂AlC, but still higher than that of the V₂SnC (1533 K) MAX phase, a known TBC material.⁹⁶ In addition, the T_m of Nb₂AC (A = Ga and P) is not only higher

than that of Nb₂AlC⁹⁴ but also comparable to that of Y₄Al₂O₉ (2000 K). T_m values of Nb₂AC (A = Ge, Tl, Zn, In, and Cd) are lower than that of Y₄Al₂O₉ (2000 K) but still reasonably high. Thus, based on the values of Θ_D , k_{\min} , and T_m of the studied phases, in comparison with those of Y₄Al₂O₉ and some other MAX phases that have already been reported as TBC materials, we conclude that the titled phases can be considered as potential TBC materials.

4 Conclusion

A DFT investigation of 211 Nb₂AC (A = Ga, Ge, Tl, Zn, P, In, and Cd) carbides has been carried out in this research. The studied phases are dynamically and mechanically stable. Among the studied phases, Nb₂PC exhibits the best combination of mechanical properties, while Nb₂TlC exhibits the lowest. The Nb₂GaC, Nb₂PC, and Nb₂InC are brittle, whereas Nb₂GeC, Nb₂TlC, Nb₂ZnC, and Nb₂CdC are ductile. The Vickers hardness of Nb₂PC is also higher than that of others considered here, while the lowest Vickers hardness is found for Nb₂TlC, in good agreement with elastic moduli. The calculated direction-dependent (2D and 3D) elastic moduli and anisotropic indices confirm the anisotropic character of the studied phases. The electronic band structure and DOS confirm the metallic nature with a dominating contribution from Nb-3d states. Partial DOS discloses strong hybridization between Nb-d and C-2p states. Mulliken's population analysis reveals the existence of both ionic bonds and covalent bonds within the studied compounds. The optical constants, such as real and imaginary parts of the dielectric function, absorption coefficient, and photoconductivity spectra, are in good accord with band structure results. The reflectivity spectra reveal the possibility of their use as coating materials to diminish solar heating. The obtained values of the Grüneisen parameter (γ) show a lower anharmonic effect within the title carbides. The low value of K_{\min} and comparatively higher melting temperature with reasonable Debye temperature suggest the studied compounds as TBC materials. The results found in this study are encouraging and hoped to attract attention from the scientific community for further investigation of new MAX phase materials.



Conflicts of interest

There are no conflicts to declare.

Acknowledgements

The authors are grateful to the Ministry of Science and Technology (MOST), Bangladesh, for providing the financial support to complete this work (Physical Science-626, 2021–2022 Special Research Grant Project). Prima Das is also grateful to the Chittagong University of Engineering and Technology (CUET) for the financial support.

References

- W. Jeitschko, H. Nowotny and F. Benesovsky, Carbides of formula T_2MC , *J. Less-Common Met.*, 1964, **7**, 133–138.
- H. Wolfsgruber, H. Nowotny and F. Benesovsky, Die kristallstruktur von Ti_3GeC_2 , *Monatsh. Chem.*, 1967, **98**, 2403–2405.
- H. Nowotny, Struktur chemieeiniger verbindungen der ubergangsmetale mit den elementen C, Si, Ge, Sn, *Prog. Solid State Chem.*, 1970, **2**, 27–70.
- H. Nowotny, J. C. Schuster and P. Rogl, Structural chemistry of complex carbides and related compounds, *J. Solid State Chem.*, 1982, **44**, 126–133.
- M. W. Barsoum and T. El-Raghy, Synthesis and characterization of a remarkable ceramic: Ti_3SiC_2 , *J. Am. Ceram. Soc.*, 1996, **79**, 1953–1956.
- M. W. Barsoum, The $M_{n+1}AX_n$ phases: a new class of solids: thermodynamically stable nanolaminates, *Prog. Solid State Chem.*, 2000, **28**, 201–281.
- M. W. Barsoum, *MAX phases: properties of machinable ternary carbides and nitrides*, Wiley VCH Verlag GmbH & Co. KGaA, 2013.
- P. Chakraborty, A. Chakrabarty, A. Dutta and T. Saha-Das gupta, Soft MAX phases with boron substitution: a computational prediction, *Phys. Rev. Mater.*, 2018, **2**, 103605.
- M. Sokol, V. Natsu, S. Kota and M. W. Barsoum, On the chemical diversity of the MAX phases, *Trends Chem.*, 2019, **1**, 210–223.
- M. S. Ali, M. A. Rayhan, M. A. Ali, R. Parvin and A. K. M. A. Islam, New MAX phase compound Mo_2TiAlC_2 : first-principles study, *J. Sci. Res.*, 2016, **8**, 109–117.
- M. A. Ali, M. M. Hossain, M. A. Hossain, M. T. Nasir, M. M. Uddin, M. Z. Hasan, A. K. M. A. Islam and S. H. Naqib, Recently synthesized $(Zr_{1-x}Ti_x)_2AlC$ ($0 \leq x \leq 1$) solid solutions: theoretical study of the effects of M mixing on physical properties, *J. Alloys Compd.*, 2018, **743**, 146–154.
- P. Li, R. Zhou and X. C. Zeng, Computational analysis of stable hard structures in the Ti-B system, *ACS Appl. Mater. Interface.*, 2015, **7**, 15607–15617.
- B. Feng, J. Zhang, Q. Zhong, W. Li, S. Li, H. Li, P. Cheng, S. Meng, L. Chen and K. Wu, Experimental realization of two-dimensional boron sheets, *Nat. Chem.*, 2016, **8**, 563–568.
- M. S. Hossain, N. Jahan, M. M. Hossain, M. M. Uddin and M. A. Ali, High pressure mediated physical properties of Hf_2AB ($A = Pb, Bi$) via DFT calculations, *Mater. Today Commun.*, 2023, **34**, 105147.
- A. Jain, G. Hautier, C. J. Moore, S. P. Ong, C. C. Fischer, T. Mueller, K. A. Persson and G. Ceder, A high-throughput infrastructure for density functional theory calculations, *Comput. Mater. Sci.*, 2011, **50**, 2295–2310.
- S. Curtarolo, G. Hart, M. B. Nardelli, N. Mingo, S. Sanvito and O. Levy, The high-throughput highway to computational materials design, *Nat. Mater.*, 2013, **12**, 191–201.
- M. F. Cover, O. Warschkow, M. M. M. Bilek and D. R. McKenzie, A comprehensive survey of M_2AX phase elastic properties, *J. Phys.: Condens. Matter*, 2009, **21**, 305403.
- V. J. Keast, S. Harris and D. K. Smith, Prediction of the stability of the $M_{n+1}AX_n$ phases from first principles, *Phys. Rev. B: Condens. Matter Mater. Phys.*, 2009, **80**, 214113.
- S. Aryal, R. Sakidja, M. W. Barsoum and W. Y. Ching, A genomic approach to the stability, elastic, and electronic properties of the MAX phases, *Phys. Status Solidi B*, 2014, **251**, 1480–1497.
- M. Ashton, R. G. Hennig, S. R. Broderick, K. Rajan and S. B. Sinnott, Computational discovery of stable M_2AX phases, *Phys. Rev. B*, 2016, **94**, 054116.
- R. Khaledialidusti, M. Khazaei, S. Khazaei and K. Ohno, High-throughput computational discovery of ternary-layered MAX phases and prediction of their exfoliation for formation of 2D MXenes, *Nanoscale*, 2021, **13**, 7294–7307.
- M. A. Hadi, Superconducting phases in a remarkable class of metallic ceramics, *J. Phys. Chem. Solids*, 2020, **138**, 109275.
- M. A. Hadi, S. R. G. Christopoulos, A. Chroneos, S. H. Naqib and A. K. M. A. Islam, Elastic behaviour and radiation tolerance in Nb-based 211 MAX phases, *Mater. Today Commun.*, 2020, **25**, 101499.
- A. Bouhemadou, Calculated structural and elastic properties of M_2InC ($M = Sc, Ti, V, Zr, Nb, Hf, Ta$), *Mod. Phys. Lett. B*, 2008, **22**, 2063–2076.
- A. Bouhemadou, Calculated structural, electronic and elastic properties of M_2GeC ($M = Ti, V, Cr, Zr, Nb, Mo, Hf, Ta$ and W), *Appl. Phys. A*, 2009, **96**, 959–967.
- W. Jeitschko, H. Nowotny and F. Benesovsky, Die H-Phasen Ti_2TiC , Ti_2PbC , Nb_2InC , Nb_2SnC and Ta_2GaC , *Monatsh. fur Chem.*, 1964, **95**, 431–435.
- I. Salama, T. El-Raghy and M. W. Barsoum, Synthesis and mechanical properties of Nb_2AlC and $(Ti, Nb)_2AlC$, *J. Alloys Compd.*, 2002, **347**, 271–278.
- W. Zhang, N. Travitzky, C. F. Hu, Y. C. Zhou and P. Greil, Reactive hot pressing and properties of Nb_2AlC , *J. Am. Ceram. Soc.*, 2009, **92**, 2396–2399.
- M. Khazaei, A. Ranjbar, K. Esfarjani, D. Bogdanovski, R. Dronskowski and S. Yunoki, Insights into exfoliation



- possibility of MAX phases to MXenes, *Phys. Chem. Chem. Phys.*, 2018, **20**, 8579–8592.
- 30 S. Zhao, Y. Dall'Agnese, X. Chu, X. Zhao, Y. Gogotsi and Y. Gao, Electrochemical interaction of Sn-containing MAX phase (Nb₂SnC) with Li-ions, *ACS Energy Lett.*, 2019, **4**, 2452–2457.
 - 31 H. Dinga, Y. Li, J. Lu, K. Luo, K. Chen, M. Li, P. O. A. Persson, L. Hultman, P. Eklund, S. Du, Z. Huang, Z. Chai, H. Wang, P. Huang and Q. Huang, Synthesis of MAX phases Nb₂CuC and Ti₂(Al_{0.1}Cu_{0.9}) N by A-site replacement reaction in molten salts, *Mater. Res. Lett.*, 2019, **7**, 510–516.
 - 32 I. R. Shein and A. L. Ivanovskii, Structural, elastic, electronic properties and Fermi surface for superconducting Mo₂GaC in comparison with V₂GaC and Nb₂GaC from first principles, *Physica C*, 2010, **470**, 533–537.
 - 33 M. A. Ghebouli, B. Ghebouli, A. Bouhemadou and M. Fatmi, Theoretical study of the structural, elastic, electronic and thermal properties of the MAX phase Nb₂SiC, *Solid State Commun.*, 2011, **151**, 382–387.
 - 34 M. D. Segall, P. J. D. Lindan, M. J. Probert, C. J. Pickard, P. J. Hasnip, S. J. Clark and M. C. Payne, First principles simulation: ideas, illustrations and the CASTEP code, *J. Phys.: Condens. Matter*, 2002, **14**, 2717–2744.
 - 35 S. J. Clark, M. D. Segall, C. J. Pickard, P. J. Hasnip, M. I. J. Probert, K. Refson and M. C. Payne, First principles methods using CASTEP, *ZeitschriftFürKrist. – Cryst. Mater.*, 2005, **220**, 567–570.
 - 36 J. P. Perdew, K. Burke and M. Ernzerhof, Generalized gradient approximation made simple, *Phys. Rev. Lett.*, 1996, **77**, 3865.
 - 37 J. P. Perdew, A. Ruzsinszky, G. I. Csonka, O. A. Vydrov, G. E. Scuseria, L. A. Constantin, X. Zhou and K. Burke, Restoring the density-gradient expansion for exchange in solids and surfaces, *Phys. Rev. Lett.*, 2008, **100**, 136406.
 - 38 O. Beckstein, J. E. Klepeis, G. L. W. Hart and O. Pankratov, First-principles elastic constants and electronic structure of α -Pt₂Si and PtSi, *Phys. Rev. B: Condens. Matter Mater. Phys.*, 2001, **63**, 134112.
 - 39 J. Islam, S. K. Mitro, M. M. Hossain, M. M. Uddin, N. Jahan, A. K. M. A. Islam, S. H. Naqib and M. A. Ali, Exploration of the physical properties of the newly synthesized kagome superconductor LaIr₃Ga₂ using different exchange–correlation functionals, *Phys. Chem. Chem. Phys.*, 2022, **24**, 29640.
 - 40 S. Masys and V. Jonauskas, A first-principles study of structural and elastic properties of bulk SrRuO₃, *J. Chem. Phys.*, 2013, **139**, 224705.
 - 41 T. H. Fischer and J. Almlof, General methods for geometry and wave function optimization, *J. Phys. Chem.*, 1992, **96**, 9768.
 - 42 H. J. Monkhorst and J. D. Pack, Special points for Brillouin-zone integrations, *Phys. Rev. B: Condens. Matter Mater. Phys.*, 1976, **13**, 5188.
 - 43 E. I. Isaev, *QHA project*, <https://qe-forge.org/qha>, accessed May 25, 2013.
 - 44 G. Hug, M. Jaouen and M. W. Barsoum, X-ray absorption spectroscopy, EELS, and full-potential augmented plane wave study of the electronic structure of Ti₂Al₃, Ti₂AlN, Nb₂AlC and (Ti_{0.5}Nb_{0.5})₂AlC, *Phys. Rev. B: Condens. Matter*, 2005, **71**, 024105.
 - 45 G. Hug, Electronic structures of and composition gaps among the ternary carbides Ti₂MC, *Phys. Rev. B: Condens. Matter*, 2006, **74**, 184113.
 - 46 M. B. Kanoun, S. Gourmi-said and M. Jaouen, Steric effect on the M site of nanolaminate compounds M₂SnC (M = Ti, Zr, Hf and Nb), *Phys. Condens. Matter*, 2009, **21**, 045404.
 - 47 A. D. Bortolozzo, Z. Fisk, O. H. Sant' Anna, C. A. M. dos Santos and A. J. S. Machado, Superconductivity in Nb₂InC, *Physica C*, 2009, **469**, 57.
 - 48 M. A. Ali and A. K. M. A. Islam, Sn_{1-x}Bi_xO₂ and Sn_{1-x}Ta_xO₂ (0 ≤ x ≤ 0.75): A first-principles study, *Phys. Rev. B: Condens. Matter Mater. Phys.*, 2012, **407**, 1020–1026.
 - 49 M. Born, On the stability of crystal lattices. I, *Math. Proc. Cambridge Philos. Soc.*, 1940, **36**, 160–172.
 - 50 Z. Sun, D. Music, R. Ahuja and J. M. Schneider, Theoretical investigation of the bonding and elastic properties of nanolayered ternary nitrides, *Phys. Rev. B: Condens. Matter Mater. Phys.*, 2005, **71**, 193402.
 - 51 S. H. Jhi, J. Ihm, S. G. Louie and M. L. Cohen, Electronic mechanism of hardness enhancement in transition-metal carbonitrides, *Nature*, 1999, **399**, 132–134.
 - 52 D. G. Pettifor, Theoretical predictions of structure and related properties of intermetallics, *J. Mater. Sci. Tech.*, 1992, **8**, 345–349.
 - 53 M. W. Qureshi, M. A. Ali and X. Ma, Screen the thermomechanical and optical properties of the new ductile 314 MAX phase boride Zr₃CdB₄: A DFT insight, *J. Alloys Compd.*, 2021, **877**, 160248.
 - 54 M. Roknuzzaman, M. A. Hadi, M. J. Abden, M. T. Nasir, A. K. M. A. Islam, M. S. Ali, K. Ostrikov and S. H. Naqib, Physical properties of predicted Ti₂CdN versus existing Ti₂CdC MAX phase: An ab initio study, *Comput. Mater. Sci.*, 2016, **113**, 148–153.
 - 55 M. W. Qureshi, M. A. Ali, X. Ma, G. Tang, M. U. Javed and D. Paudyal, Verification of stability and unraveling the electronic and physical properties of bulk and (001)-surfaces of newly synthesized Ti₂ZnX (X = C, N) MAX phases, *Surf. Interfaces*, 2022, **31**, 102032.
 - 56 R. Hill, The elastic behaviour of a crystalline aggregate, *Proc. Phys. Soc., London, Sect. A*, 1952, **65**, 349–354.
 - 57 W. Voigt, *Lehrbuch der Kristallphysik*, Teubner, Leipzig, 1928.
 - 58 A. Reuss, Berechnung der fließgrenze von mischkristallen auf grund der plastizitätsbedingung für einkristalle, *J. Appl. Math. Mech.*, 1929, **9**, 49–58.
 - 59 M. A. Ali, M. Roknuzzaman, M. T. Nasir, A. K. M. A. Islam and S. H. Naqib, Structural, elastic, electronic and optical properties of Cu₃MTe₄ (M = Nb, Ta) sulvanites —An ab initio study, *Int. J. Mod. Phys. B*, 2016, **30**, 1650089.
 - 60 M. A. Ali, M. A. Hossain, M. A. Rayhan, M. M. Hossain, M. M. Uddin, M. Roknuzzaman, K. Ostrikov, A. K. M. A. Islam and S. H. Naqib, First-principles study



- of elastic, electronic, optical and thermoelectric properties of newly synthesized $\text{K}_2\text{Cu}_2\text{GeS}_4$ chalcogenide, *J. Alloys Compd.*, 2018, **781**, 37–46.
- 61 X. Wang, H. Xiang, X. Sun, J. Liu, F. Hou and Y. Zhou, Mechanical properties and damage tolerance of bulk $\text{Yb}_3\text{Al}_5\text{O}_{12}$ ceramic, *J. Mater. Sci. Technol.*, 2015, **31**, 369–374.
 - 62 M. A. Ali, A. K. M. A. Islam, N. Jahan and S. Karimunnesa, First-principles study of SnO under high pressure, *Int. J. Mod. Phys. B*, 2016, **30**, 1650228.
 - 63 X. Q. Chen, H. Niu, D. Li and Y. Li, Modeling hardness of polycrystalline materials and bulk metallic glasses, *Intermetallics*, 2011, **19**, 1275–1281.
 - 64 N. Miao, B. Sa, J. Zhou and Z. Sun, Theoretical investigation on the transition-metal borides with Ta_3B_4 -type structure: A class of hard and refractory materials, *Comput. Mater. Sci.*, 2011, **50**, 1559–1566.
 - 65 M. Radovic and M. W. Barsoum, MAX phases: Bridging the gap between metals and ceramics, *Am. Ceram. Soc. Bull.*, 2013, **92**, 20–27.
 - 66 M. Mebrek, A. Mokaddem, B. Doumi, A. Yakoubi and A. Mir, A novel theoretical study of elastic and electronic properties of M_2CdC ($\text{M} = \text{Zr}, \text{Hf}, \text{and Ta}$) MAX phases, *Acta Phys. Pol. A*, 2018, **133**, 76–81.
 - 67 S. F. Pugh, Relations between the elastic moduli and the plastic properties of polycrystalline pure metals, *Philos. Mag. J. Sci.*, 1954, **45**, 823–843.
 - 68 M. Roknuzzaman, M. A. Hadi, M. A. Ali, M. M. Hossain, N. Jahan, M. M. Uddin, J. A. Alarco and K. Ostrikov, First hafnium-based MAX phase in the 312 family, Hf_3AlC_2 : A first-principles study, *J. Alloys Compd.*, 2017, **727**, 616–626.
 - 69 I. R. Shein and A. L. Ivanovskii, Graphene-like titanium carbides and nitrides $\text{Ti}_{n+1}\text{C}_n$, $\text{Ti}_{n+1}\text{N}_n$ ($n = 1, 2$, and 3) from de-intercalated MAX phases: First-principles probing of their structural, electronic properties and relative stability, *Comput. Mater. Sci.*, 2012, **65**, 104.
 - 70 I. R. Shein and A. L. Ivanovskii, Elastic properties of superconducting MAX phases from first-principles calculations, *Phys. Status Solidi B*, 2011, **248**, 228–232.
 - 71 H. Gou, L. Hou, J. Zhang and F. Gao, Pressure-induced incompressibility of ReC and effect of metallic bonding on its hardness, *Appl. Phys. Lett.*, 2008, **92**, 2419.
 - 72 P. Barua, M. M. Hossain, M. A. Ali, M. M. Uddin, S. H. Naqib and A. K. M. A. Islam, Effects of transition metals on physical properties of M_2BC ($\text{M} = \text{V}, \text{Nb}, \text{Mo}$ and Ta): a DFT calculation, *J. Alloy. Compd.*, 2018, **770**, 523–534.
 - 73 Y. Zhou and Z. Sun, Electronic structure and bonding properties of layered machinable and ceramics, *Phys. Rev. B: Condens. Matter Mater. Phys.*, 2000, **61**, 12570–12573.
 - 74 M. A. Ali and S. H. Naqib, Recently synthesized $(\text{Ti}_{1-x}\text{Mo}_x)_2\text{AlC}$ ($0 \leq x \leq 0.20$) solid solutions: deciphering the structural, electronic, mechanical and thermodynamic properties via ab initio simulations, *RSC Adv.*, 2020, **10**, 31535–31546.
 - 75 A. Chowdhury, M. A. Ali, M. M. Hossain, S. H. Naqib and A. K. M. A. Islam, Predicted MAX phase Sc_2InC : dynamical stability, vibrational and optical properties, *Phys. Status Solidi B*, 2018, **255**, 1700235.
 - 76 H. M. Ledbetter and A. Migliori, A general elastic-anisotropy measure, *J. Appl. Phys.*, 2006, **100**, 063516.
 - 77 J. Chang, G. P. Zhao, X. L. Zhou, K. Liu and L. Y. Lu, Structure and mechanical properties of tantalum mononitride under high pressure: a first-principles study, *J. Appl. Phys.*, 2012, **112**, 083519.
 - 78 R. Gaillac, P. Pullumbi and F. X. Coudert, ELATE: an open-source online application for analysis and visualization of elastic tensors, *J. Phys.: Condens. Matter*, 2016, **28**, 275201.
 - 79 H. M. Ledbetter, Elastic properties of zinc: a compilation and a review, *J. Phys. Chem. Ref. Data*, 1977, **6**, 1181–1203.
 - 80 A. K. M. A. Islam, A. S. Sikder and F. N. Islam, NbB_2 : a density functional study, *Phys. Lett. A*, 2006, **350**, 288–292.
 - 81 J. Wang, Y. Zhou, T. Liao and Z. Lin, First-principles prediction of low shear-strain resistance of Al_3BC_3 : a metal borocarbide containing short linear BC_2 units, *Appl. Phys. Lett.*, 2006, **89**, 021917.
 - 82 *Anisotropy in single crystal refractory compound*, ed. D. H. Chung, W. R. Buessem, F. W. Vahldiek and S. A. Mersol, Plenum Press, New York, 1968, vol. 2.
 - 83 S. I. Ranganathan and M. Ostoja-Starzewski, Universal elastic anisotropy index, *Phys. Rev. Lett.*, 2008, **101**, 055504.
 - 84 S. Li, R. Ahuja, M. W. Barsoum, P. Jena and B. Johansson, Optical properties of Ti_3SiC_2 and Ti_4AlN_3 , *Appl. Phys. Lett.*, 2008, **92**, 221907.
 - 85 M. F. Li, *Physics of Semiconductor*, Science Press, Beijing, 1991.
 - 86 R. C. Fang, *Solid Spectroscopy*, Chinese Science Technology University Press, Hefei, 2003.
 - 87 Y. Zhang and W. M. Shen, *Basic of Solid Electronics*, Zhe Jiang University Press, Hangzhou, 2005.
 - 88 M. T. Nasir, M. A. Hadi, M. A. Rayhan, M. A. Ali, M. M. Hossain, M. Roknuzzaman, *et al.*, First-principles study of superconducting ScRhP and ScIrP pnictides, *Phys. Status Solidi B*, 2017, **254**, 1700336.
 - 89 F. Sultana, M. M. Uddin, M. A. Ali, M. M. Hossain, S. H. Naqib and A. K. M. A. Islam, First principles study of M_2InC ($\text{M} = \text{Zr}, \text{Hf}$ and Ta) MAX phases: the effect of M atomic species, *Results Phys.*, 2018, **11**, 869–876.
 - 90 K. Akter, F. Parvin, M. A. Hadi and A. K. M. A. Islam, Insights into the predicted Hf_2SN in comparison with the synthesized MAX phase Hf_2SC : a comprehensive study, *Comput. Condens. Matter.*, 2020, **24**, e00485.
 - 91 N. Haddad, E. G. Caurel, L. Hultman, M. W. Barsoum and G. Hug, Dielectric Properties of Ti_2AlC and Ti_2AlN MAX Phases: The Conductivity Anisotropy, *J. Appl. Phys.*, 2008, **104**, 023531.
 - 92 M. A. Ali and M. W. Qureshi, Newly synthesized MAX phase Zr_2SeC : DFT insights into physical properties towards possible applications, *RSC Adv.*, 2021, **11**, 16892.
 - 93 O. L. Anderson, A simplified method for calculating in the Debye temperature from elastic constants, *J. Phys. Chem. Solids*, 1963, **24**, 909–917.
 - 94 M. A. Hadi, N. Kelaidis, S. H. Naqib, A. K. M. A. Islam, A. Chroneos and R. V. Vovk, Insights into the physical properties of a new 211 MAX phase Nb_2CuC , *J. Phys. Chem. Solids*, 2020, **149**, 109759.



- 95 M. A. Ali, M. M. Hossain, M. M. Uddin, M. A. Hossain, A. K. M. A. Islam and S. H. Naqib, Physical properties of new MAX phase borides M_2SB ($M = Zr, Hf$ and Nb) in comparison with conventional MAX phase carbides M_2SC ($M = Zr, Hf$ and Nb): Comprehensive insights, *J. Mater. Res. Tech.*, 2021, **11**, 1000–1018.
- 96 M. A. Hadi, M. Dahlqvist, S. R. G. Christopoulos, S. H. Naqib, A. Chroneos and A. K. M. A. Islam, Chemically stable new MAX phase V_2SnC : a damage and radiation tolerant TBC material, *RSC Adv.*, 2020, **10**, 43783–43798.
- 97 Y. Zhou, X. Lu, H. Xiang, Z. Feng and Z. Li, Theoretical prediction on mechanical and thermal properties of a promising thermal barrier material: $Y_4Al_2O_9$, *J. Adv. Ceram.*, 2015, **4**, 83–93.
- 98 G. A. Slack, The thermal conductivity of nonmetallic crystals, *Solid State Phys.*, 1979, **34**, 1–71.
- 99 V. N. Belomestnykh and E. P. Tesleva, Interrelation between anharmonicity and lateral strain in quasi-isotropic polycrystalline solids, *Tech. Phys.*, 2004, **49**, 1098–1100.
- 100 S. I. Mikitishin, Interrelationship of Poisson's ratio with other characteristics of pure metals, *Sov. Mater. Sci.*, 1982, **18**, 262–265.
- 101 M. E. Fine, L. D. Brown and H. L. Marcus, Elastic constants versus melting temperature in metals, *Scr. Metall.*, 1984, **18**, 951–956.



Supplementary Information File

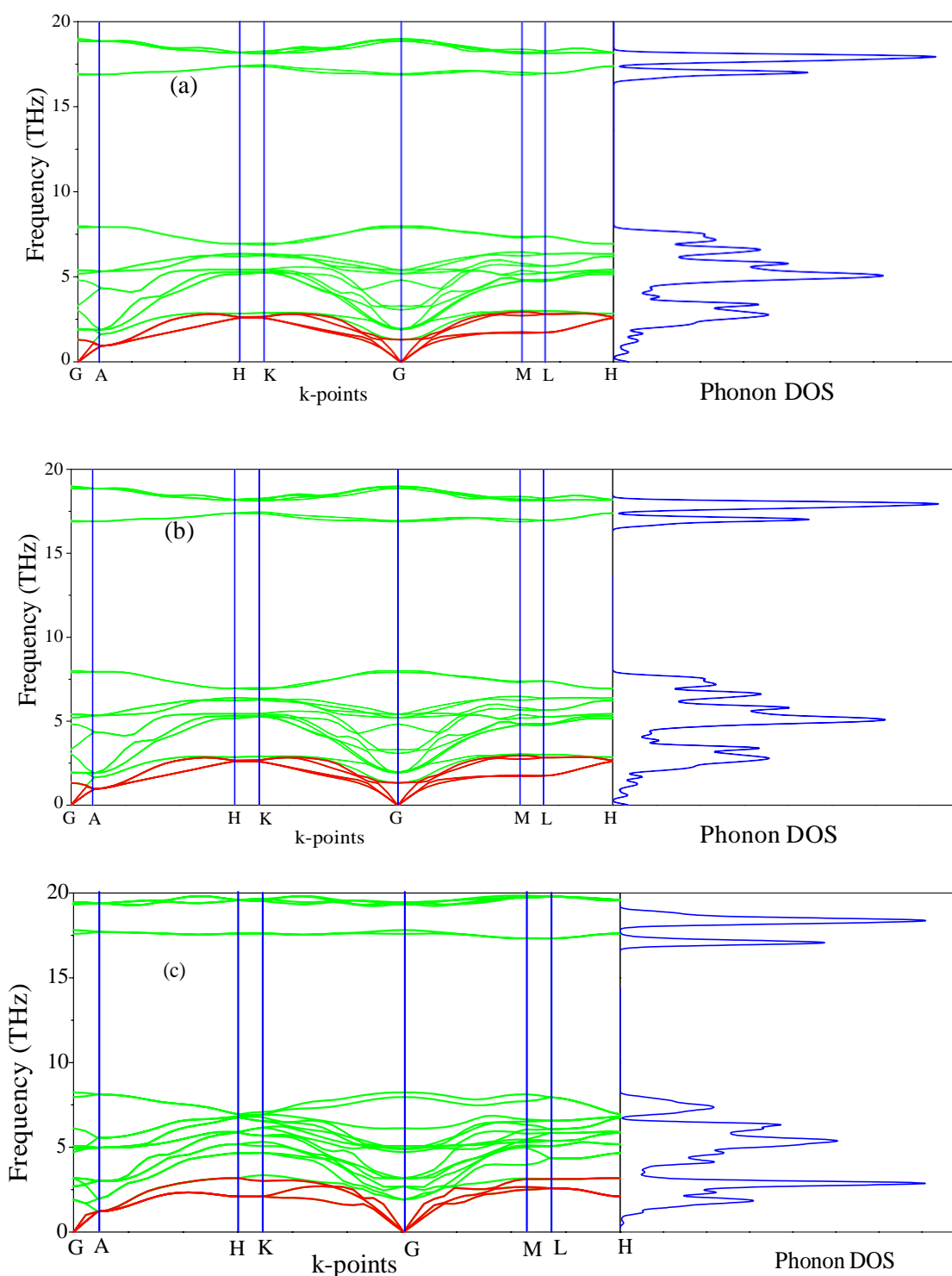
DFT insights into Nb-based 211 MAX phase carbides:

Nb_2AC (A= Ga, Ge, Tl, Zn, P, In, Cd)

Prima Das, N. Jahan*, M. A. Ali*

Department of physics, Chittagong University of Engineering and Technology (CUET)

Chattogram-4349, Bangladesh



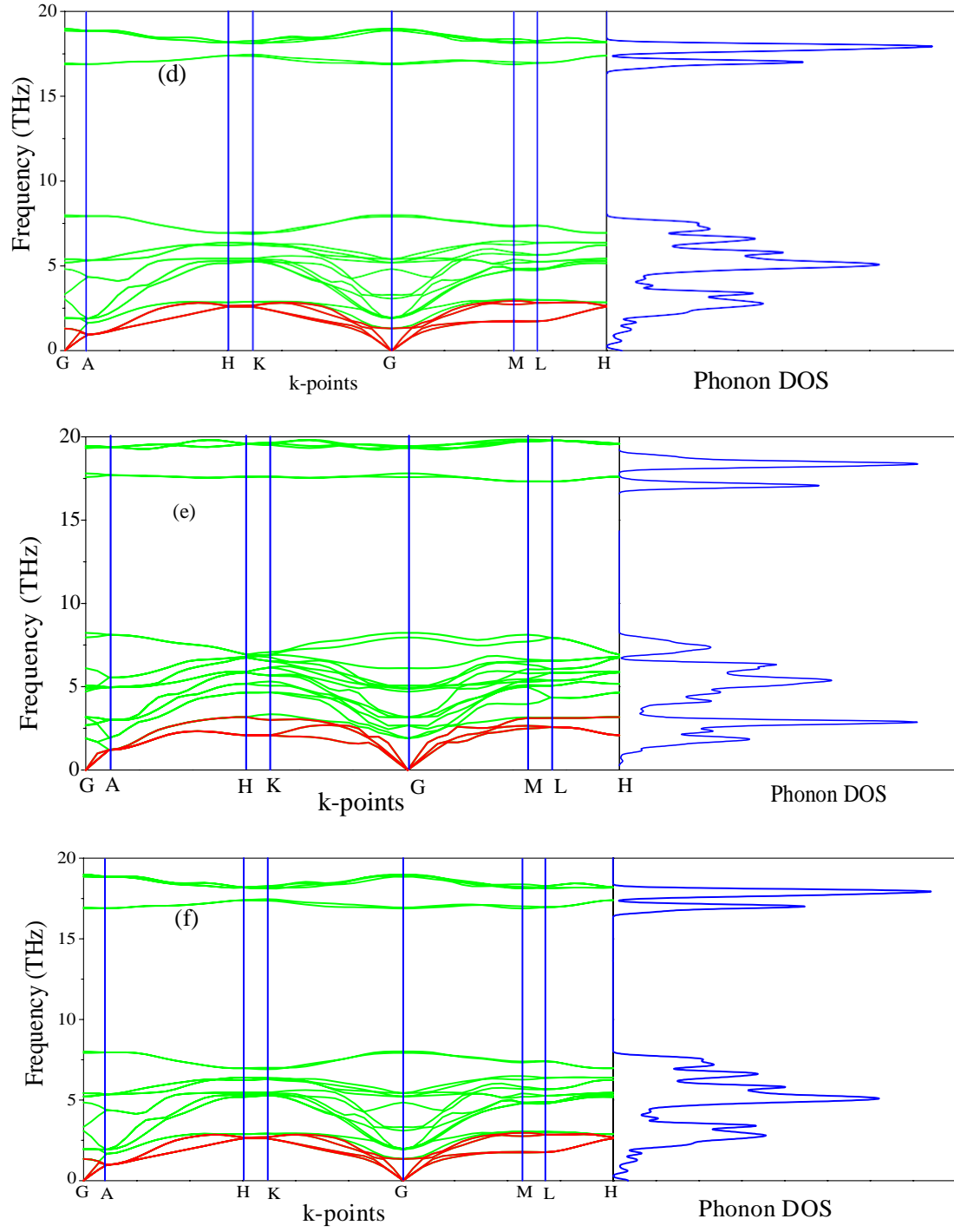


Fig.S-1: Phonon dispersion curve and phonon DOS of (a) Nb₂GeC, (b) Nb₂TiC, (c) Nb₂ZnC, (d) Nb₂PC, (e) Nb₂InC and (f) Nb₂CdC calculated using GGA PBEsol.

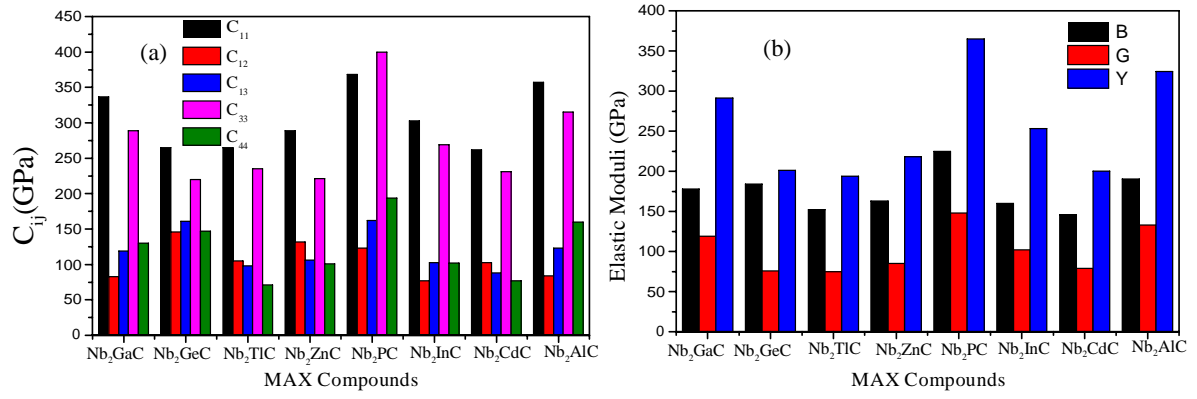


Fig.S-2: (a) The stiffness constant and (b) elastic moduli of Nb₂AC (A = Ga, Ge, Ti, Zn, P, In, Cd, Al) MAX phases calculated using GGA PBE.

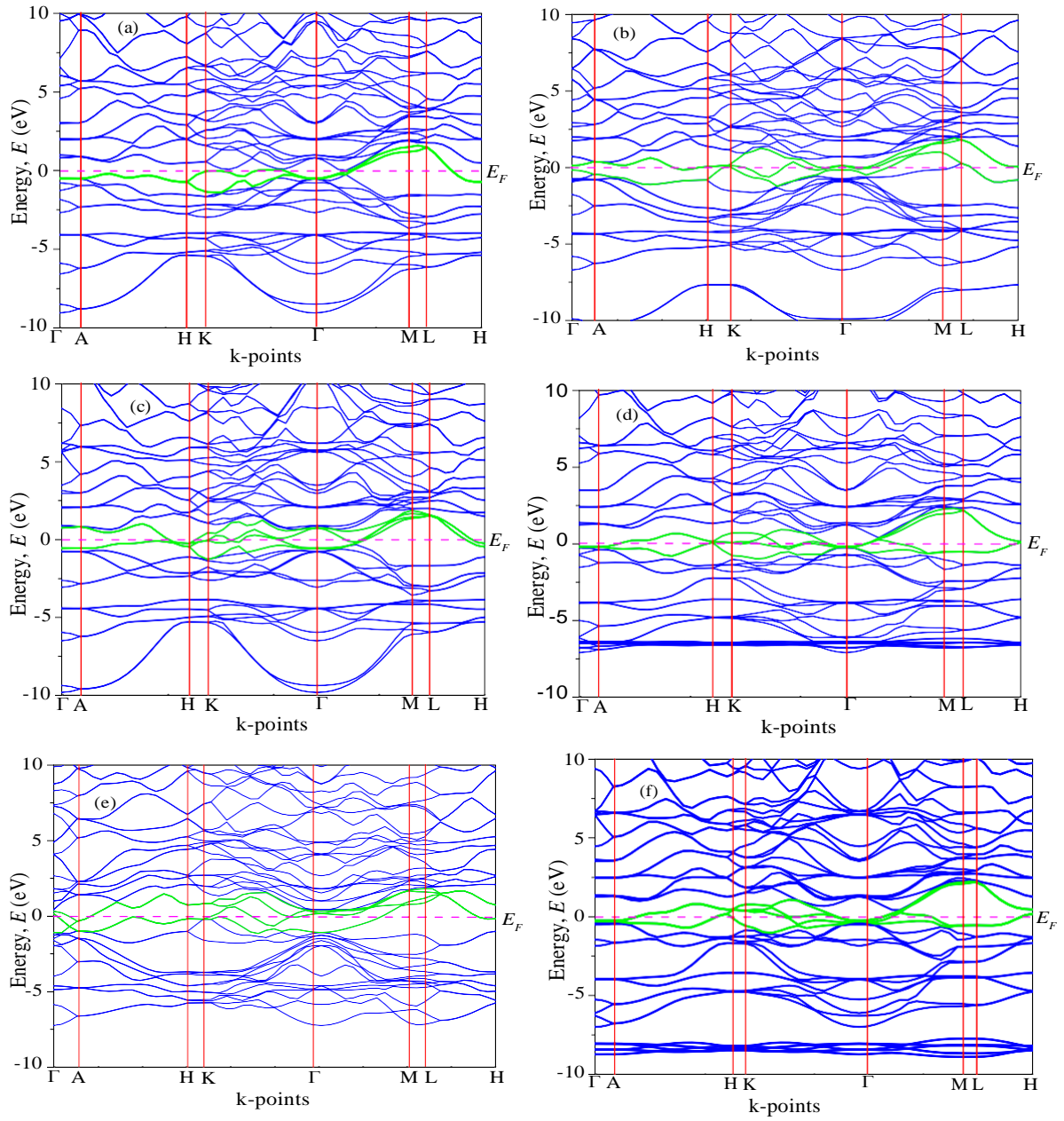


Fig.S-3: Band Structure of a) Nb_2GeC , b) Nb_2TiC , c) Nb_2ZnC , d) Nb_2PC , e) Nb_2ZnC and f) Nb_2CdC calculated using GGA PBEsol.

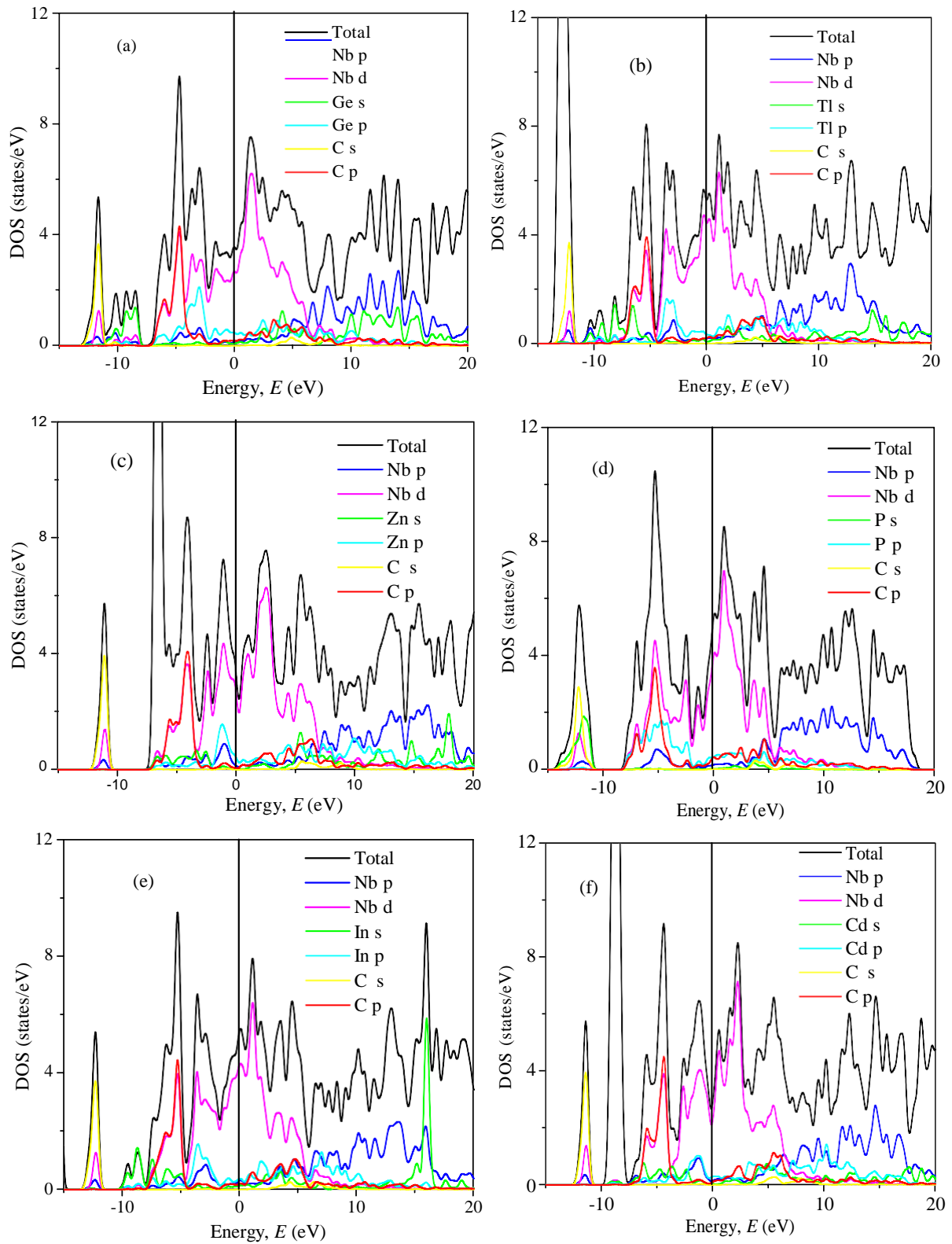
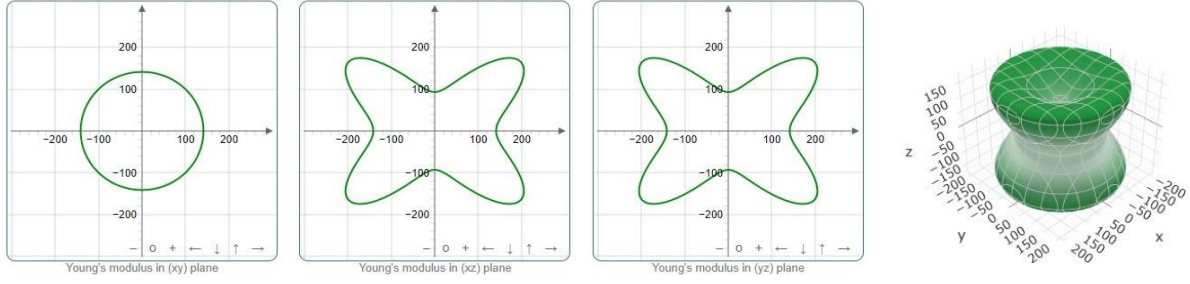
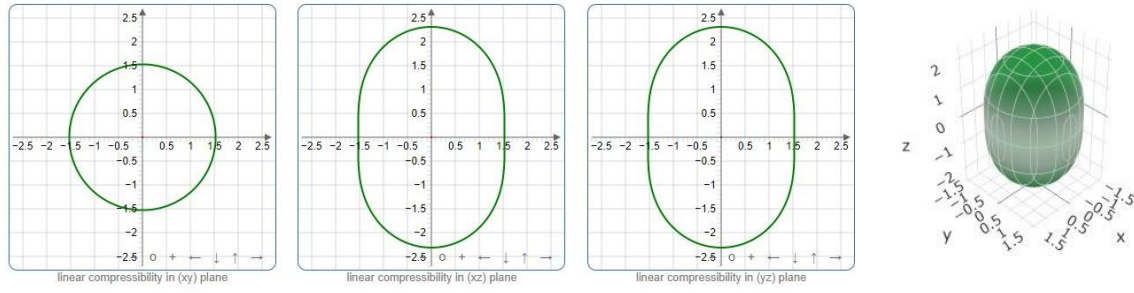


Fig.S-4: Total and Partial DOS of a) Nb₂GeC, b) Nb₂TiC, c) Nb₂ZnC, d) Nb₂PC, e) Nb₂InC and f) Nb₂CdC calculated using GGA PBEsol.

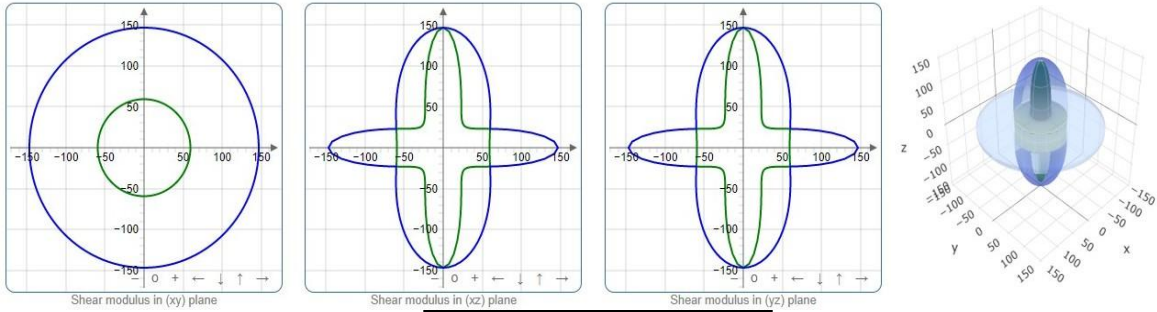
(a) Young's modulus



(b) Compressibility



(c) Shear modulus



(d) Poisson's ratio

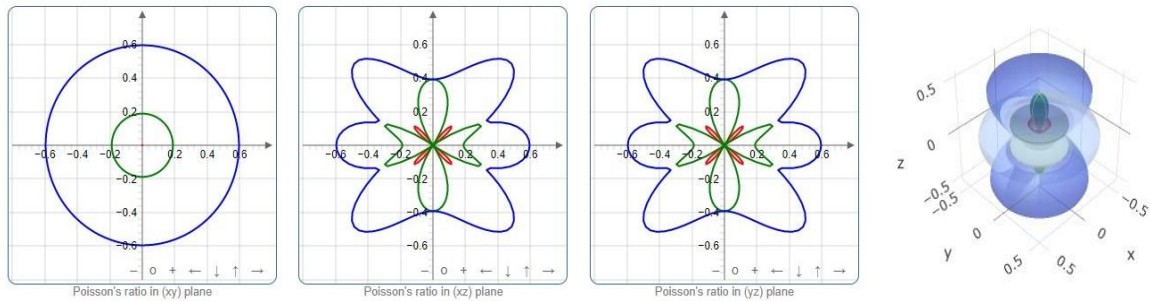


Fig.S-5: The 2D and 3D plots of (a) Y, (b) K, (c) G and (d) ν of Nb₂GeC calculated using GGA PBEsol.

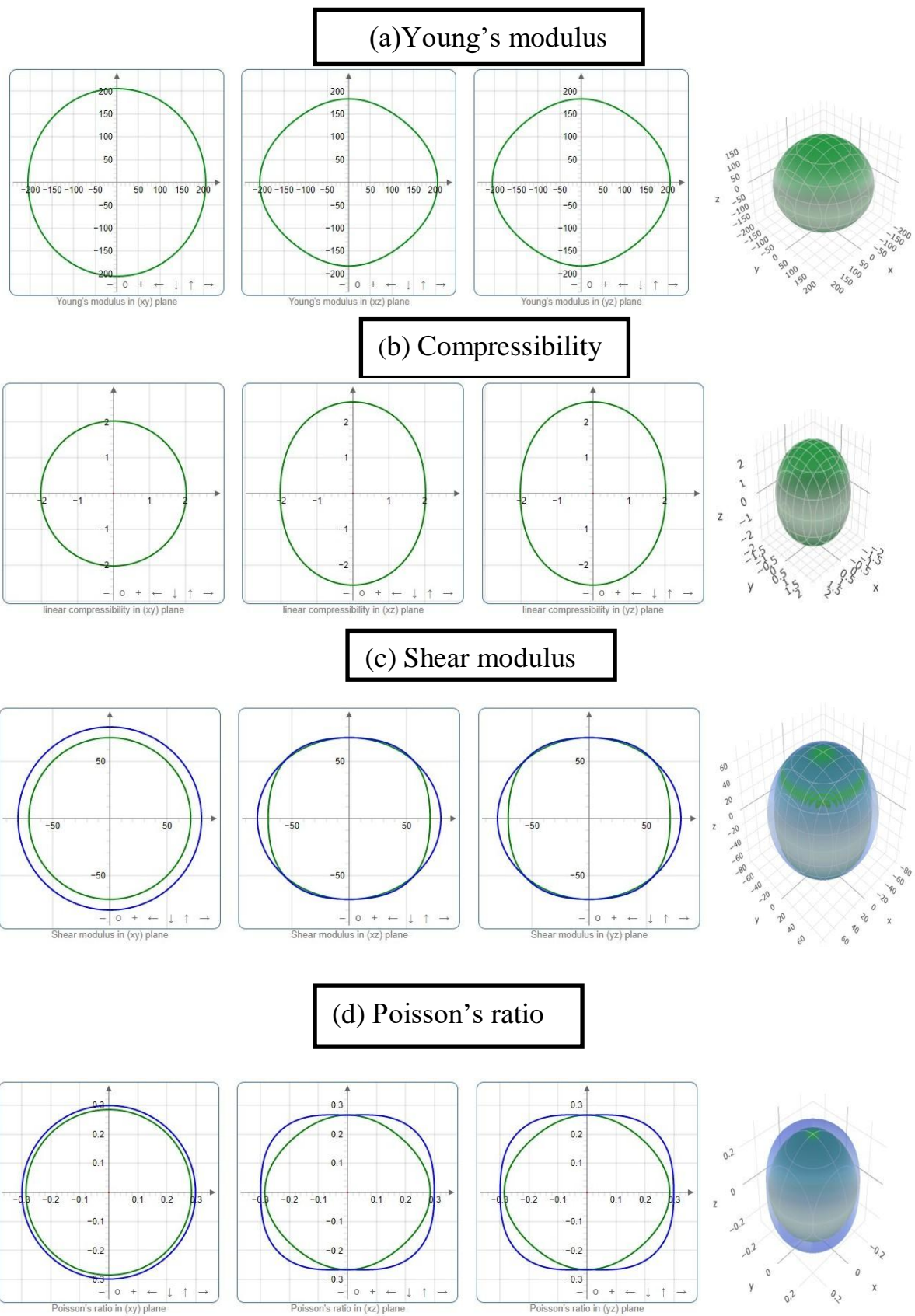
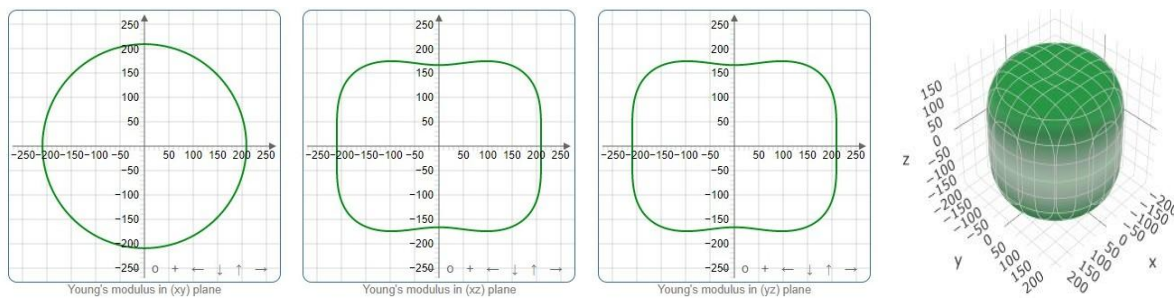
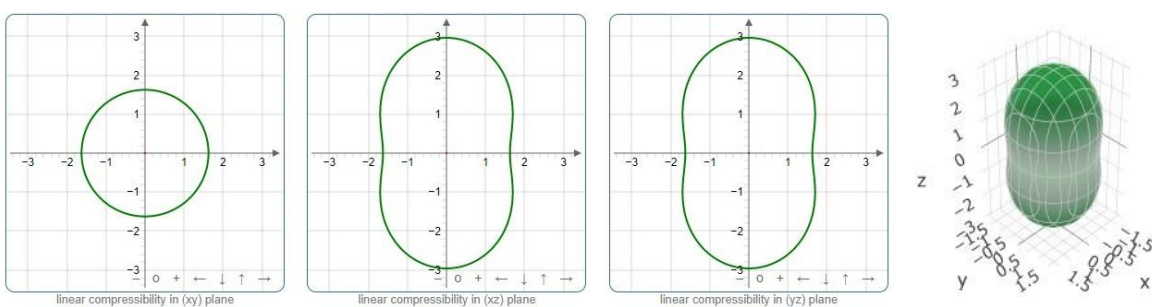


Fig.S-6: The 2D and 3D plots of (a) Y , (b) K , (c) G and (d) ν of Nb_2TIC calculated using GGA PBEsol.

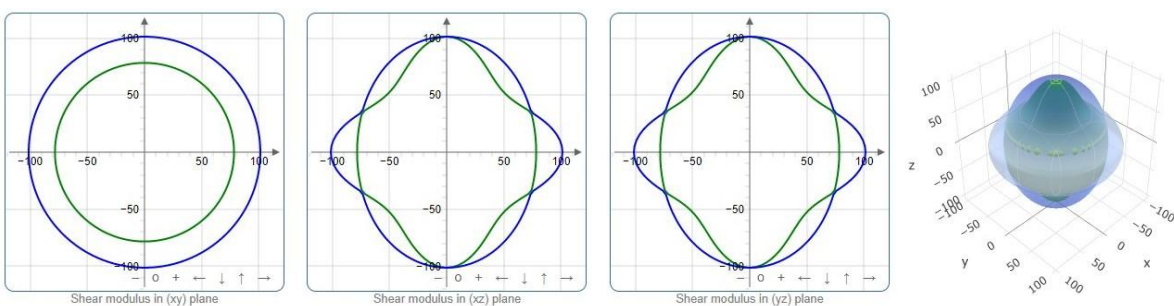
(a) Young's modulus



(b) Compressibility



(c) Shear modulus



(d) Poisson's ratio

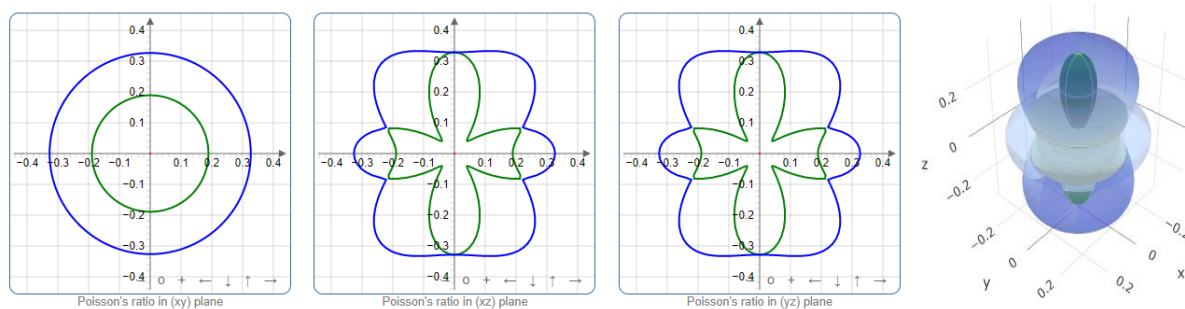
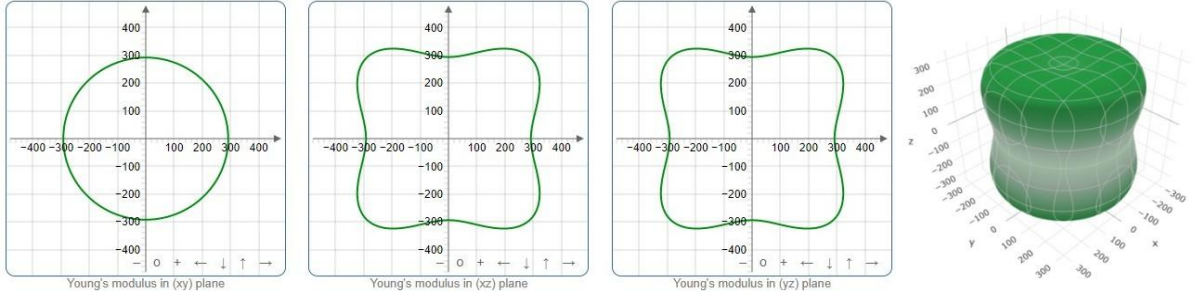
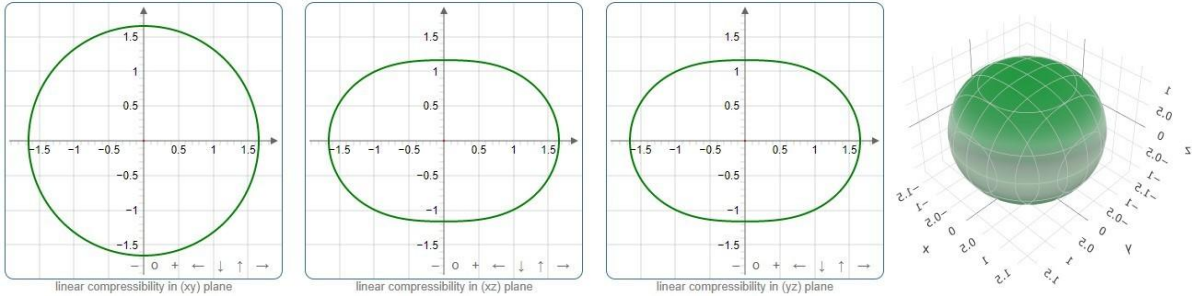


Fig.S-7: The 2D and 3D plots of (a) Y, (b) K, (c) G and (d) ν of Nb_2ZnC calculated using GGA PBEsol.

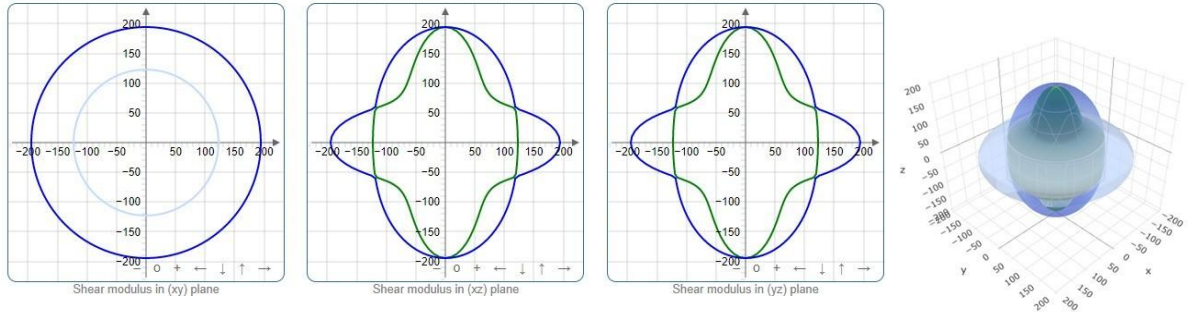
(a) Young's modulus



(b) Compressibility



(c) Shear modulus



(d) Poisson's ratio

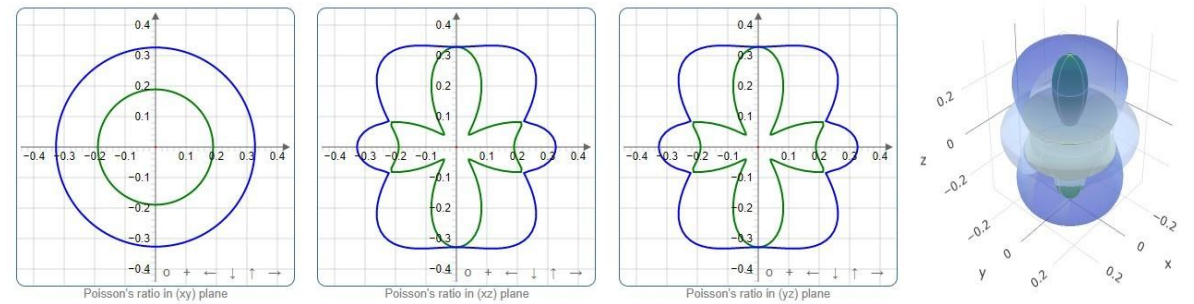
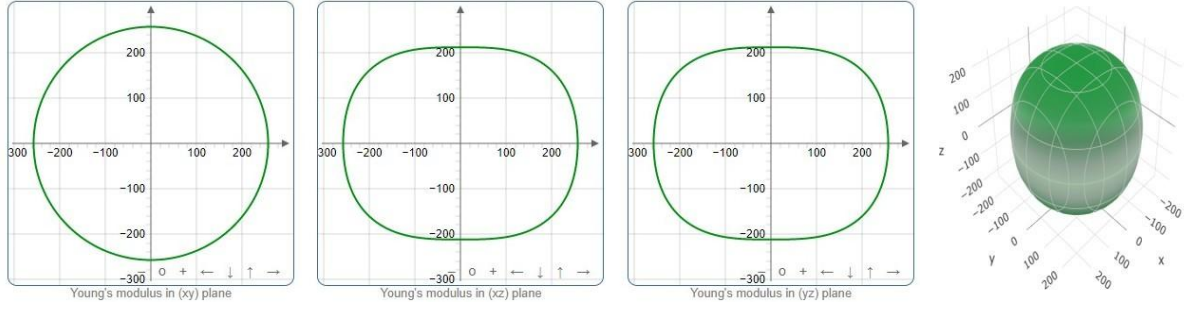
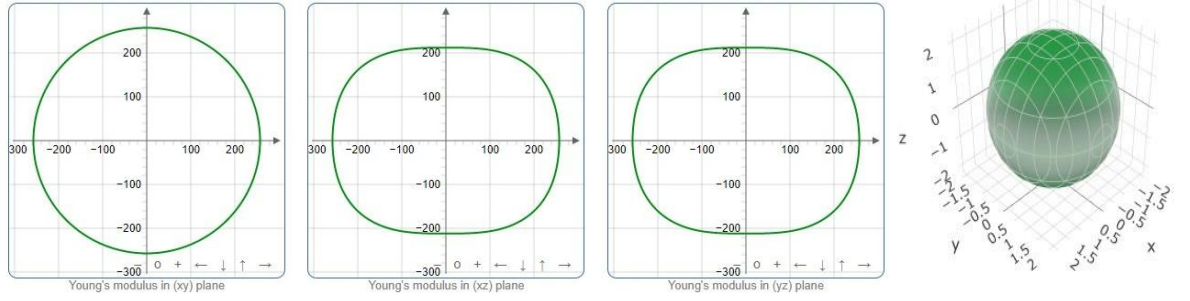


Fig.S-8: The 2D and 3D plots of (a) Y, (b) K, (c) G and (d) ν of Nb₂PC calculated using GGA PBEsol.

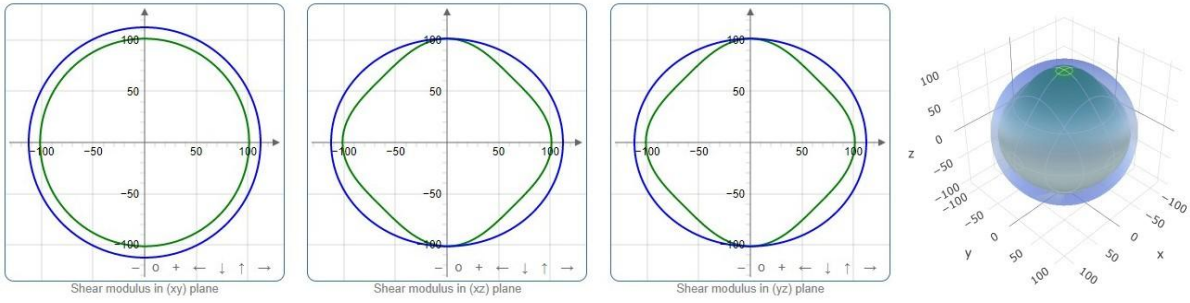
(a) Young's modulus



(b) Compressibility



(c) Shear modulus



(d) Poisson's ratio

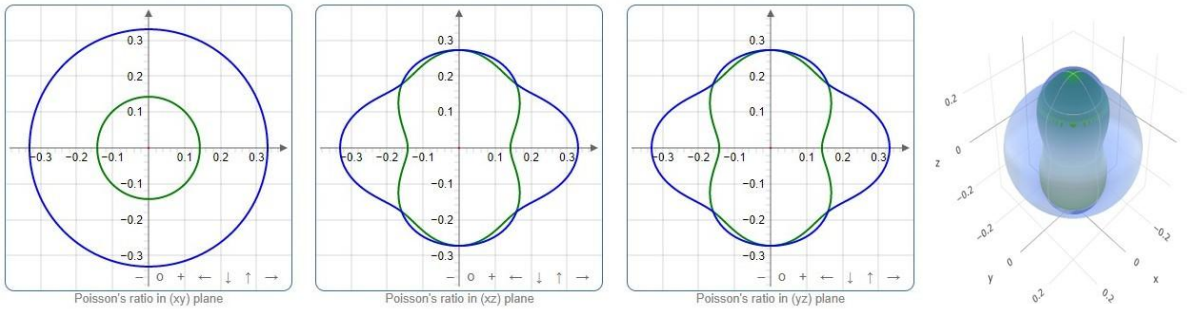
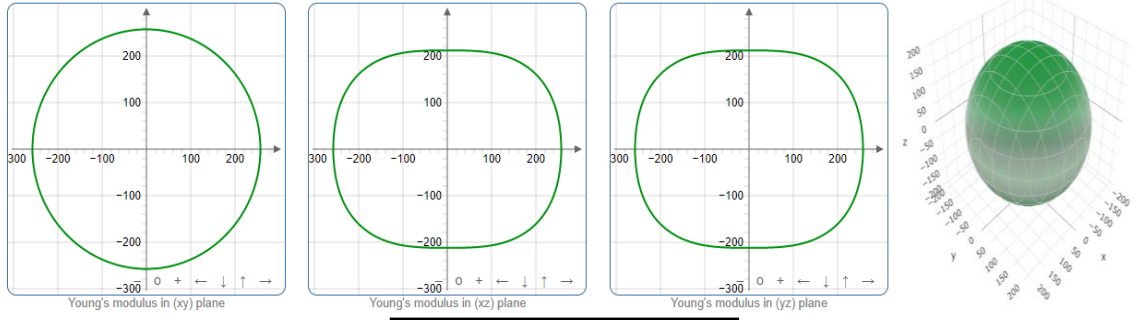
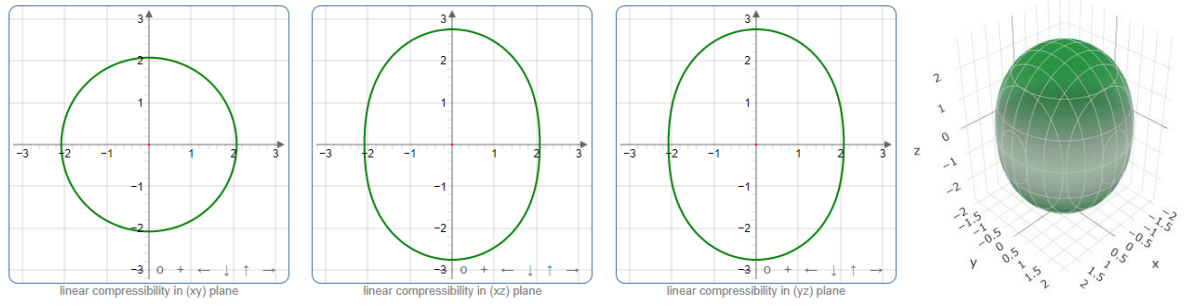


Fig.S-9: The 2D and 3D plots of (a) Y, (b) K, (c) G and (d) ν of Nb₂InC calculated using GGA PBEsol.

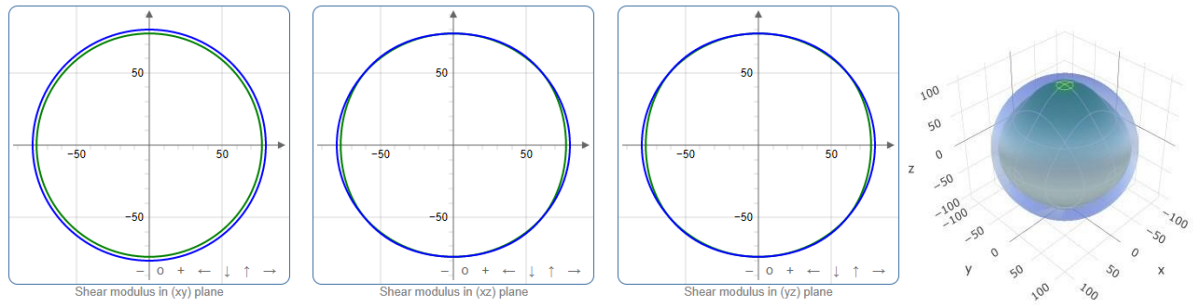
(a) Young's modulus



(b) Compressibility



(c) Shear modulus



(d) Poisson's ratio

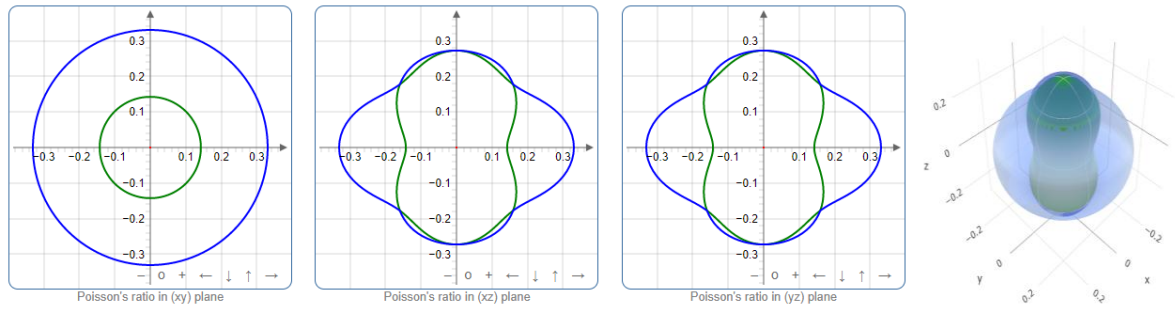


Fig.S-10: The 2D and 3D plots of (a) Y, (b) K, (c) G and (d) ν of Nb₂InC calculated using GGA PBEsol.

Table S-1: Mulliken atomic and bond overlap population (BOP) calculated using GGA-PBE.

Phases	Atoms	s	p	d	Total	Charge(e)	Bond	Bond number n^u	Bond overlap population P^u	Ref.
Nb ₂ GaC	C	1.44	3.23	0.00	4.67	-0.67	C-Nb	4	0.93	This
	Ga	0.87	1.84	9.99	12.70	0.30				
	Nb	2.27	6.63	3.92	12.82	0.18				
Nb ₂ GeC	C	1.44	3.22	0.00	4.66	-0.66	C-Nb	4	0.99	This
	Ge	1.01	2.54	10.00	13.55	0.45				
	Nb	2.33	6.61	3.96	12.89	0.11				
Nb ₂ TlC	C	1.45	3.24	0.00	4.69	-0.69	C-Nb	4	0.94	This
	Tl	1.04	1.79	10.02	12.85	0.15				
	Nb	2.25	6.55	3.93	12.73	0.27				
Nb ₂ ZnC	C	1.44	3.23	0.00	4.67	-0.67	C-Nb	4	0.92	This
	Zn	0.53	1.32	9.93	11.78	0.22				
	Nb	2.28	6.64	3.85	12.77	0.23				
Nb ₂ PC	C	1.45	3.21	0.00	4.66	-0.66	C-Nb	4	1.01	This
	P	1.58	3.48	0.00	5.06	-0.06	P-Nb	4	0.98	
	Nb	2.24	6.45	3.95	12.64	0.36				
Nb ₂ InC	C	1.44	3.22	0.00	4.66	-0.66	C-Nb	4	0.96	This
	In	0.98	1.81	9.97	12.77	0.23				
	Nb	2.23	6.64	3.92	12.79	0.21				
Nb ₂ CdC	C	1.45	3.24	0.00	4.70	-0.70	C-Nb	4	0.99	This
	Cd	0.56	1.27	9.92	11.75	0.25				
	Nb	2.28	6.63	3.87	12.78	0.22				
Nb ₂ AlC	C	1.43	3.21	0.00	4.65	-0.65	C-Nb	4	0.98	This
	Al	0.96	1.81	0.00	2.77	0.23				
	Nb	2.20	6.62	3.97	12.79	0.21				

Table S-2: Anisotropy factors $A_1, A_2, A_3, k_c/k_a, B_a, B_c$ percentage anisotropy factors A_G and A_B and universal anisotropic index A^u calculated using GGA-PBE.

Phase	A_1	A_2	A_3	B_a	B_c	K_c/k_a	A_B	A_G	A^u	Ref.
Nb ₂ GaC	0.669	1.0236	0.685	453.71	1017.29	1.07	0.003	0.013	0.134	This
Nb ₂ GeC	0.2347	2.4706	0.5798	440.74	1886.74	1.51	0.003	0.016	1.846	This
Nb ₂ TlC	1.0516	0.8875	0.9333	513.49	982.77	1.27	0.002	0.002	0.024	This
Nb ₂ ZnC	0.7244	1.2866	0.9321	455.93	713.39	1.82	0.014	0.013	0.160	This
Nb ₂ PC	0.552	1.584	0.874	526.67	1773.29	0.70	0.002	0.032	0.328	This
Nb ₂ InC	0.827	0.903	0.747	440.46	941.15	1.05	0.003	0.005	0.050	This
Nb ₂ CdC	1.123	0.969	0.648	523.91	884.98	1.32	0.005	0.001	0.019	This
Nb ₂ AlC	0.618	1.236	0.764	491.08	1029.15	1.09	0.003	0.016	0.165	This

Table S-3: Calculated density (ρ), longitudinal, transverse and average sound velocities (v_l , v_t , and v_m , respectively), Debye temperature (Θ_D), minimum thermal conductivity (K_{min}) and Grüneisen parameter (γ) of Nb₂AC (A = Ga, Ge, Tl, Zn, P, In, Cd, Al) calculated using GGA-PBE..

Phases	ρ (g/cm ³)	v_l (m/s)	v_t (m/s)	v_m (m/s)	Θ_D (K)	K_{min} (W/mk)	γ	T_m (K)	Ref.
Nb ₂ GaC	7.59	6660	3959	4031	533	0.91	1.41	1799	This
Nb ₂ GeC	7.76	6064	3129	3239	428	0.75	2.06	1479	This
Nb ₂ TlC	10.18	4975	2714	2794	354	0.59	1.71	1502	This
Nb ₂ ZnC	7.43	6098	3382	3480	457	0.79	1.66	1553	This
Nb ₂ PC	8.28	7140	4227	4682	736	1.81	1.41	2058	This
Nb ₂ InC	11.49	5074	2978	3301	492	1.15	1.45	1667	This
Nb ₂ CdC	8.06	5584	3130	3484	411	0.76	1.60	1487	This
Nb ₂ AlC	6.34	7520	4474	4953	612	0.83	1.37	1897	This

PP-39: DFT insights into Nb-based 211 MAX phase Carbides: Nb₂AC (A = Ga, Ge, Tl, Zn)

Prima Das, M. A. Ali*, N. Jahan, M. M. Hossain, and M. M. Uddin

Department of Physics, Chittagong University of Engineering and Technology (CUET),
Chattogram-4349, Bangladesh
Email: ashrafphy31@cuet.ac.bd

In this study, 211 MAX phase Carbides Nb₂AC (A= Ga, Ge, Tl, Zn) have been studied by using density functional theory (DFT) based first-principles calculations. The thermo-mechanical properties of Nb₂AC (A= Ga, Ge, Tl, Zn) have been focused. The structural properties agree well with the previous results. The value of stiffness constants, elastic moduli, and Vickers hardness has been calculated. The Nb₂GaC shows the best mechanical properties with highest hardness values whereas Nb₂GeC possesses the lowest values of mechanical properties. We have calculated different anisotropic indices and 2D and 3D plots of Young's modulus, compressibility, shear modulus, and Poisson's ratio to demonstrate the anisotropy of the elastic properties. We have calculated the important thermal properties characterizing parameters such as Debye temperature (Θ_D), minimum thermal conductivity (K_{min}), melting temperature (T_m), Grüneisen parameter (γ). The values of these parameters suggest that the titled carbides can be used as thermal barrier coating (TBC) materials.